

Electronic Thesis and Dissertation Repository

---

3-4-2011 12:00 AM

## Pushing the Boundaries in Gradient and Shim Design for MRI

Parisa Hudson, *The University of Western Ontario*

Supervisor: Dr. Blaine Chronik, *The University of Western Ontario*

A thesis submitted in partial fulfillment of the requirements for the Doctor of Philosophy degree in Physics

© Parisa Hudson 2011

Follow this and additional works at: <https://ir.lib.uwo.ca/etd>



Part of the [Physics Commons](#), and the [Sustainability Commons](#)

---

### Recommended Citation

Hudson, Parisa, "Pushing the Boundaries in Gradient and Shim Design for MRI" (2011). *Electronic Thesis and Dissertation Repository*. 99.

<https://ir.lib.uwo.ca/etd/99>

This Dissertation/Thesis is brought to you for free and open access by Scholarship@Western. It has been accepted for inclusion in Electronic Thesis and Dissertation Repository by an authorized administrator of Scholarship@Western. For more information, please contact [wlsadmin@uwo.ca](mailto:wlsadmin@uwo.ca).

# **PUSHING THE BOUNDARIES IN GRADIENT AND SHIM DESIGN FOR MRI**

(Spine title: Design of high performance gradient and shim coils)

(Thesis format: Integrated- Article)

by

Parisa Hudson

Graduate Program in Physics and Environment and sustainability

A thesis submitted in partial fulfillment  
of the requirements for the degree of  
Doctor of Philosophy

The School of Graduate and Postdoctoral Studies  
The University of Western Ontario  
London, Ontario, Canada

© Parisa Hudson 2011

THE UNIVERSITY OF WESTERN ONTARIO  
School of Graduate and Postdoctoral Studies

**CERTIFICATE OF EXAMINATION**

Supervisor

Examiners

\_\_\_\_\_  
Dr. Blaine A. Chronik

\_\_\_\_\_  
Dr. Michael D. Noseworthy

Supervisory Committee

\_\_\_\_\_  
Dr. Eugene Wong

\_\_\_\_\_  
Dr. David S. Rosner

\_\_\_\_\_  
Dr. Paul A. Wiegert

\_\_\_\_\_  
Dr. Tamie L. Poepping

\_\_\_\_\_  
Dr. Charles A. McKenzie

\_\_\_\_\_  
Dr. Robert Lannigan

The thesis by

**Parisa Hudson**

entitled:

**Pushing the boundaries in gradient and shim design for MRI**

is accepted in partial fulfillment of the  
requirements for the degree of  
Doctor of Philosophy

\_\_\_\_\_  
Date

\_\_\_\_\_  
Chair of the Thesis Examination Board

# Abstract

High performance gradient and shim coils are highly interested for high-field magnetic resonance imaging and spectroscopy to correct for large  $B_0$  inhomogeneities created by the magnetic susceptibility differences between tissues, bone, and air. In chapter two, complete sets of high-performance gradient and shim coils are designed using two different methods: the minimum inductance and the minimum power target field methods. A quantitative comparison of shim performance in terms of merit of inductance,  $ML$ , and merit of resistance,  $MR$ , is made for shim coils designed using the minimum inductance and the minimum power design algorithms. The coils designed using the target field method are not controlled over the length of the coil. In order to produce realistic coils for use in human or small-animal studies, direct control over the length of the coils is necessary. Therefore in chapter three, an extended Fourier series method for the design of shim coils with predetermined length is presented. This simple method is based on a truncated Fourier series expansion of the current density to allow for explicit control over the coil length. This method is mathematically simple, easy to implement and computationally fast. Also a quantitative comparison of figures of merit for inductance and resistance is made as a function of shim coil length. Coils of 40 cm diameter are designed with lengths of 50 cm, 60 cm, 80 cm, and 100 cm.

Pushing the boundaries of shim design in MRI, we designed a region specific, custom shim coil to correct for large field inhomogeneities that are consistent among subjects. In chapter four, we have designed a custom shim coil for the medial temporal lobe of the human head to correct for the significant field inhomogeneities caused by magnetic susceptibility differences at air/tissue interfaces. The custom coil was designed using the boundary element method. This method is capable of designing coils wound on arbitrarily shaped surfaces so as to produce specific field shapes. We propose that, the addition of this custom coil to the MRI systems can improve the field inhomogeneities significantly. A systematic displacement of head within the custom coil is also presented in this chapter as a method of investigating the sensitivity of the customized shim coil to small differences in subject positioning.

**Keywords:** Magnetic Resonance Imaging, Shim Coil, Gradient Coil, Minimum Inductance, Minimum Power, Target Field Method, Fourier Series Method, Boundary Element Method, Magnetic Resonance Spectroscopy

# **Co-Authorship Statement**

This thesis contains material from published journal articles co-authored by Parisa Hudson, Stephen Hudson, William Handler, Timothy Scholl, and Blaine Chronik. Versions of the original journal Articles appeared in chapters 2 and 3 were written by Parisa Hudson.

# Acknowledgments

I express my appreciation to all those who have helped me academically and personally throughout this research. I express many thanks and appreciation to my supervisor, Blaine Chronik, for his guidance and insight throughout the completion of this Ph.D. project. Blaine has always given me valuable suggestions and comments to make this project successful.

Special thanks to William Handler who has been like a second supervisor to me. Will has been a great mentor and a wonderful adviser during this project. His assistance and knowledge has been invaluable to me during this work. Mr. Handler, I will never forget your kindness and support over the past five years.

I have been fortunate to work with wonderful colleges and friends over the course of this project. Many thanks to Tim Scholl, Jamu Alford, Chad Harris, Kyle Gilbert, Dustin Haw and Rebecca Feldman. It has been a great pleasure to work with such wonderful friends.

I would like to show my gratitude to Joe Gati and Martyn Klassen for providing the field maps and anatomical images for this project.

Lastly, I would like to thank my incredible husband who is been helping me and supporting throughout this Ph. D. project. Without him every step towards the completion of thesis would have been impossible. Steve, you have been shining in the darkest moments of my life.

# Table of Contents

CERTIFICATE OF EXAMINATION .....	ii
Abstract .....	iii
Co-Authorship Statement.....	v
Acknowledgments .....	vi
Table of Contents.....	vii
List of Tables.....	x
List of Figures.....	xi
List of Appendices .....	xvi
List of Abbreviations and Symbols .....	xvii
Chapter 1 .....	1
1 Introduction.....	1
1.1 A Brief History of Magnetic Resonance Imaging.....	1
1.1.1 The MRI Scanner.....	2
1.2 Magnetic Field Inhomogeneities.....	4
1.2.1 Imperfect Magnet and Magnetic Environment .....	5
1.2.2 Susceptibility-Induced Magnetic Field Inhomogeneities .....	5
1.2.3 Field Inhomogeneities in the Slice Select Direction.....	6
1.2.4 Field Inhomogeneities in the Plane of the Slice.....	6
1.3 Correcting the Field, Shimming.....	7
1.3.1 FID Shimming.....	7
1.3.2 Field Map-Based Shimming.....	8
1.3.3 z-Shimming .....	9
1.3.4 Dynamic Shimming.....	10



1.3.5	Local Passive Shimming.....	11
1.4	Spherical Harmonic.....	12
1.5	Designing Shim and Gradient Coils.....	15
1.5.1	Biot Savart Law.....	15
1.5.2	Coil Performance.....	16
1.5.3	Coils with Discrete Windings.....	17
1.5.3.1	Zonal Coils: Helmholtz and Maxwell Coils.....	18
1.5.3.2	Tesseral Coils: Golay Coil.....	19
1.5.4	Coils with Distributed Windings.....	20
1.5.4.1	Matrix Inversion Methods.....	21
1.5.4.2	Stream Function Method.....	22
1.5.4.3	Target Field Methods.....	24
1.5.4.4	Fourier Series Method: Finite Length Coil Design.....	25
1.5.4.5	The Boundary Element Method.....	26
1.6	Scope of This Thesis.....	26
1.7	References or Bibliography.....	27
Chapter 2	.....	32
2	Quantitative comparison of minimum inductance and minimum power algorithms for the design of shim coils for small animal imaging.....	32
2.1	Introduction.....	32
2.2	Theory.....	34
2.3	Methods.....	37
2.4	Results and Discussion.....	41
2.5	References or Bibliography.....	48
2.6	Appendix A.....	50
Chapter 3	.....	53

3 Finite-length shim coil design using a Fourier series minimum inductance and minimum power algorithm.....	53
3.1 Introduction.....	53
3.2 Theory.....	55
3.3 Methods .....	58
3.4 Results and Discussion .....	63
3.5 References or Bibliography .....	68
Chapter 4 .....	70
4 A novel custom shim coil designed for spectroscopy to correct the field inhomogeneities in the medial temporal lobe of the human brain .....	70
4.1 Introduction.....	70
4.2 Methods .....	72
4.3 Results and Discussion .....	77
4.4 Conclusions.....	84
4.5 References or Bibliography .....	85
4.6 Appendix B.....	87
Chapter 5 .....	94
5 Conclusions.....	94
5.1 Thesis Summary.....	94
5.2 Future Work.....	96
5.3 Final Conclusions.....	97
Letters of Permission .....	98
Curriculum Vitae .....	133

# List of Tables

Table 2.1 Performance values for ten shim axes designed using minimum inductance and minimum power algorithms. In every design case, the improvement in  $ML$  provided by the minimum inductance method is less than 10% of the value obtained using the minimum power method and the improvements in  $MR$  provided by the minimum power method are less than 15% of the values obtained using the minimum inductance method. The merit of inductance calculated with the discrete method agrees with the merit of inductance calculated with the continuous method within 3.5% in all cases. The difference between the merits of power calculated with the discrete and the continuous methods ranges between 10% and 30%. ..... 47

Table 3.1 Inductive merit,  $ML$ , values for all 28 distinct shim axis pairs designed using minimum inductance and minimum power algorithms. The differences in  $ML$  between the minimum inductance and minimum power designs were less than 6% in all cases. Across most shim axes, the 80 cm length designs had the highest inductive merit values. .... 66

Table 3.2 Resistive merit,  $MR$ , values for all 28 distinct shim axis pairs designed using minimum inductance and minimum power algorithms. The differences in  $MR$  between the minimum inductance and minimum power designs were less than 6% in all cases. Across all shim axes, the 80 cm length designs had the highest resistive merit values. .... 66

Table 4.1 Calculated standard deviations of the frequency inhomogeneities when no shim, system shims, and the simulated custom plus system shims were used for all three subjects. The addition of the custom shim improves the field inhomogeneities by up to 30%. .... 83

# List of Figures

Figure 1.1 A recent transverse <i>in vivo</i> T <sub>2</sub> -weighted MR image of a normal human wrist acquired by Uchiyama <i>et al.</i> is shown in a) and the first transverse MR image of a normal human wrist acquired by Hinshaw <i>et al.</i> is shown in b).	2
Figure 1.2 Schematic of an MRI scanner is shown with cut-away section including the principle components.	4
Figure 1.3 FID signals received from a) a well-shimmed sample and b) a poorly-shimmed sample.	8
Figure 1.4 An example of z-shimming by Yang <i>et al.</i> (29) shows axial gradient-echo images of brain. a) The first image is acquired with no compensation. b) The second image is acquired with a 20% slice refocusing gradient area offset and the third image is acquired with a 40% of slice refocusing gradient area offset, and (d) shows the sum of images (a), (b), and (c) which is an artifact free image.	10
Figure 1.5 Non-oblique-sliced DSU homogeneity improvement for selected slices in a 32-slice acquisition, a) shows the field maps acquired using static global FASTMAP and b) the field maps acquired using second-order dynamic shimming updating.	11
Figure 1.6 Residual magnetic field maps near auditory air cavities of a mouse are presented using a) no shim, b) a one-material (zirconium) passive shim and c) a two- material passive shim.	12
Figure 1.7 Plots of the spherical harmonics are shown up to 3rd order on the surface of a sphere. The equations for the spherical harmonics are given in spherical (r, $\theta$ , $\phi$ ) and Cartesian (x, y, z) coordinates.	14
Figure 1.8 The elemental form of Biot-Savart law is shown with $I d\mathbf{l}$ as the source of magnetic field and $d\mathbf{B}$ as the resulting field.	16
Figure 1.9 a) An arrangement of a Helmholtz coil is shown with two loops of wire arranged on an axis perpendicular to the plane of the loops, separated by a distance, $a$ , equal to the	

radius of the loop. b) The $z$ -component of the magnetic field is plotted as function of $z$ within the region of interest.....	18
Figure 1.10 a) An arrangement of a Maxwell coil is shown with two loops of wire separated by a distance $\sqrt{3}a$ and anti-parallel currents. b) the $z$ -component of the magnetic field is plotted as function of $z$ within the region of interest. ....	19
Figure 1.11 a) An arrangement of a Y coil is shown with coil spacing for optimal gradient uniformity. b) The $z$ -component of the magnetic field is plotted as function of $z$ within the region of interest.....	20
Figure 1.12 A plot of the stream function $S(z,0)$ , for $\phi = 0$ , for a transverse gradient coil is shown. The arcs position is then determined by finding the equally spaced contours of the stream function. The wire pattern of the coil is shown figure 1.13. ....	23
Figure 1.13 The wire pattern of a transverse gradient coil resulting by the stream function given by Eq. [1.21] is shown.....	24
Figure 2.1 The upper half ( $z > 0$ ) of the $Z^2$ wire pattern given by (a) minimum inductance and (b) minimum power methods. The bottom halves of the coils are mirror images of the top halves not shown in this figure. Minimum power designs tend to feature longer, less compact wire patterns than minimum inductance designs.....	38
Figure 2.2 The upper half ( $z > 0$ ) of the $X^2-Y^2$ wire pattern given by (a) minimum inductance and (b) minimum power methods. The bottom halves of the coils are mirror images of the top halves not shown in this figure. Minimum inductance designs tend to give more complex wire and more compact wire patterns than minimum power designs.....	40
Figure 2.3 a) Magnetic field profile for $Z^2$ , normalized to the edge of the region of interest, on the $z$ -axis (solid line). (b) Calculated magnetic field profile in the $x$ and $y$ directions for the $X^2-Y^2$ shim coil with a radius of $a = 0.1$ m. For the $Z^2$ coil, the field targets (circles) were specified over a region of $z = \pm 0.5a$ , the magnetic field profile meets the field targets within this region of interest. It can be seen that for this coil, quadratic behavior of the magnetic field continues well outside the region of interest. ....	41

Figure 2.4 One quadrant of the relative residual fields (top figures) and the absolute residual fields (bottom figures) in the  $xy$  plane for the  $X^2-Y^2$  shim coils designed using minimum inductance (a, c) and minimum power methods (b, d). Within the ROI and in the  $xy$  plane, the average relative residual fields are  $<2\%$  and the average absolute residual fields are  $<10^{-7}$  T when evaluated using both design methods. The magnetic fields produced by the coils designed using minimum power and minimum inductance methods were scaled to have the same efficiency (17 mT/ m<sup>2</sup>/A)..... 43

Figure 2.5 One quadrant of the relative residual fields (top figures) and the absolute residual fields (bottom figures) in the  $yz$  plane for the  $X^2-Y^2$  shim coils designed using minimum inductance (a, c) and minimum power methods (b, d). Within the ROI and in the  $yz$  plane, the average relative residual fields are  $<4\%$  and the average absolute residual fields are  $<10^{-6}$  T when evaluated using both design methods. The magnetic fields produced by the coils designed using minimum power and minimum inductance methods were scaled to have the same efficiency (17 mT/ m<sup>2</sup>/A). ..... 44

Figure 3.1 Half-wire-patterns for ten coils: X, Y, Z, XY,  $X^2-Y^2$ , YZ, XZ,  $Z^2$ ,  $Z^3$ , and  $Z^4$  at four different lengths given by minimum inductance and minimum resistance methods. All coils are symmetric about the cuts chosen. The minimum resistance designs tend to feature less oscillation with less number of loops than minimum inductance designs at the same coil length..... 61

Figure 3.2 The  $z$ -component of the magnetic field profile in the  $z-y$  plane ( $x = 0$ ) for a  $Z^2$  shim coil with a radius of  $a = 0.2$  m. The region shown is larger than the originally specified region of interest, and it can be seen that the quadratic behavior of the magnetic field continues well outside the region of interest..... 62

Figure 3.3 The  $z$ -component of the magnetic field profile in the  $x-y$  plane ( $z = 0$ ) for an XY shim coil with a radius of  $a = 0.2$  m. .... 63

Figure 3.4 The relative residual fields in the  $xy$  (a, b) and  $yz$  (c, d) planes for the 80 cm length XY shim coil designed using minimum inductance (left column; a, c) and minimum power methods (right column; b, d). The average relative residual fields within the ROI in the  $xy$

and $yz$ planes are less than 5% for both formulations, indicating that both produced comparable field uniformity.....	64
Figure 4.1 A schematic view of a custom coil with a diameter of 40 cm and the length of 30 cm is shown. The coil's region of interest has dimensions of 8 cm × 5 cm × 4 cm and is off centered. ....	73
Figure 4.2 A cylindrical surface mesh with 8300 elements, with a diameter of 40 cm, and a length of 30 cm was created using Comsol Multiphysics (Burlington, MA). ....	75
Figure 4.3 parts a), d) and g) show sagittal anatomical images and parts b), e) and h) show sagittal images of the unshimmed field inhomogeneity maps of all three subject heads respectively. The field map of each subject head was overlaid with the anatomical image and the results are shown in parts c), f), and i). For each subject the white rectangle, shown in parts c), f), and i) encompasses the hippocampi.....	78
Figure 4.4 The wire pattern of the coil is shown with 1 mm diameter wire and 60 windings. The inductance of the coil was calculated to be 960 $\mu$ H and the resistance of the coil was 1.65 $\Omega$ . ....	79
Figure 4.5 The $z$ -component of the magnetic field is shown along $x$ , $y$ and $z$ -axes, within the region of interest.....	80
Figure 4.6 Planar slices of the field inhomogeneity through the centre of the region of interest when a) no shims, b) simulated custom shim and the existing system shims were used. The simulated custom shim reduces the field inhomogeneity by a factor of 1.3 when added to the system shims as compared to that obtained using the shim system only.....	81
Figure 4.7 Parts a), b), and c) show the simulated histograms of the frequency inhomogeneities for three subjects. Each figure shows the histogram of the unshimmed frequency inhomogeneities, the residual frequency inhomogeneities after shimmed with the system shims and the residual frequency inhomogeneities after shimmed with the simulated custom plus system shims. In all three subjects the line-width of the histogram of frequency inhomogeneities decreases after the addition of the custom coil to the system. ....	82

Figure 4.8 The standard deviation of residual frequency inhomogeneities after shimmed with the simulated custom plus system shims was calculated for many misalignments of one subject's head within the custom coil. This figure shows that the misalignment of up to  $\pm 1$  cm could be tolerated in  $x$ -,  $y$ - and  $z$ - directions..... 83

Figure 4.9 The discretized current carrying surface is shown in a), the current element and the basis function  $f_n$  for the  $n^{\text{th}}$  node are shown in b), and the length,  $d_{ni}$ , and the width,  $e_{ni}$ , vectors of one of the triangles associated with the selected node are shown in c)..... 87



# List of Appendices

Appendix A ..... 50

Appendix B ..... 87

# List of Abbreviations and Symbols

MRI	magnetic resonance imaging
MRS	magnetic Resonance spectroscopy
RF	radio frequency
SNR	signal to noise ratio
FID	free induction decay
FASTMAP	fast automatic shimming technique by mapping along projections
RASTAMAP	robust automated shimming technique using arbitrary mapping acquisition parameters
FOV	field of view
DSU	dynamic shimming updating
BEM	boundary element method
ROI	region of interest
RMS	root mean squared
DC	direct current
fMRI	functional MRI
PCA	principle component analysis
$T_2$	spin-spin relaxation time
$TE$	echo time

$TR$	repetition time
$MR$	merit of resistance
$ML$	merit of inductance
$\eta$	efficiency
$L$	inductance
$R$	resistance
$P$	power
$M$	torque
$G$	gradient
$B$	magnetic field
$J$	current density
$S$	stream function
$U$	optimization functional for current
$\sigma$	standard deviation

# Chapter 1

## 1 Introduction

### 1.1 A Brief History of Magnetic Resonance Imaging

Magnetic Resonance Imaging has proven to be a powerful imaging technique for the visualization of internal structure of the body. It has the ability to create contrast between different soft tissues of the body, it possesses sensitivity to a broad range of tissue properties, and it allows for the early diagnosis of many diseases, in particular neurological, musculoskeletal, and cardiovascular diseases, and cancer.

Although several scientists like Larmor (1857-1942) (1), Isaac Rabi (1930's), Bloch and Purcell (1952) (2,3), and Damadian (1970's) (4) introduced some basic steps towards the development of magnetic resonance imaging, first *in vivo* cross-sectional magnetic resonance images of a finger were acquired by Mansfield and Maudsley (5) in 1973. In the late 1970's and early 1980's a number of groups of scientists and manufacturers showed promising results of MRI *in vivo*. The first commercial MR scanner in Europe (from Picker Ltd.) was installed in 1983 in the Department of Diagnostic Radiology at the University of Manchester Medical School (Professor I Isherwood & Professor B Pullen). Since then there has been an explosion of technology and science in the field and we have moved from crude noisy images to highly sophisticated measurements. Figure 1.1 shows a) a recent transverse *in vivo* T<sub>2</sub>-weighted MR image a normal human wrist acquired by Uchiyama *et al.* (6) and b) the first transverse MR image of a normal human wrist acquired by Hinshaw (7) *et al.* in 1977.

A modern MRI scanner is capable of providing exquisite anatomical detail as well as functional information in perfusion and diffusion studies of the brain. Two- and three-dimensional MR angiography provide a roadmap of vessels in any part of the body, together with the ability to obtain functional velocity profiling of blood flow. This non-invasive imaging modality with a virtually limitless future is continuing today to make further major advances in diagnosing diseases.

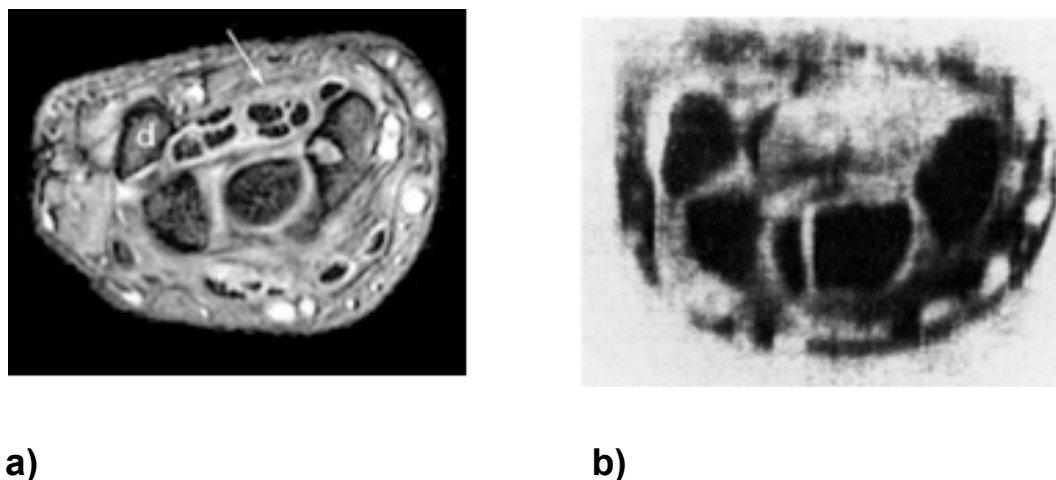


**Figure 1.1** A recent transverse *in vivo* T<sub>2</sub>-weighted MR image of a normal human wrist acquired by Uchiyama *et al.* is shown in a) and the first transverse MR image of a normal human wrist acquired by Hinshaw *et al.* is shown in b).

### 1.1.1 The MRI Scanner

An MRI scanner consists of four important subsystems: the main magnet, the shim coils, the gradient coils and the radio frequency (RF) coil. A schematic view of an MRI system is shown in figure 1.2. The major component of an MRI scanner is the main magnet. This magnet, which is the largest component, is used to create a constant and uniform magnetic field in the imaging region. Three kinds of magnets are available: resistive magnets, permanent magnets and super-conducting magnets. Resistive magnets (8) are composed of current carrying coils with the geometry that will generate a uniform magnetic field. This technology is limited in the achievable field strength due to the mass of conductor required to achieve high fields and is only used for low field systems.

Permanent magnets are constructed with ferromagnetic materials and do not require electricity to run. However, these magnets are limited to low magnetic field strength. Super-conducting magnets (9) are most commonly used clinically and are composed of super-conducting material, such as Niobium-Titanium (Nb<sub>3</sub>Ti). The super-conducting windings are immersed in liquid helium to reduce the temperature of the alloy to a level that makes them superconductive.

Shim coils (10) are located within the magnet bore and create magnetic fields in a variety of shapes to compensate for the field inhomogeneities in the magnetic field and make the field more uniform for imaging (This process is further explained in detail in this chapter). Shim coils may be super-conducting and/or room-temperature resistive coils of wire.

Gradient coils (10) are usually located inside the shim coils and are designed to produce linear magnetic field gradients in the imaging region, which collectively and sequentially are superimposed on the main magnetic field,  $B_0$ , for the selective spatial excitation of the imaging volume. There are typically three sets of gradient coils creating three orthogonal field gradients in the  $x$ -,  $y$ - and  $z$ -directions in conventional MRI coordinates. The gradient in the  $z$ -direction,  $G_z$ , is conventionally used in the slice selecting process. This gradient is defined as a slice select gradient that causes a linear variation in the resonant frequency in  $z$ -direction across the sample. When a slice is selected by irradiating the sample with an RF pulse, in the presence  $G_z$ , only a slice of finite thickness,  $\Delta z$ , is excited. The gradient in the  $x$ -direction,  $G_x$ , is conventionally used in the frequency encoding process. This gradient is perpendicular to the slice select gradient. This gradient applies a field gradient and causes a linear variation in the resonant frequency in  $x$ -direction in order to encode the  $x$ -position of the sample. The third gradient,  $G_y$ , is conventionally used in the phase encoding process. This gradient, which is perpendicular to  $G_x$  and  $G_z$ , is turned on before the frequency encoding gradient to encode the  $y$ -position via the phase of the signal.

The fourth component of an MRI system is the radio frequency (RF) coil (10), which is usually located inside the gradient coils. An RF coil creates a high frequency

electromagnetic field that excites the protons at their resonant frequency, and also detects the signal generated by the precessing spins after excitation. During the excitation, the slice thickness is determined by the spectral bandwidth of the RF pulse along with the strength of the gradient field. RF coils can be divided into three general categories: transmit and receive coils, receive only coils, and transmit only coils. Transmit and receive coils serve as the transmitter of the RF field and receiver of signals from the imaged object. A transmit only coil is used to create the magnetic field and a receive only coil is used in conjunction with the transmit coil to detect or receive signals from the imaged object.

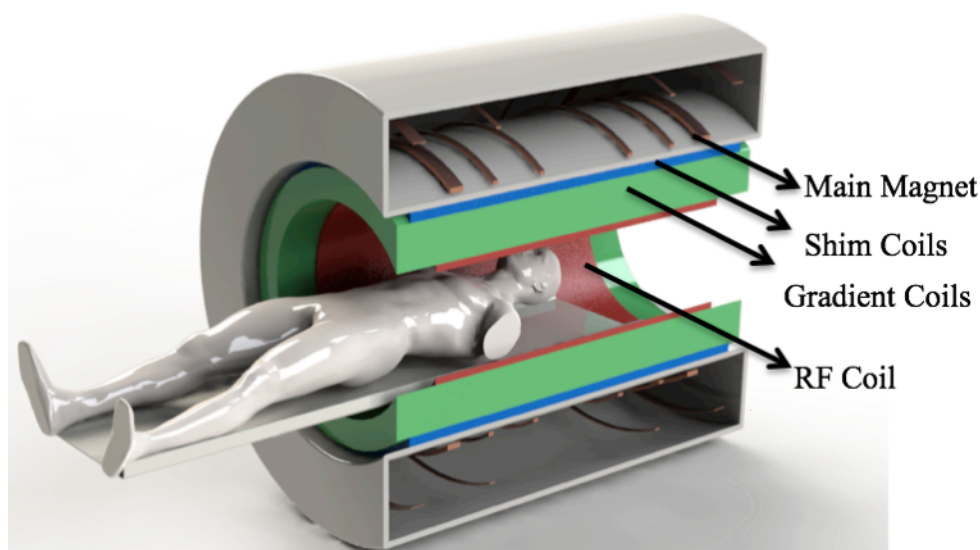


**Figure 1.2** Schematic of an MRI scanner is shown with cut-away section including the principle components.

## 1.2 Magnetic Field Inhomogeneities

The demand for making more powerful magnets to generate stronger magnetic fields is increasing. With increasing magnetic field strength, the signal to noise ratio (SNR) increases in MRI. This increase in field strength is accompanied by many technical challenges. One challenge is the requirement for the static magnetic field to be highly homogeneous. The fractional deviation of the main magnetic field from the

average value of the field is known as field inhomogeneities. The inhomogeneities of the static main magnetic field are caused by two major sources: the imperfect magnet and the magnetic environment, and the susceptibility of the imaging object.

### **1.2.1 Imperfect Magnet and Magnetic Environment**

In practice it is not possible to build a perfect magnet. Imperfections in the main magnet design and construction create field inhomogeneities that should be addressed. Ferromagnetic objects in the vicinity of the magnet, the metal impurities in gradient systems and magnet shielding around the scanner room also contributes to the creation of the field inhomogeneities. These field inhomogeneities are usually on the order of 100 parts per million (ppm) and are often corrected by placing magnetic materials close to the area that experiences large field inhomogeneities and allowing the field to be shimmed.

### **1.2.2 Susceptibility-Induced Magnetic Field Inhomogeneities**

The imaging objects such as a human subject, an animal or a device perturb the magnetic field due to their susceptibilities when placed in an MRI scanner. Such susceptibility induced field inhomogeneities have been simulated by several authors (11-13) and the field inhomogeneities have been shown to be sharper and stronger at boundaries between materials with different susceptibilities. The strength of the field inhomogeneities scales with the strength of the magnetic field. Thus at higher magnetic field, the field inhomogeneities generated at the interface of tissues of different magnetic susceptibilities are higher (14,15). These field inhomogeneities are usually a few parts per million (ppm).

The field inhomogeneities generated by the imperfect magnet and susceptibility of an imaging object are known as static field inhomogeneities, and cause signal loss and therefore image distortion. An image is distorted due to field inhomogeneities created in two directions: distortion due to field inhomogeneities in the slice selection direction,  $G'_z$  and distortion due to field inhomogeneities in plane of the slice,  $G'_x$  and  $G'_y$ .



### 1.2.3 Field Inhomogeneities in the Slice Select Direction

The effect of field inhomogeneities in the slice select direction,  $G'_z$  on the signal are found by looking at phase behavior. The equation for a signal received from a region of a sample at a time  $t$  (10) could be written as:

$$S(t) \propto \int \int \int \rho(r) e^{i\phi(t)} dx dy dz \quad (1.1)$$

where  $\rho(r)$  is the spin density and  $\phi(t)$  is the phase that could be written as:

$$\phi(t) = \gamma(\mathbf{G}(r) \cdot \mathbf{r})t. \quad (1.2)$$

$\mathbf{G}(r)$  is the field gradient. Without the effect of the field inhomogeneities:

$$\mathbf{G}(r) = G_x \mathbf{i} + G_y \mathbf{j} + G_z \mathbf{k}. \quad (1.3)$$

During the slice select process, the equation for signal is:

$$S(t) \propto \int \rho(r) e^{iG_z z t} dz \quad (1.4)$$

The presence of the field inhomogeneities in the slice select direction,  $G'_z$ , can cause misregistration of the signal as a function of slice location since the measured signal is now affected by  $G'_z$ :

$$S(t) \propto \int \rho(r) e^{i(G_z + G'_z) z t} dz \quad (1.5)$$

The addition of  $G'_z$  to  $G_z$  can also lead to a slice thickness different from the designed value because the slice thickness is inversely proportional to  $G_z + G'_z$ .

### 1.2.4 Field Inhomogeneities in the Plane of the Slice

Magnetic field gradients  $G_x$  and  $G_y$  are used to encode the MR signal spatially. The presence of field inhomogeneities along the  $x$ - and  $y$ - directions during the slice

select process could cause the excited plane to be rotated (10). During the phase encoding process this could cause slice distortion resulting in positional misregistration of the signal.

## 1.3 Correcting the Field, Shimming

Magnetic field inhomogeneities can be reduced using ferrosims and shim coils. Ferrosims are pieces of ferromagnetic materials placed in the bore of the magnet or areas that suffer from large field inhomogeneities so as to correct the inhomogeneities. This process is described in detail in section 1.3.4. Shim coils are resistive coils of wire carrying currents controlled by the user to minimize the field inhomogeneities. In section 1.4, various techniques that have been developed to design high performance shim coils are described. Several methods have been developed to reduce the field inhomogeneities by either using the ferrosims or shim coils.

### 1.3.1 FID Shimming

One way to correct for the field inhomogeneities is free induction decay shimming. The free induction decay signal coming from a sample is affected by the field inhomogeneities through the signal decay time,  $T_2^*$ . The increase in the field inhomogeneities, decreases  $T_2^*$  and therefore causes the FID signal to decay more quickly. Figure 1.3 shows two free-induction decay (FID) signals received from a) a well-shimmed sample and b) a poorly-shimmed sample. The shimming is performed by adjusting the currents in shim coils manually to minimize the rate of the signal decay (16,17). Automatic shimming (18-20) could be also performed by finding the shim currents that maximizes the time integral of the magnitude of the FID signal with a minimization algorithm such as the simplex algorithm. Since in this shimming method, the field inhomogeneities are not measured directly, this method is known as a blind shimming.

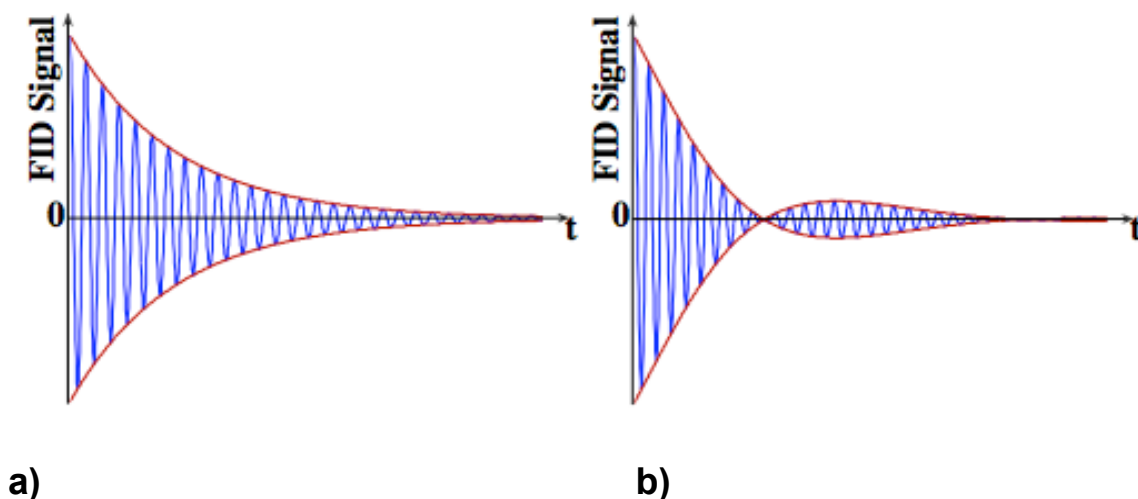


**Figure 1.3** FID signals received from a) a well-shimmed sample and b) a poorly-shimmed sample.

### 1.3.2 Field Map-Based Shimming

This method of shimming relies on the measurement of the field inhomogeneities that need to be shimmed. In this method, a 3D field generated by each shim coil is measured for a phantom at the center of the shim coils and a matrix describing all the shim fields,  $\mathbf{B}^{\text{shim}}$  is created (21). The optimal shim currents vector,  $\mathbf{I}$ , is obtained by multiplying the pseudo inverse,  $\dagger$ , of  $\mathbf{B}^{\text{shim}}$  with a vector of field values,  $\mathbf{b}$ , required to null the field inhomogeneities at each spatial position throughout the sample:

$$\mathbf{I} = \left(\mathbf{B}^{\text{shim}}\right)^{\dagger} \mathbf{b}. \quad (1.6)$$

To create  $\mathbf{B}^{\text{shim}}$ , chemical shift imaging (22,23) and phase mapping (24,25) techniques have been used. These techniques require long acquisition time and therefore are relatively slow. Fast automatic shimming technique by mapping along projections (FASTMAP) was developed by Gruetter (26,27) to offer a time efficient field mapping approach. In this method, the field inhomogeneities are measured along 6 ‘pencil-beam’

lines to give enough information for the determination of shim currents. However this method incorrectly assumes that shim coil fields are always fully characterized by a minimal set of spherical harmonics. Later, robust automated shimming technique using arbitrary mapping acquisition parameters (RASTAMAP) (28) was developed by using a fast, accurate, and flexible pulse sequence that can compensate for phase errors and generate absolute field maps regardless of the field of view (FOV) resolution, and acquisition geometry, making it ideally suited for automated shimming applications. In this method the shim fields are fitted to the field inhomogeneity map using linear least squares fitting in order to find the optimum current in each shim coil.

### 1.3.3 $z$ -Shimming

The presence of the field inhomogeneities in the slice select direction,  $G'_z$  could be eliminated by  $z$ -shimming (29). As mentioned in section 1.2.3, the gradient field in the slice direction could be separated into two terms;  $G_z$  and  $G'_z$ , where  $G_z$  is the gradient field generated by the slice select gradient and  $G'_z$  is the field inhomogeneities in the slice select direction. The effect of  $G'_z$  could be removed by applying a compensation gradient offset,  $G_c$  in time duration  $t_c$  such that:

$$G'_z t - G_c t_c = 0 \quad (1.7)$$

To perform the  $z$ -shimming technique, a normal image (figure 1.4a) with  $G_c = 0$  is acquired. This image shows large signal loss in the inferior frontal cortex and inferior lateral temporal regions. Two subsequent images (figures. 1.4b and 1.4c) were acquired with increasing compensation gradient,  $G_c t_c$ . Figures 1.4b and 1.4c show the enhancement in the signal only in regions where the field inhomogeneities are compensated by  $G_c$ . All three images were combined to obtain an artifact free image as shown in figure 1.4d.

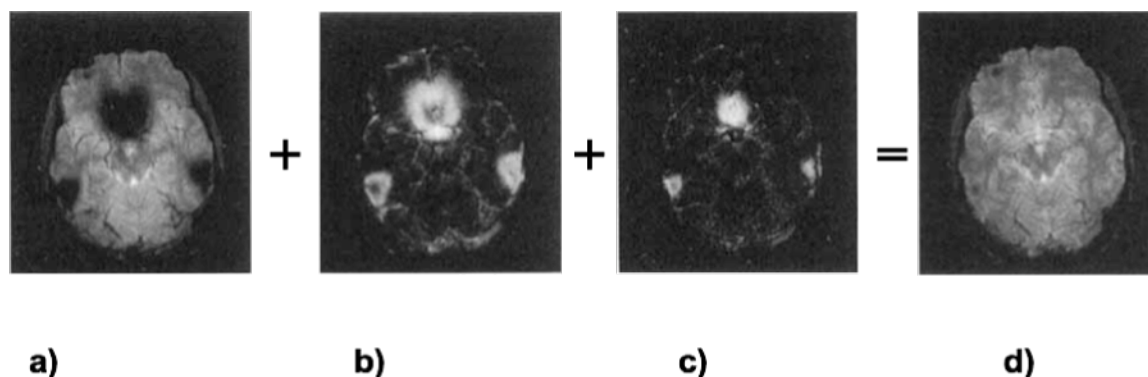


**Figure 1.4** An example of z-shimming by Yang *et al.* (29) shows axial gradient-echo images of brain. a) The first image is acquired with no compensation. b) The second image is acquired with a 20% slice refocusing gradient area offset and the third image is acquired with a 40% of slice refocusing gradient area offset, and (d) shows the sum of images (a), (b), and (c) which is an artifact free image.

### 1.3.4 Dynamic Shimming

Similar to field-map-based shimming, dynamic shimming updating (DSU) uses the linear least squares fitting to fit the shim fields with the field inhomogeneity map in order to find the optimum currents in shim coils. However in dynamic shimming the fitting is performed separately for each slice during a multi-slice imaging acquisition that allows for optimal local modeling and updating of shim currents for separate slices. This method of shimming removes the locally manageable field inhomogeneities in a global fashion. Figure 1.5 shows the field maps of brain for selected slices in a 32-slice acquisition after a) static global FASTMAP optimized shimming and b) second order dynamic shimming. As shown in the field maps, dynamic shimming significantly reduces the field inhomogeneities in frontal lobe as compared to FASTMAP shimming (30). The current in the shim coils needs to be switched rapidly during dynamic shimming. Therefore the shim coils required for performing dynamic shimming should be designed with low inductance to allow for shorter switching time. To limit the effect of the eddy currents, (the currents in the bore of the scanner induced by a time varying

magnetic field that is generated during switching currents in the shim coils) the shim coils may be actively shielded.

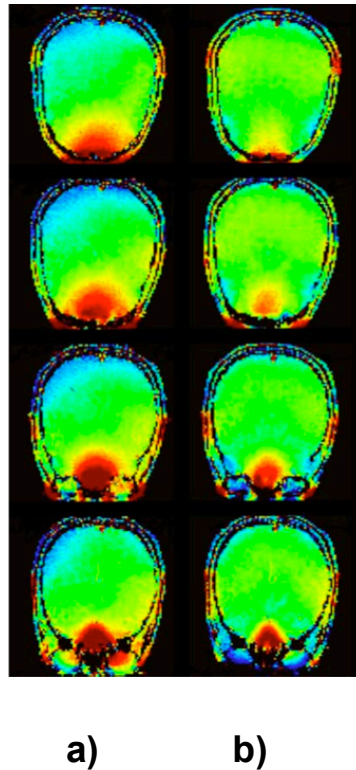


**Figure 1.5** Non-oblique-sliced DSU homogeneity improvement for selected slices in a 32-slice acquisition, a) shows the field maps acquired using static global FASTMAP and b) the field maps acquired using second-order dynamic shimming updating.

### 1.3.5 Local Passive Shimming

Paramagnetic, ferromagnetic or diamagnetic materials could be located near the areas suffering from large field inhomogeneities to locally shim the susceptibility induced field inhomogeneities. It has been shown that the static field inhomogeneities in the inferior frontal cortex of human brain are significantly reduced by placing a small amount of strongly diamagnetic material (Highly oriented pyrolytic graphite) in the roof of the mouth (31).

Similarly, Koch *et al.* (32) have shown that a prototype shim comprised of both diamagnetic (bismuth) and paramagnetic (zirconium) materials improve the field inhomogeneities significantly in a mouse brain. Figure 1.6 shows an example of the residual field maps when a) no shimming, b) one material passive shimming and c) two-material passive shimming were performed.

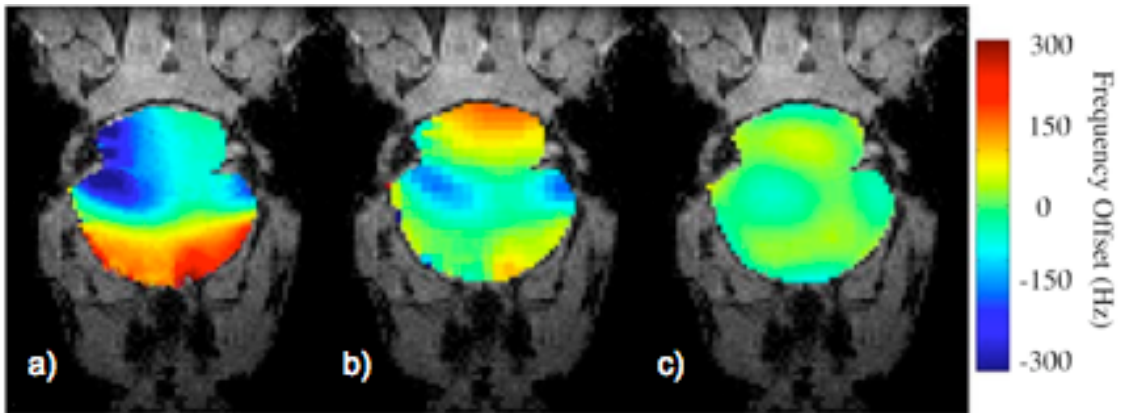


**Figure 1.6** Residual magnetic field maps near auditory air cavities of a mouse are presented using a) no shim, b) a one-material (zirconium) passive shim and c) a two-material passive shim.

## 1.4 Spherical Harmonic

In regions of space with free sources of current density,  $\mathbf{J}$ , the Maxwell equations that govern the magnetic field are simplified to (36):

$$\nabla \times \mathbf{B} = \mathbf{0} \quad (1.8)$$

$$\nabla \cdot \mathbf{B} = 0 \quad (1.9)$$

Using the vector identity  $\nabla \times \nabla \times \mathbf{B} = \nabla(\nabla \cdot \mathbf{B}) - \nabla^2 \mathbf{B}$ , Eqs. [1.8] and [1.9], Laplace's equation is derived:

$$\nabla^2 \mathbf{B} = \mathbf{0}. \quad (1.10)$$

If only the  $z$ -component of the magnetic field is considered, Laplace's equation could be simplified to:

$$\nabla^2 B_z = 0. \quad (1.11)$$

The general solution of Laplace's equation in spherical coordinates is a linear combination of spherical harmonic functions (36):

$$B_z(\mathbf{r}) = \sum_{n=0}^{\infty} \sum_{m=-n}^n C_n^m r^n P_n^m(\cos\theta) e^{im\phi} \quad (1.12)$$

where  $P_n^m$  are Legendre polynomials with positive integer order  $n$  and positive integer degree  $m \leq n$ .  $C_n^m$  is the amount of the  $n^{\text{th}}$  order,  $m^{\text{th}}$  degree spherical harmonic present in  $B_z(\mathbf{r})$ . Figure 1.7 shows all the 0<sup>th</sup>, 1<sup>st</sup>, 2<sup>nd</sup> and 3<sup>rd</sup> order spherical harmonic functions plotted on the surface of a sphere. The order, degree, name, and the equations in spherical and Cartesian coordinates of each harmonic are given next to the plot.



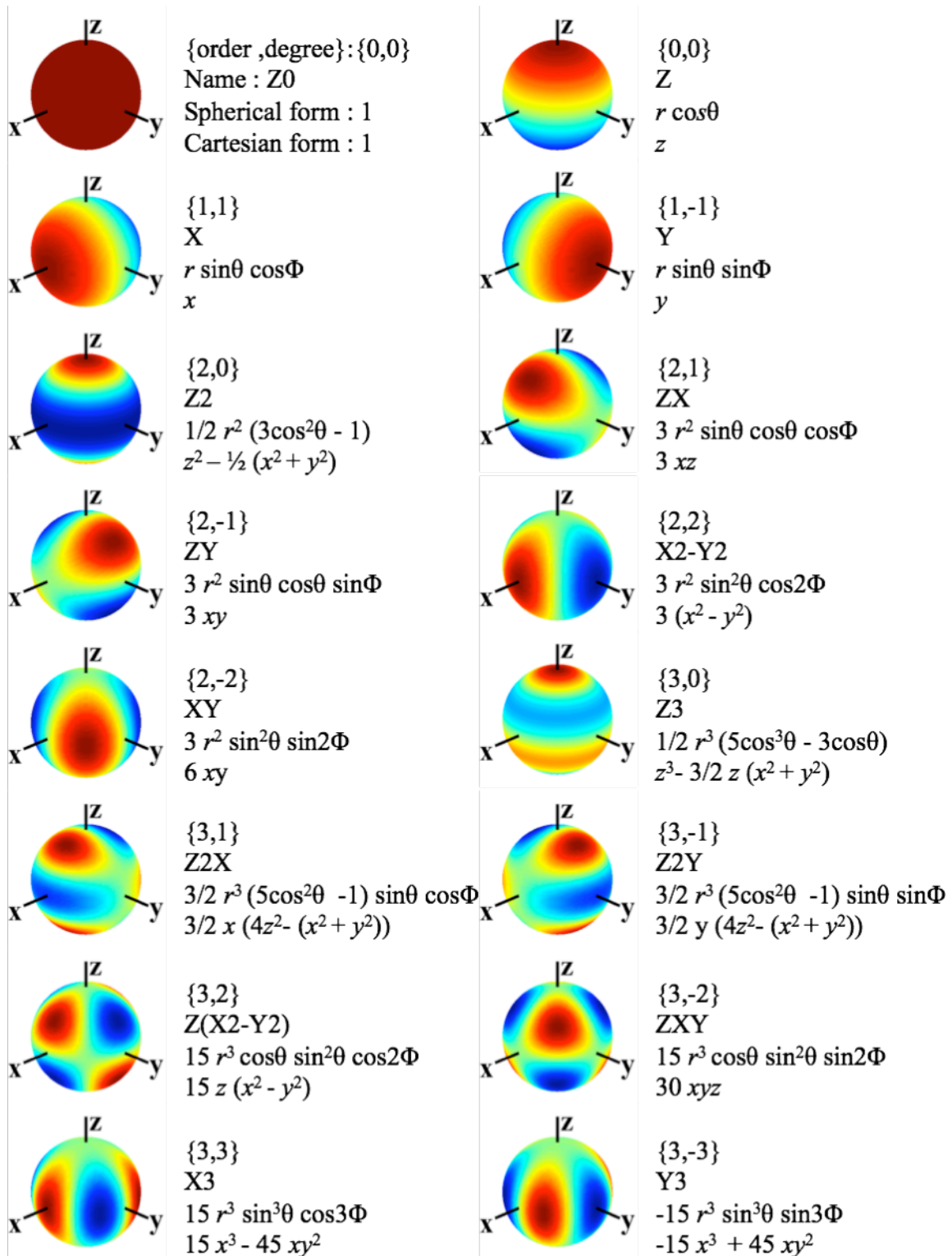


**Figure 1.7** Plots of the spherical harmonics are shown up to 3rd order on the surface of a sphere. The equations for the spherical harmonics are given in spherical ( $r, \theta, \phi$ ) and Cartesian ( $x, y, z$ ) coordinates.

Since the magnetic field vector can be described by spherical harmonic functions, the deviation from homogeneities can also be expressed on that basis. Active shimming capitalizes on this principle by using a set of shim coils, each generating one component of magnetic field that correspond to one spherical harmonic. These coils minimize the magnetic field inhomogeneities by superimposing a shim field with the same special distribution and magnitude but opposite sign to inhomogeneities.

## 1.5 Designing Shim and Gradient Coils

With a serious need for better quality gradient and shim coils, various methods have been developed to design these current-carrying coils of wire to generate magnetic field whose axial component is in shape of a spherical harmonic. These methods are categorized under the discrete windings method and the distributed windings method.

### 1.5.1 Biot Savart Law

One of the most fundamental equations used in coil design is the Biot-Savart law. Using this equation, the elemental magnetic field  $d\mathbf{B}(\mathbf{r})$  generated by a current  $I$ , through a wire element of length  $d\mathbf{l}$  could be written as (37):

$$d\mathbf{B} = \frac{\mu_0 I d\mathbf{l} \times \mathbf{r}}{4\pi r^3} \quad (1.13)$$

where  $\mathbf{r}$  is the distance between the point at which the magnetic field is calculated and the wire element and  $r$  is the magnitude of vector  $\mathbf{r}$  as shown in figure 1.8. The total magnetic field produced by a coil is calculated by integration of Eq. [1.13] over the whole circuit.

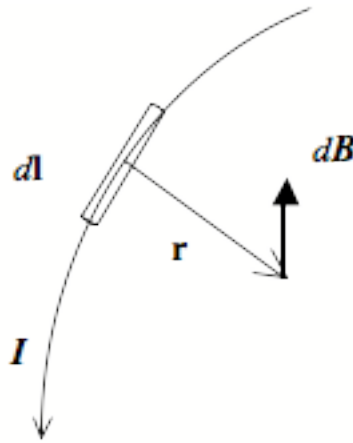


**Figure 1.8** The elemental form of Biot-Savart law is shown with  $I dl$  as the source of magnetic field and  $d\mathbf{B}$  as the resulting field.

## 1.5.2 Coil Performance

The performance of a coil depends on the application for which it is used. This includes the efficiency of the coil, the field uniformity, the inductance, the resistance, the torque, and the figure of merits.

The efficiency,  $\eta$ , of a coil is defined as the amount of spherical harmonic magnetic field generated by the coil per unit current and has the unit of  $\text{Tm}^{-n}\text{A}^{-1}$ , where  $n$  is the order of the spherical harmonic generated by the coil. The accuracy with which the desired magnetic field is generated by the coil could be defined as the field uniformity. To characterize the field uniformity, the relative field residual defined as the percent difference between the actual field and the assumed ideal shape of the field in the region of interest could be calculated.

The inductance,  $L$ , the resistance,  $R$ , and the torque,  $M$ , of a coil govern the speed at which the current can be switched in the coil, the amount of power dissipated in the

coil, and the amount of the torque that coil experiences in an intense static magnetic field respectively.

Inductive and resistive merits suggested by Turner (38) are used for comparing the performance of the gradient and shim coils. These two quantities defined such that they are independent of the number of turns of wire used in the coil.

The inductive merit is defined as:

$$ML = \frac{\eta}{\sqrt{L}} \quad (1.14)$$

and resistive merit for a rectangular wire is defined as:

$$MR = \frac{\eta}{\sqrt{R}}. \quad (1.15)$$

### 1.5.3 Coils with Discrete Windings

Gradient and shim coils were originally designed using the discrete winding method. Taylor expansion was widely employed in the design of coils with discrete paths. Later, by expanding the magnetic field in spherical harmonics (39), spherical harmonic generating coils were designed. This process involved the annulment of the unwanted harmonics so as to leave the desired harmonics as the dominant form of field variation. The annulment was done by placing the loops of wire at a specified position such that the harmonic with lower order and higher order than that of the desired harmonic was annulled. Zonal spherical harmonic generating coils (those with no  $\phi$  dependence,  $m = 0$ ) were designed by placing loops of wire placed symmetrically (or anti-symmetrically) about  $z = 0$  to generate only even (or odd) zonal harmonics. Tesseral ( $m = 0$ ) and sectoral ( $m = n$ ) harmonic generating coils were designed by placing arcs of wire on a cylindrical surface and changing the angular length of the arcs

and their  $z$ -positions to dictate the degree,  $m$ , of the harmonics and annuls lower and some higher remaining unwanted harmonics.

### 1.5.3.1 Zonal Coils: Helmholtz and Maxwell Coils

Helmholtz and Maxwell coils are designed by only keeping the zonal spherical harmonic (those with no  $\phi$  dependence,  $m = 0$ ) expansion (39) of the magnetic field. A Helmholtz coil with  $m = 0$  and  $n = 0$  consists of two coaxial circular loops separated by a distance  $a$ , equal to the radius of loops. This coil generates a uniform magnetic field at center of the coil and is used to operate as Z0 shim coil within the MRI systems. Using this coil, a magnetic field with deviation of up to 5% is obtained within a sphere of radius  $0.5a$ . Figure 1.9 shows a) the Helmholtz coil arrangement and b) the  $z$ -component of the magnetic field as function of  $z$ , within the region of interest.

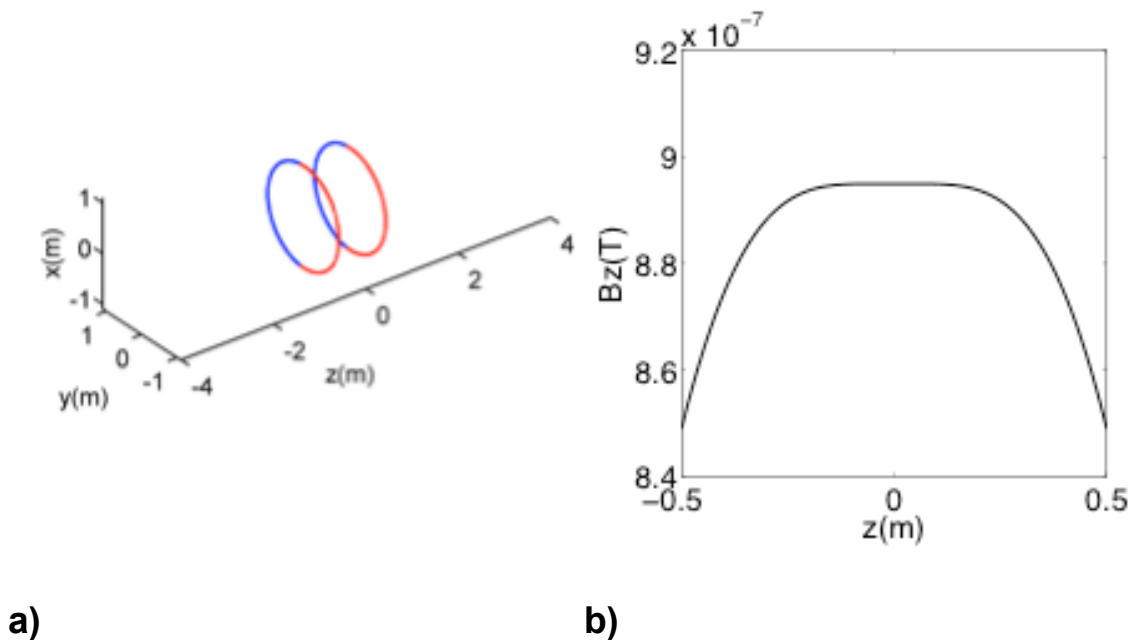


**Figure 1.9** a) An arrangement of a Helmholtz coil is shown with two loops of wire arranged on an axis perpendicular to the plane of the loops, separated by a distance,  $a$ , equal to the radius of the loop. b) The  $z$ -component of the magnetic field is plotted as function of  $z$  within the region of interest.

A Maxwell coil with  $m = 0$  and  $n = 1$ , also consists of two circular loops but with the loop separation of  $\sqrt{3} a$ , and currents flowing in reverse directions in the loops (39), such that a magnetic field varying linearly with  $z$  is produced. This coil could be operated as a Z gradient coil within an MRI system. Similar to a Helmholtz coil, this coil also generates a magnetic field with deviation of up to 5% within a sphere of radius  $0.5a$ . An arrangement of a Maxwell coil is shown in figure 1.10a and the  $z$ -component of the magnetic field as a function of  $z$  within the region of interest is shown in 1.10b.

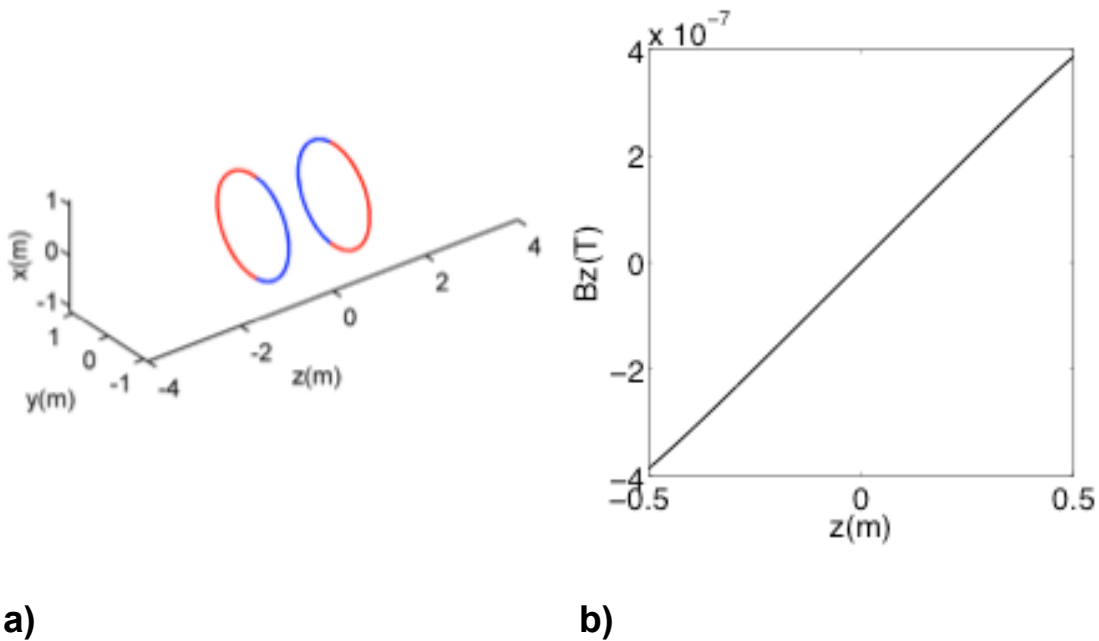


**Figure 1.10** a) An arrangement of a Maxwell coil is shown with two loops of wire separated by a distance  $\sqrt{3}a$  and anti-parallel currents. b) the  $z$ -component of the magnetic field is plotted as function of  $z$  within the region of interest.

### 1.5.3.2 Tesseral Coils: Golay Coil

A Golay or double-saddle coil (40) that generates the first order and the first degree ( $m = n = 1$ ) spherical harmonics shaped magnetic field is designed by placing the arcs of wire on a cylindrical surface as building blocks. This coil operates as an X or Y gradient coil within MRI systems. Figure 1.11 shows a) a Y gradient coil designed by

placing  $120^\circ$  circular arcs of current with opposite sense at appropriate  $z$  positions. The  $z$  component of the magnetic field as function of  $y$  is shown in b).

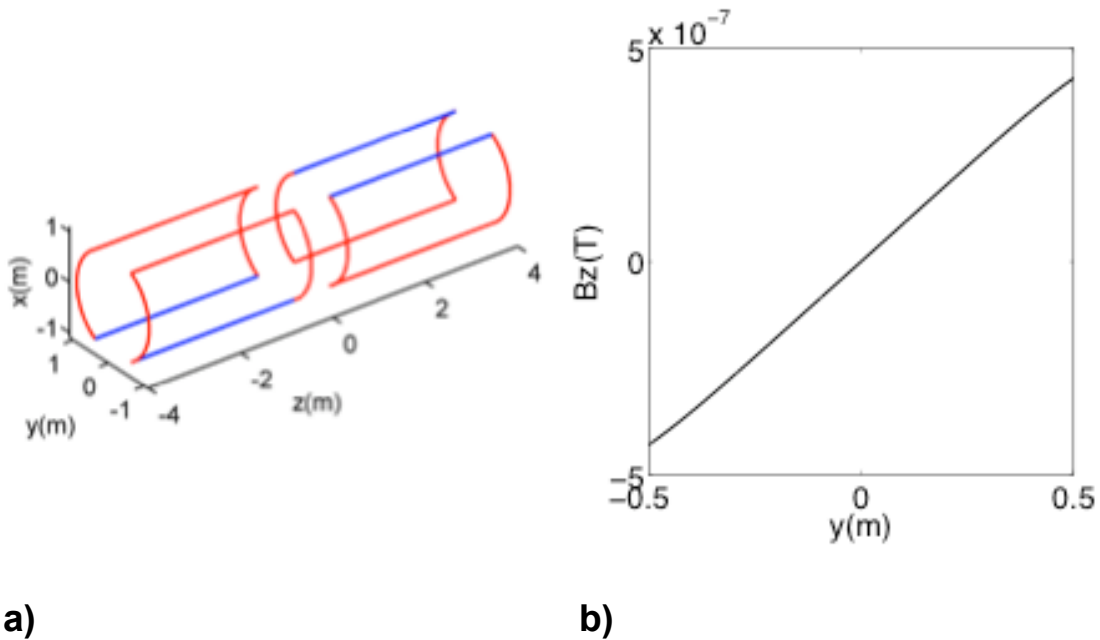


**Figure 1.11 a)** An arrangement of a Y coil is shown with coil spacing for optimal gradient uniformity. **b)** The  $z$ -component of the magnetic field is plotted as function of  $z$  within the region of interest.

In order to achieve high magnetic field intensity, many loops of wire should be used with the discrete design and using many number of loops forces the loops to be positioned farther from the correct location and therefore introduces field errors. Furthermore the inductance of such coils is higher, since the loops are close together.

### 1.5.4 Coils with Distributed Windings

Coils with distributed windings are designed with a continuous varying current density on formers of cylindrical shells, planes or arbitrary surfaces to have higher efficiency and lower inductance. Several methods for designing coils with distributed windings have been developed. These methods include matrix inversion techniques,

stream function methods, target field methods, the Fourier series method and the boundary element methods.

### 1.5.4.1 Matrix Inversion Methods

This method relies on the expansion of the magnetic field to find the optimal current flowing on surface of the coil. In 1997 Holt (41) suggested that the axial component of the magnetic field generated by a coil could be written as:

$$B_z = \sum_{n=1}^N A_{mn} I_n \quad (1.16)$$

where:

$$A_{mn} = \frac{\mu_0 a^2}{2 \left[ (z_m - z_n)^2 + a^2 \right]^{3/2}} \quad (1.17)$$

is a matrix that relates the axial component of the field at point  $z_m$  on the axis to the current  $I_n$  flowing in the  $n^{\text{th}}$  circular loop located at a position  $z_n$  of a solenoid of radius  $a$ . To find a set of currents at  $N$  positions, the matrix  $A_{mn}$  is inverted. The major weakness of this method is that the field could be specified in such a way the matrix becomes singular. Further improvements were made by Compton (42) who introduced a predetermined error by departing the magnetic field created by the coil from the desired field. In this method, the surface of the coil was divided into 2048 equally sized elementary areas and similar to Holt's approach the axial component of the magnetic field at position  $k$  can be written:

$$B_{zk} = \sum_{j=1}^n A_{kj} I_j \quad (1.18)$$

where  $A_{kj}$  is a matrix for which each entry is the coefficient of the magnetic field at the point  $a$  resulting from a current  $I_j$  at a differential surface element  $j$ . By subtracting this field from desired field,  $B_{zk}^0$ :



$$E_k = B_{zk}^0 - B_{zk} = B_{zk}^0 - \sum_{j=1}^n A_{kj} I_j \quad (1.19)$$

and minimizing  $\sum_{k=1}^{\text{vol}} E_k^2$  with respect to the current elements  $I_j$ , a set of  $n$  simultaneous equations is derived that could be solved by a matrix inversion method to find the surface current elements  $I_j$ . The wire pattern can be found by integrating over the elements of surface area until the current required for the coil in a discrete wire is accumulated. The transverse and longitudinal gradient coils designed using this method, create optimal field uniformity over the volume of the interest. However this method is computationally slow since a  $2048 \times 2048$  matrix is inverted. Furthermore inductance or power is not constrained in this method.

#### 1.5.4.2 Stream Function Method

The continuity equation for the current density,  $\nabla \cdot \mathbf{J} = 0$ , allows the current density to be described as the curl of a scalar function, the stream function,  $S(z, \phi)$ :

$$\mathbf{J} = \nabla \times S \hat{\mathbf{e}}_r \quad (1.20)$$

Various gradient coils with distributed windings have been designed by considering simple stream functions capable of generating gradient fields of the desired symmetry. In this method the stream function is used to represent a current flow. Since a special change in the value of the stream function corresponds to an equivalent change in the current density, the contour plots of  $S(z, \phi)$  gives the locations of the discrete wire carrying equal currents. By defining a proper stream function, a desired gradient field can be generated. To design a transverse gradient field, Edelstein *et al.* (43) defined a stream function expressed as:

$$\begin{aligned}
 S(z, \phi) &= \frac{I_0 z}{d} \cos \phi & |z| < d \\
 &= \frac{I_0 (c - z)}{(c - d)} \cos \phi & d < |z| < c \\
 &= 0 & \text{elsewhere}
 \end{aligned}
 \tag{1.21}$$

where  $I_0$  is the total current flowing in the coil,  $c$  and  $d$  are the parameters that could be adjusted to allow for some degree of optimization. For example, considering large values for  $c$  and  $d$ , results in a linear transverse gradient field over a large volume. Figure 1.12 shows the plot of the stream function for  $\phi = 0$  for Edelstein-type transverse gradient coil.

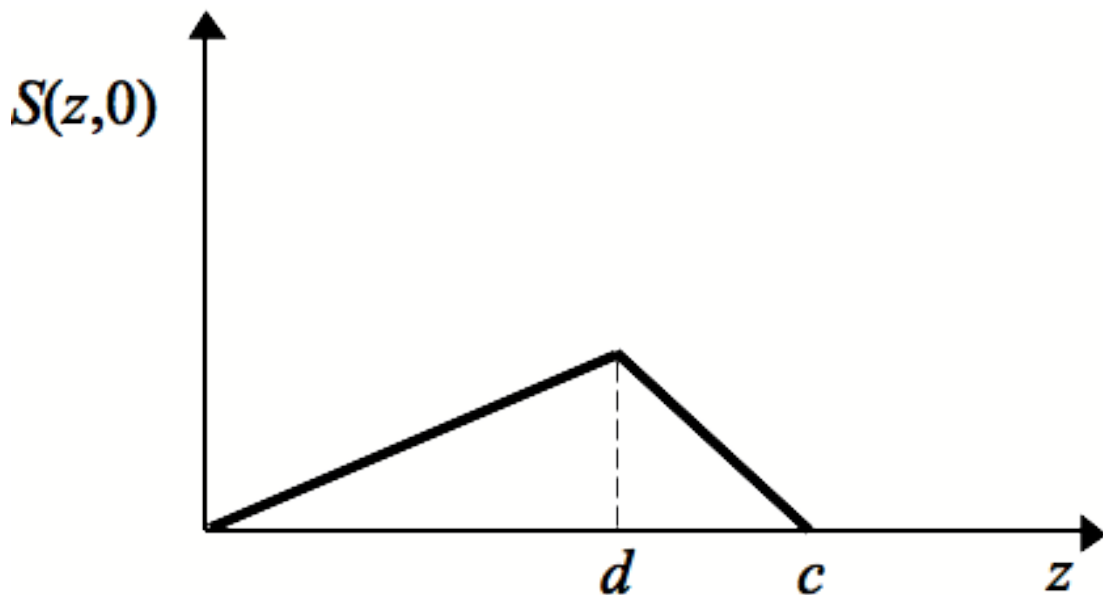


**Figure 1.12** A plot of the stream function  $S(z, 0)$ , for  $\phi = 0$ , for a transverse gradient coil is shown. The arcs position is then determined by finding the equally spaced contours of the stream function. The wire pattern of the coil is shown figure 1.13.

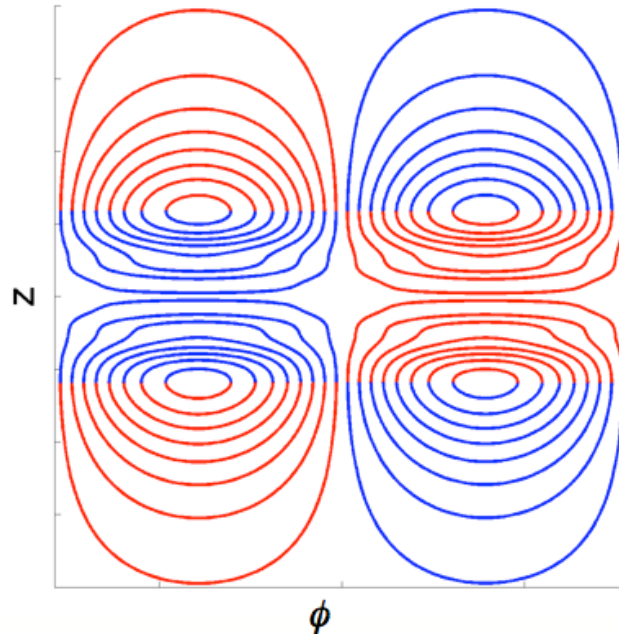


**Figure 1.13** The wire pattern of a transverse gradient coil resulting by the stream function given by Eq. [1.21] is shown.

Coils designed with the stream function method generally have a good efficiency, but the gradient homogeneity tends to be poor.

### 1.5.4.3 Target Field Methods

Turner developed the powerful target field method (44) that uses the expansion of the Green's function,  $\mathbf{G}(\mathbf{r}, \mathbf{r}') = \frac{1}{|\mathbf{r} - \mathbf{r}'|}$ , for the Laplacian, in cylindrical coordinates to relate the desired magnetic field to the current density on a cylindrical surface in the Fourier domain. The current density is then calculated from the desired fields in the Fourier domain. The stream function can be evaluated from the current density and the position of wires can be determined from the contours of the stream function. Further, Turner modified the target field (38) method by minimizing the coil inductance or power. A functional then was made of the deviation of the magnetic field from the desired target

fields and the inductance. This functional was then minimized to give the optimal current density. The complete mathematical derivation for the target field method is presented in chapter two where the minimum inductance design is compared with the minimum power design for a set of gradient and shim coils.

#### 1.5.4.4 Fourier Series Method: Finite Length Coil Design

The length of cylindrical or planar coils designed with the target field method is unbounded and could not be controlled. Chronik and Rutt (45) modified the target field method by constraining the extent of the current density. This method is computationally slow since a large number of current constraints are used to force the current density to remain contained within a finite length. For the design of gradient coils with finite length, Carlson *et al* (46) developed a Fourier series method. In their method, the current density is expanded as a sum of odd sinusoidal functions for the Z gradient coil:

$$\begin{aligned} j_{\phi}^m(\rho, z) &= \delta(\rho - a) \sum_{n=-N}^N \lambda_n \sin\left(\frac{n\pi z}{l}\right) & |z| \leq l \\ j_{\phi}^m(\rho, z) &= 0 & |z| > l \end{aligned} \quad (1.22)$$

and a sum of even sinusoidal functions for transverse gradient coils (X or Y coil):

$$\begin{aligned} j_{\phi}^m(\rho, z) &= \delta(\rho - a) \sum_{n=-N}^N \lambda_n \cos\left(\frac{n\pi z}{l}\right) & |z| \leq l \\ j_{\phi}^m(\rho, z) &= 0 & |z| > l \end{aligned} \quad (1.23)$$

In Eqs. [1.22] and [1.23],  $a$  is the radius of the coil,  $l$  is the length of the coil and  $\lambda_n$  are the unknown coefficients. Using a functional that includes the magnetic field, inductance, power or both, the optimal current density can be derived via  $\lambda_n$  while minimizing the inductance, the power or both. In chapter three this method is extended to design a set of shim coils by introducing a general 2D-Fourier series expansion of current density on the surface of a cylinder. The complete derivation for the Fourier series method is presented in chapter three.

#### 1.5.4.5 The Boundary Element Method

This method is capable of designing gradient and shim coils wound on an arbitrary surface. This method, which was first developed by Pissanetzky (47), relies on discretization of the current density into elements on a mesh. A functional was made of the magnetic field, the inductance and the torque and minimized to allow for finding the optimal discretized current density while minimizing the inductance and the torque. Further Pool and Bowtell (48) modified this method by adding a power term to the functional to also minimize the power dissipation in the coil. In chapter four, the complete derivation of the boundary element method for the design of region specific custom shim coils is presented.

### 1.6 Scope of This Thesis

In chapter two, the minimum inductance and minimum power target field methods are described, and the mathematical derivations for both are presented. A quantitative comparison of minimum inductance and the minimum power algorithms is made for the design of shim coils for small animal imaging.

As previously mentioned, Carlson *et al.* developed a Fourier series method to design gradient coils with finite length. In chapter three, the technique of Carlson is extended to design shim coils with finite length by introducing a general 3D Fourier series of the current density. Also a quantitative comparison of shim coils performance at four lengths: 50 cm, 60 cm, 80 cm, and 100 cm designed using minimum power and minimum inductance algorithms is made.

In chapter four, the boundary element method, which is capable of designing coils wounds on arbitrarily shaped surfaces is used so as to design region specific custom coils. In this chapter, a design of a custom shim coil for the medial temporal lobe of the human head is presented and used to correct for the significant field inhomogeneities caused by magnetic susceptibility differences at air/tissue interfaces.

## 1.7 References or Bibliography

1. Tubridy N, McKinsty CS. Neuroradiological history: Sir Joseph Larmor and the basis of MRI physics. *Neuroradiology* 2000;42(11):852-855.
2. Purcell EM, Torrey HC, Pouond RV. Resonance absorption by nuclear magnetic moments in a solid. *Phys Rev* 1946;69:37-38.
3. Bloch F. The Principle of Nuclear Induction. *Science* 1953;118(3068):425-430.
4. Kjelle MM. Raymond Damadian and the Development of MRI (Unlocking the Secrets of Science): Mitchell Lane Publishers; 2002. 48 pages p.
5. Mansfield P, Maudsley AA. Medical Imaging by NMR. *Br J Radiol* 1977;50(592):188-194.
6. Uchiyama S, Itsubo T, Yasutomi T, Nakagawa H, Kamimura M, Kato H. Quantitative MRI of the wrist and nerve conduction studies in patients with idiopathic carpal tunnel syndrome. *J Neurol Neurosurg Psychiatry* 2005;76(8):1103-1108.
7. Hinshaw WS, Bottomley PA, Holland GN. Radiographic thin-section image of the human wrist by nuclear magnetic resonance. *Nature* 1977;270(5639):722-723.
8. Hugon C, D'Amico F, Aubert G, Sakellariou D. Design of arbitrarily homogeneous permanent magnet systems for NMR and MRI: theory and experimental developments of a simple portable magnet. *J Magn Reson* 2010;205(1):75-85.
9. Wilson MN. *Superconducting Magnets*: Oxford University Press, USA; 1984. 352 p.
10. Haacke EM, Brown RW, Thompson MR, Venkatesan R. *Magnetic Resonance Imaging*: Wiley-Liss; 1999. 914 p.
11. Li S, Williams GD, Frisk TA, Arnold BW, Smith MB. A computer simulation of the static magnetic field distribution in the human head. *Magn Reson Med* 1995;34(2):268-275.

12. Bhagwandien R, van Ee R, Beersma R, Bakker CJ, Moerland MA, Lagendijk JJ. Numerical analysis of the magnetic field for arbitrary magnetic susceptibility distributions in 2D. *Magn Reson Imaging* 1992;10(2):299-313.
13. Bhagwandien R, Moerland MA, Bakker CJ, Beersma R, Lagendijk JJ. Numerical analysis of the magnetic field for arbitrary magnetic susceptibility distributions in 3D. *Magn Reson Imaging* 1994;12(1):101-107.
14. Truong TK, Clymer BD, Chakeres DW, Schmalbrock P. Three-dimensional numerical simulations of susceptibility-induced magnetic field inhomogeneities in the human head. *Magn Reson Imaging* 2002;20(10):759-770.
15. Shmueli K, Thomas DL, Ordidge RJ. Design, construction and evaluation of an anthropomorphic head phantom with realistic susceptibility artifacts. *J Magn Reson Imaging* 2007;26(1):202-207.
16. Conover W. *Practical Guide to Shimming Superconducting NMR Magnets*: John Wiley & Sons, Ltd; 1984.
17. Chmurnuy GN, Hoult DI. The Ancient and Honourable Art of Shimming. *Concept Magn Reson* 1990;2(3):131-149.
18. Ernst RR. Measurement and Control of Magnetic Field Homogeneity. *Review of Scientific Instruments* 1968;39(7):998-1012.
19. Tochtrop M, Vollmann W, Holz D, Leussler C. Automatic Shimming of Selected Volumes in Patients. *Proceedings of the Society for Magnetic Resonance in Medicine*. Volume 6; 1987. p 816.
20. Holz D, Jensen D, Proksa R, Tochtrop M, Wllmann W. Automatic Shimming For Localized Spectroscopy. *Med Phys* 1988;15(6):Medical Physics.
21. Prammer MG, Haselgrove JC, Shinnar M, Leigh JS. A New Approach to Automatic Shimming. *J Magn Reson* 1988;77:40-52.

22. Schneider E, Glover G. Rapid *in vivo* proton shimming. *Magn Reson Med* 1991;18:335-346.
23. Mackenzie IS, Robinson EM, Wells AN, Wood B, . A simple field map for shimming. *Magn Reson Med* 1987;5:262–268.
24. Jaffer FA, Wen H, Balaban RS, Wolff SD. A method to improve the B<sub>0</sub> homogeneity of the heart *in vivo*. *Magn Reson Med* 1996;36:375-383.
25. Kanayama S, Kuhara S, Satoh K. *In vivo* rapid magnetic field measurement and shimming using single scan differential phase mapping. *Magn Reson Med* 1996;36:637–642.
26. Gruetter R, Boesch C. Fast, Noniterative Shimming of Spatially Localized Signals. *In Vivo Analysis of the Magnetic Field along Axes*. *J Magn Reson* 1992;96: 323–334.
27. Gruetter R. Automatic, localized *in vivo* Adjustment of All First- and Second-Order Shim Coils. *Magn Reson Med* 1993;29(6):804-811.
28. Klassen LM, Menon RS. Robust Automated Shimming Technique Using Arbitrary Mapping Acquisition Parameters. *Magn Reson Med* 2004;51:881-887.
29. Yang QX, Dardzinski BJ, Li S, Eslinger PJ, Smith MB. Multi-Gradient Echo with Susceptibility Inhomogeneity Compensation (MGESIC): Demonstration of fMRI in the Olfactory Cortex at 3.0 T. *Magn Reson Med* 1997;37(3):331–335.
30. Koch KM, McIntyre S, Nixon TW, Rothman DL, de Graaf RA. Dynamic shim updating on the human brain. *J Magn Reson* 2006;180(2):286-296.
31. Koch KM, Rothman DL, de Graaf RA. Optimization of static magnetic field homogeneity in the human and animal brain *in vivo*. *Prog Nucl Magn Reson Spectrosc* 2009;54(2):69-96.
32. Koch KM, Brown PB, Rothman DL, de Graaf RA. Sample-specific diamagnetic and paramagnetic passive shimming. *J Magn Reson* 2006;182(1):66-74.



33. Chen N, Wyrwicz AM. Removal of intravoxel dephasing artifact in gradient-echo images using a field-map based RF refocusing technique. *Magn Reson Med* 1999;42(4):807-812.
34. Stenger VA, Boada FE, Noll DC. Multishot 3D slice-select tailored RF pulses for MRI. *Magn Reson Med* 2002;48(1):157-165.
35. Stenger VA, Boada FE, Noll DC. Variable-density spiral 3D tailored RF pulses. *Magn Reson Med* 2003;50(5):1100-1106.
36. Jackson JD. *Classical Electrodynamics*. New York: John Wiley & Sons; 1998.
37. Reitz JR, Milford FJ, Christy RW. *Foundation of electromagnetic Theory*. New York: Addison Wesley; 1989.
38. Turner R. Minimum inductance coils. *J Phys [E]* 1988;21:948-995.
39. Romeo F, Hoult DI. Magnet field profiling: analysis and correcting coil design. *Magn Reson Med* 1984;1(1):44-65.
40. Golay MJE; Magnetic Field control apparatus. US Patent. 1957.
41. Hoult DI. [Ph. D. Thesis]: Oxford Univeristy; 1977.
42. Compton RA; Gradient-coil apparatus for a magnetic resonance system. Us Patent. 1982.
43. Schenck JF, Hussein MA, Edelstein WA; Transverse gradient coils for nuclear magnetic resonance imaging. US Patent. 1983.
44. Turner R. A target field approach to optimal coil design. *J Phys [D]* 1986;19:L147-L151.
45. Chronik BA, Rutt BK. Constrained length minimum inductance gradient coil design. *Magn Reson Med* 1998;39(2):270-278.
46. Carlson JW, Derby KA, Hawryszko KC, Weideman M. Design and evaluation of shielded gradient coils. *Magn Reson Med* 1992;26(2):191-206.

47. Pissanetzky S. Minimum Energy MRI Gradient Coils of General Geometry. *Measurement Science and Technology* 1992;3(7):667–673.
48. Poole M, Bowtell R. Novel gradient coil designed using a boundary element method. *Concept Magn Reson [B]* 2007;31B:162-175

# Chapter 2

## 2 Quantitative comparison of minimum inductance and minimum power algorithms for the design of shim coils for small animal imaging

### 2.1 Introduction

A high-field clinical magnetic resonance imaging (MRI) scanner, such as a 3T scanner, has the potential to operate with a high signal-to-noise ratio (SNR), allowing the acquisition of high-quality magnetic resonance spectroscopy (MRS) data and high-resolution MR images, provided that the field inhomogeneities are well shimmed (1). At higher magnetic field, field inhomogeneities can be larger, resulting in phase and frequency instability in MRI signals and line broadening and frequency shifts in MRS (1,2). To correct the larger field inhomogeneities, gradient and shim coils with higher performance than those available in typical clinical MRI scanners are required. High-performance gradient and shim coils require low inductance,  $L$ , to allow short switching times, low resistance,  $R$ , to minimize power dissipation, and high efficiency,  $\eta$ , to produce the desired field (3). However, when designing high-performance coils, the

---

A version of this chapter has been published: Hudson P, Hudson SD, Handler WB, Scholl TJ, Chronik BA. Quantitative Comparison of Minimum Inductance and Minimum Power Algorithms for the Design of Shim Coils for Small Animal Imaging. Concepts Magn Reson Part B Magn Reson Eng 2010;37B(2):65-74

trade-offs between different coil characteristics should be considered. For example, minimum inductance coil designs allow faster switching speeds while minimum power coil designs optimize the power consumption.

A target-field approach for designing gradient coils was devised by Turner (4). His method relies on inverse Fourier transformations to determine a continuous current distribution, confined to flow on cylindrical shells or on planes, that yields the desired field. With this method, a functional that includes the deviation of the desired field from the calculated field over the region of interest (ROI) is formed. The current density in the reciprocal domain is found by minimizing the functional with respect to the current density. Turner further developed the target field method by adding inductance to the functional (5). This minimized the inductance while maintaining a specified field over the desired ROI.

Carlson *et al.* modified Turner's inductance minimization technique by expanding the current density as a sum of truncated sinusoidal functions, allowing the length of gradient coils to be constrained (6). Bowtell and Robyr allowed the current density to vary in the radial direction in addition to the axial and azimuthal directions, for the design of multilayer, cylindrical gradient coils (7). In their design algorithm, power and inductance of the coil were minimized simultaneously. Further developments were made by Forbes and Crozier in a series of papers (8-10), for the design of shielded zonal and tesseral shim coils on cylindrical and planar surfaces.

Poole and Bowtell applied the boundary element method to design gradient coils wound on arbitrarily shaped surfaces, by discretizing the current density into a mesh of triangles (11). The inductance, resistance, and torque were derived in terms of current density, allowing for a functional capable of simultaneously minimizing the square of the difference between the target field and the actual field, the stored energy, the power loss, and the torque exerted on the coils.

As mentioned, many methods have been developed for the design of gradient and shim coils. These methods are able to minimize properties such as power and inductance, allowing coils to be optimized for a variety of applications in MRI and MRS. In an

International Society of Magnetic Resonance in Medicine proceeding, Turner reported on the comparison of gradient coil performance for coils designed using the minimum inductance and minimum power methods (12). To the best of the authors' knowledge, no quantitative comparison of minimum inductance and minimum power design algorithms have been published for a shim coil set designed for small animal imaging.

In this paper, the method of Turner was applied to design high order shim sets containing ten independent axes. The shim sets were designed using both minimum inductance and minimum power algorithms, and a quantitative comparison was made between coil performances obtained with the two methods. These quantitative comparisons are critical first steps for the optimization of practical, high-power, high-order shim sets, designed for MRI and MRS applications in small animals.

## 2.2 Theory

For the design of the cylindrical shims used in MRI, the axial component of the magnetic field,  $B_z(\rho, \phi, z)$ , is of interest. For a current constrained to flow on a surface of a cylinder, only the azimuthal component of the current density,  $J_\phi(\phi, z)$ , contributes to the axial component of the magnetic field. Inside a coil of radius  $a$  (i.e. in the region where  $\rho < a$ ), the axial component of the magnetic field can be represented in terms of cylindrical harmonics (13,14):

$$B_z(\rho, \phi, z) = -\mu_0 a \sum_{m=-\infty}^{\infty} \int_{-\infty}^{\infty} dk e^{im\phi} e^{i2\pi kz} j_\phi^m(k) |k| I_m(|2\pi k \rho|) K'_m(|2\pi k a|) \quad (2.1)$$

where  $I_m$  and  $K'_m$  are the modified Bessel functions (15,16) and  $K'_m$  is the derivative of  $K_m$  which can be written:  $K'_m = \frac{-1}{2}(K_{m+1} + K_{m-1})$ . The Fourier transform of the azimuthal component of current density is given by:

$$j_\phi^m(k) = \int_{-\pi}^{\pi} d\phi e^{-im\phi} \int_{-\infty}^{\infty} dz e^{-i2\pi kz} J_\phi(\phi, z). \quad (2.2)$$

Our goal is to find an optimal current density,  $j_\phi^m(k)$ , in order to achieve a desired magnetic field in the region of interest (ROI), as well as to minimize some physical parameters of the coil (such as inductance or power dissipation). Considering these requirements, we introduce a functional,  $U\{j_\phi^m(k)\}$ , that consists of two terms:

$$U\{j_\phi^m(k)\} = Z\{j_\phi^m(k)\} + \sum_{n=1}^N \lambda_n [B_z(\rho_n, \phi_n, z_n) - B_{zn}] \quad (2.3)$$

where  $B_{zn}$  are the desired  $z$ -components of the magnetic field at the target points,  $N$  is the number of field targets,  $\lambda_n$  are the Lagrange multipliers (5), and  $Z$  is the physical characteristic of the coil that should be minimized. For example  $Z$  could be Power, Inductance or their combination.

In order to minimize a physical parameter of the coil, it must be expressed in terms of the current density. For designing coils with minimized inductance, inductance is represented in terms of the current distribution over the coil by (3,5):

$$L = \frac{-\mu_0 a^2}{2\pi I^2} \sum_{m=-\infty}^{\infty} \int_{-\infty}^{\infty} dk |j_\phi^m(k)|^2 I'_m(2\pi ka) K'_m(2\pi ka) \quad (2.4)$$

where  $I$  is the current required to produce the current surface density.

If minimum power designs are desired, power dissipation resulting from a current density flowing on the surface of a cylinder of thickness  $t$  and resistivity  $\rho$  can be expressed as (3,5):

$$P = \frac{\rho a}{2\pi t} \sum_{m=-\infty}^{\infty} \int_{-\infty}^{\infty} dk |j_\phi^m(k)|^2 \left( 1 + \frac{m^2}{(2\pi ka)^2} \right). \quad (2.5)$$

Since both inductance and power are quadratic in  $j_\phi^m(k)$  (Eqs. [2.4,2.5]), absolute minima of inductance and power are attainable. These minima, subject to the field constraints, are found when:

$$\frac{dU(j_\phi^m(k))}{dj_\phi^m(k)} = 0. \quad (2.6)$$

This gives an expression relating  $j_\phi^m(k)$  and  $\lambda$  which can be substituted back into Eq. [2.1], allowing  $B_z$  to be written in terms of  $\lambda$ . Substituting this expression for  $B_z$  into:

$$B_z(\rho_n, \phi_n, z_n) - B_{zn} = 0 \quad (2.7)$$

gives a set of linearly independent equations that can be assembled into a matrix equation and solved for the set of  $\{\lambda_n\}$  using singular value decomposition. The matrix has dimensions  $N \times N$ , where  $N$  is the number of field targets. Having the set of  $\{\lambda_n\}$ , current density can be derived over the surface of the coil via substitution. The complete derivation for the minimum inductance method has been shown by Turner (5) and Chronik et al. (17). The complete derivation for the minimum power method is presented in Appendix A.

Optimum accuracy of the magnetic field and the resistance would be achieved by building a coil with a continuous current density. In practice, it is only possible to build a coil that approximates the continuous current density. The current density was approximated with a finite set of current carrying loops. To determine the loop positions under the condition  $\nabla \cdot J = 0$ , we define a stream function,  $S(z)$ , that corresponds to the surface current density,  $J_\phi(\phi, z)$ , (18) as:

$$S(z) = \int_{-z}^z J_\phi(\phi, z') dz'. \quad (2.8)$$

The stream function is discretized into some contours using the contouring function of Matlab version 7.5 (The Mathworks, Inc., Natick, MD, USA). Contours were found at a fixed number of values (levels) of the stream function. The contours of the stream function are the discrete wire patterns that approximate the continuous current

density. Wires were positioned along the contours of the stream function and each contour represents one or more closed loops on the cylindrical surface of the coil (18).

## 2.3 Methods

The calculations and design algorithms were implemented in Matlab, version 7.5 (The Mathworks, Inc., Natick, MD, USA). The following ten separate gradient and shim axes were designed using both the minimum inductance and the minimum power methods: X, Y, Z, XY,  $X^2-Y^2$ , YZ, XZ,  $Z^2$ ,  $Z^3$ , and  $Z^4$ . For the remainder of this discussion, all of these will be referred to as shim coils (i.e., gradient coils will be considered as first order shims). All coils were designed with a radius of 10 cm.

For each axis, identical magnetic field constraints were used for both the minimum inductance and the minimum power methods. The magnetic field was specified at nine evenly spaced points, between  $z = \pm 0.5a$  where  $a$  is the radius of the coil, parallel to the  $z$ -axis. Increasing the number of field constraints over the same region increases both the accuracy of the field and the size of the region of uniformity, at the expense of coil efficiency. For zonal axes, the field targets were located on the  $z$ -axis, with the appropriate pure polynomial variation with  $z$ , and for tesseral axes, the field targets were offset from the  $z$ -axis by  $0.5a$  at an angle of zero radians. Using field targets at multiple radial locations did not significantly affect the design of tesseral coils. The current density of tesseral axes were found by limiting the expansion to have only the azimuthal order necessary for that shim; for the first order shims we included only  $m = \pm 1$  in the current density expansion, for the second order shims we included only  $m = \pm 2$ , etc (see Appendix A).



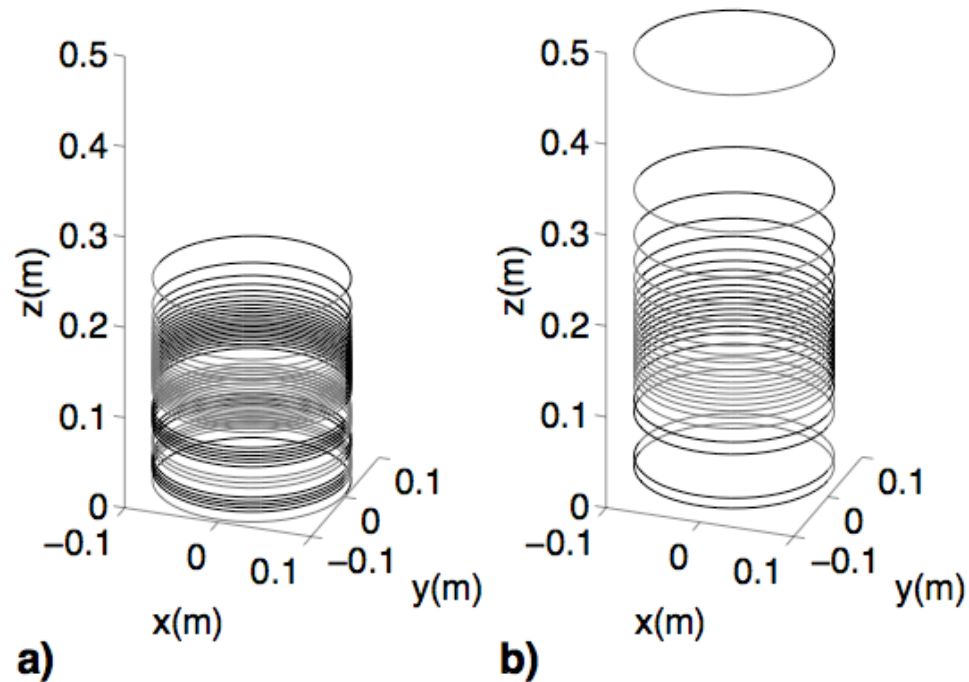


**Figure 2.1** The upper half ( $z > 0$ ) of the  $Z^2$  wire pattern given by (a) minimum inductance and (b) minimum power methods. The bottom halves of the coils are mirror images of the top halves not shown in this figure. Minimum power designs tend to feature longer, less compact wire patterns than minimum inductance designs.

The continuous current density was approximated as loops of current carrying wire. The location of wire was determined from contours of the stream function using the Matlab contouring function. Once the wire pattern was obtained, it was discretized into an array of elements characterized by their positions and lengths, each carrying current  $I$ . The magnetic field generated by each coil was calculated using the elemental Biot-Savart equation on the array of wire elements (14). For each coil, it was verified that the numerically calculated field met the field targets. Coils designed with the two methods were compared using inductive merit,  $ML$ , and resistive merit,  $MR$ .

Inductive and resistive merits were calculated with both discrete and continuous methods. For the discrete method, inductance was evaluated by applying the Neumann formula (13,14) to the wire element array.

Resistance was calculated by summing the resistances of the wire elements in the element array. In the case of rectangular wire, the radial thickness of the conducting layer used for coil fabrication was assumed to be constant and the width of the conducting path was assumed to be equal to the minimum spacing. The cross-sectional area of each wire element would then be the thickness multiplied by the minimum spacing. If round wire were considered, the cross sectional-area would be the area of a circle with a diameter equal to the minimum spacing.

Regardless of the cross-section of a discrete wire, efficiency varies linearly with the number of loops while inductance varies quadratically. Using this information, an equation for inductive merit independent of the number of loops was created. Inductive merit is defined as  $\frac{\eta}{L^{1/2}}$  where  $L$  is the coil inductance and  $\eta$  is the field efficiency of the coil (7).

In order to develop a figure of merit for resistance or power, the dependence of resistance on the number of loops must first be determined for the cases of rectangular and circular cross-section wires separately. The wire length increases linearly with the number of loops for both rectangular and round wires. The cross-sectional area of round wire ( $\pi$  multiplied by one-half the minimum spacing squared) is inversely proportional to the number of loops squared because the minimum spacing is proportional to the number of loops. Combining these two effects, the coil resistance ( $R$ ) for round wire is found to vary as the third power of the number of loops. For rectangular wire the thickness is held constant, and therefore the cross-sectional area (thickness multiplied by the minimum spacing) is inversely proportional to the number of loops. This causes the coil resistance for rectangular wire to vary with the number of loops. To obtain a resistive merit equation independent of the number of loops,  $MR$  was therefore defined as  $\frac{\eta}{R^{1/2}}$  for

rectangular wire and  $\frac{\eta}{R^{1/3}}$  for round wire (7). The coil radius is not included in the merit equations for this work because it was held constant for coils designed with both the minimum inductance and the minimum power methods.

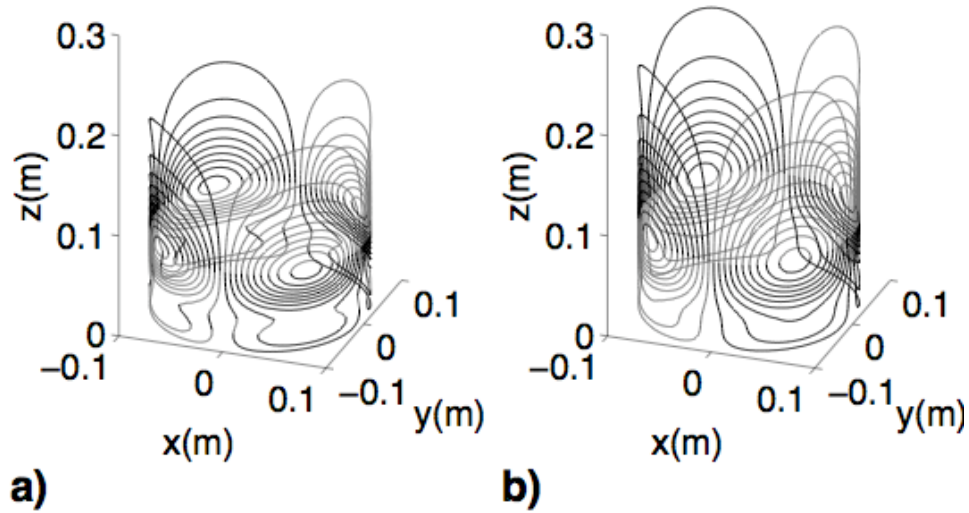


**Figure 2.2** The upper half ( $z > 0$ ) of the  $X^2-Y^2$  wire pattern given by (a) minimum inductance and (b) minimum power methods. The bottom halves of the coils are mirror images of the top halves not shown in this figure. Minimum inductance designs tend to give more complex wire and more compact wire patterns than minimum power designs.

For the continuous method, the continuous current density was directly substituted into equations for magnetic field, inductance, and power (3). As with the discrete method, mathematical functions were fit to the analytically calculated field in order to obtain the efficiencies of the individual shim coils.

$ML$  and  $MR$  were calculated for the minimum power and the minimum inductance designs with both discrete and continuous methods. Absolute field residuals, defined as the difference between the actual field and the assumed ideal shape of the field (i.e., the difference between the field created by the shim and the fitted field profile), were calculated inside a cylindrical volume with a radius of  $0.9a$  and a length of  $1.8a$  (approximately 6 times the volume of the ROI). Relative field residuals, defined as the

percent difference between the actual field and the assumed ideal shape of the field were also calculated in the same region. Relative field residuals were not calculated where the value of the ideal function used to describe the shape of the field was expected to be equal to zero. Both absolute and relative field residuals were calculated for all shim axes as a method of characterizing field uniformity.

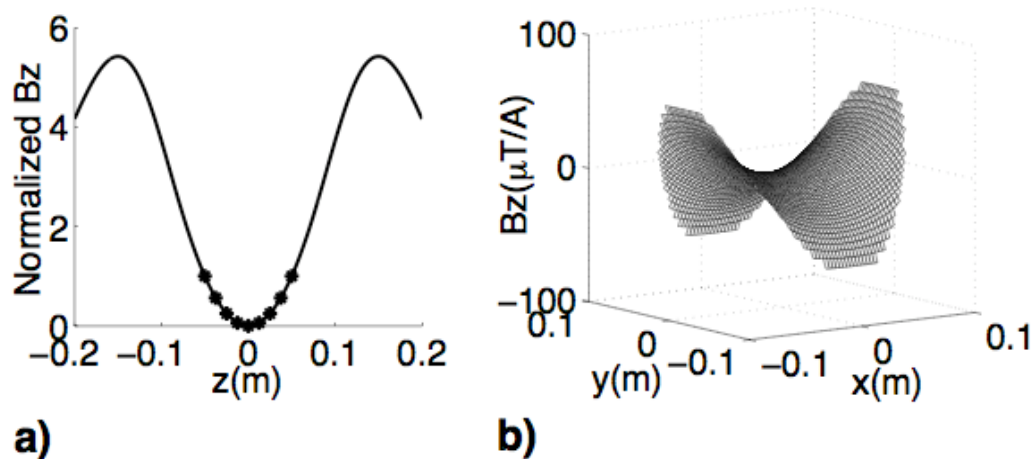


**Figure 2.3** a) Magnetic field profile for  $Z^2$ , normalized to the edge of the region of interest, on the  $z$ -axis (solid line). (b) Calculated magnetic field profile in the  $x$  and  $y$  directions for the  $X^2-Y^2$  shim coil with a radius of  $a = 0.1$  m. For the  $Z^2$  coil, the field targets (circles) were specified over a region of  $z = \pm 0.5a$ , the magnetic field profile meets the field targets within this region of interest. It can be seen that for this coil, quadratic behavior of the magnetic field continues well outside the region of interest.

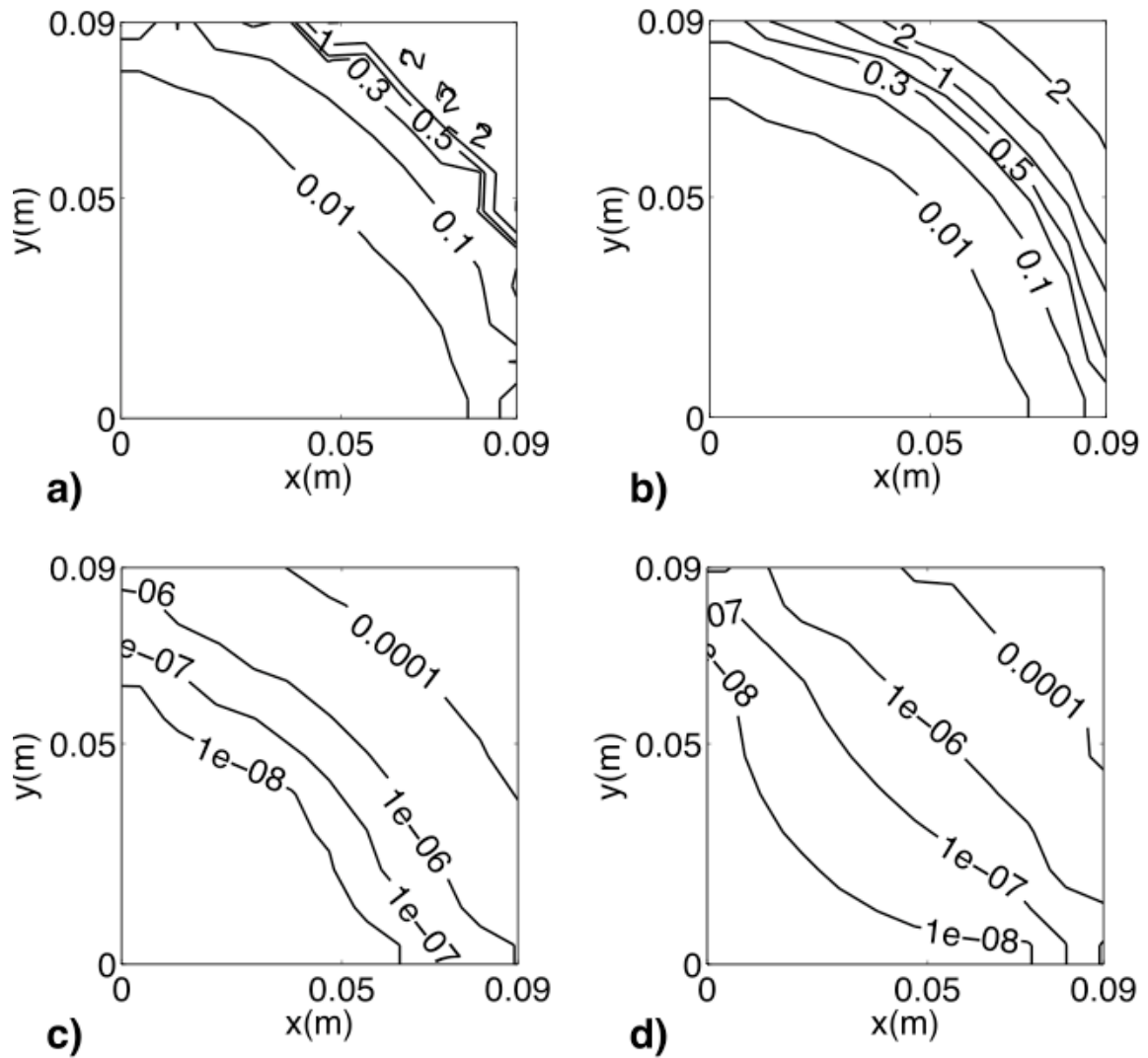
## 2.4 Results and Discussion

Figure 2.1 shows the upper halves of the  $Z^2$  wire patterns and Figure 2.2 shows the upper halves of the  $X^2-Y^2$  wire patterns created using (a) the minimum inductance and (b) the minimum power design algorithms. The bottom halves of the coils are mirror images of the top halves. Both algorithms prevent current density from spreading out indefinitely over the coil surface. The basic features characteristic of the two methods are apparent: minimum inductance designs tend to feature oscillations within the current density and minimum power designs tend to feature longer, less rapidly-varying current

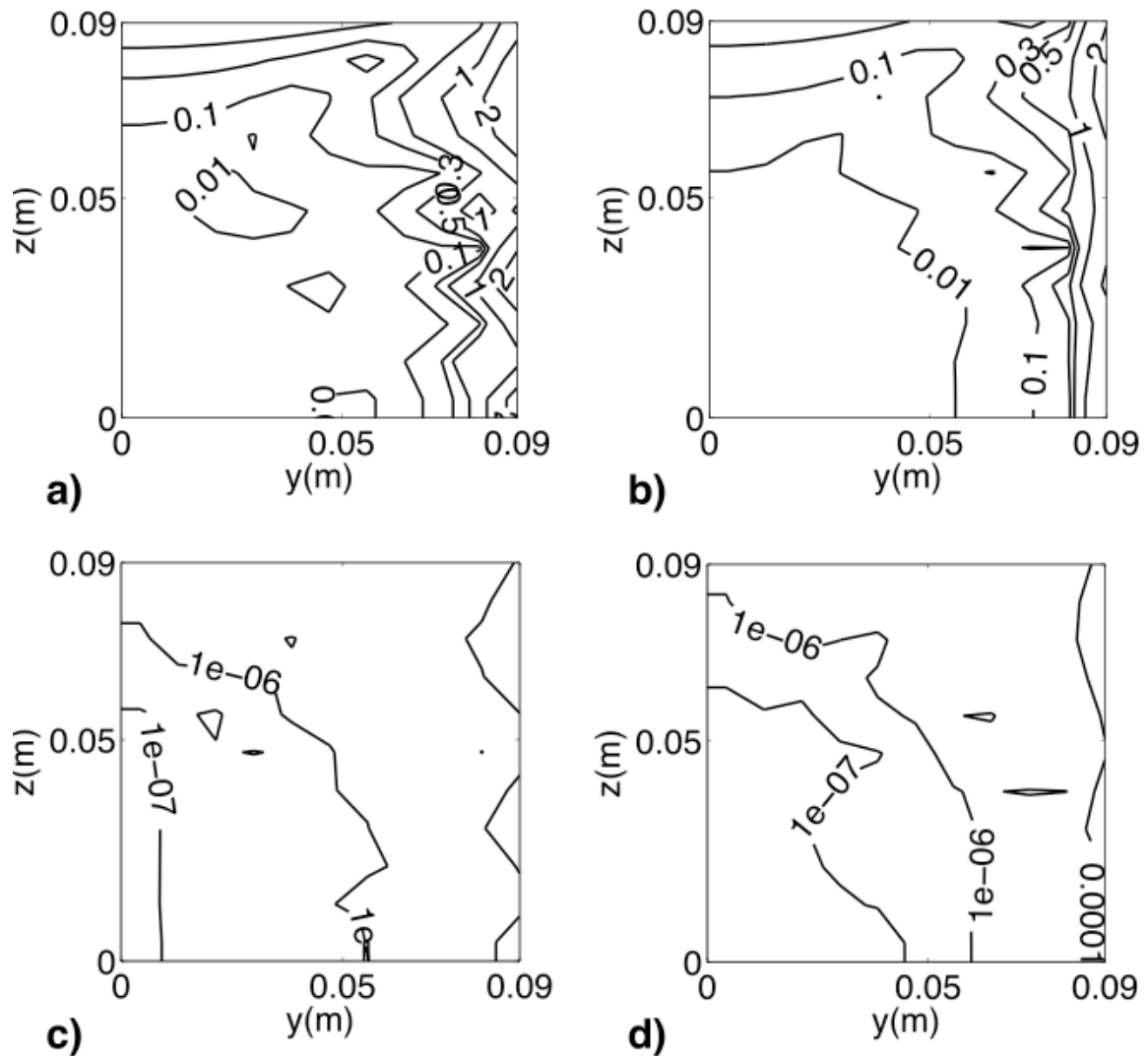
densities and a lower power dissipation. These features are consistent across all shim axes designed using these two methods.

Figure 2.3a illustrates the calculated magnetic field profile and the field targets versus  $z$  for the  $Z^2$  coil. Within the ROI (the cylinder of length  $a$  and radius  $0.5a$ ), the field profile, having an absolute error of  $10^{-6}$ , shows negligible deviation from the field targets, and the quadratic behavior of the magnetic field continues well outside of the ROI. The field profile for an  $X^2$ - $Y^2$  shim coil, calculated in the  $xy$  plane within the ROI, is shown in Figure 2.3b. The magnetic field deviates from the  $x^2$ - $y^2$  behavior more quickly than for the  $Z^2$  coil.

The field profiles given by the two design methods are almost identical within the ROI. However, small differences can be measured by comparing the relative residual fields given by each method. The relative and absolute residual fields for the  $X^2$ - $Y^2$  coils are shown in the  $xy$  plane and the  $yz$  plane in Figures 2.4 and 2.5, respectively. In each figure, subfigures a & c show the relative and absolute residual fields for the minimum inductance design, respectively, and subfigures b & d show the relative and absolute residual fields for the minimum power design, respectively. Due to symmetry, only one quadrant of the relative residual fields is shown. For all tesseral coils, the average relative field residuals are less than 2% and the average absolute field residuals are less than  $10^{-7}$  T in the  $xy$  plane within the ROI, when evaluated using both design methods. In the  $yz$  plane within the ROI, the average relative residual fields are less than 4% and the average absolute residual fields are less than  $10^{-6}$  T for all tesseral coils made with both design methods. For all zonal coils made with both design methods, the average relative residual fields are less than 2% and the average absolute residual fields are less than  $10^{-8}$  T in the  $yz$  plane within the ROI. The magnetic fields produced by the coils designed using the minimum power and the minimum inductance methods are scaled to have the same efficiency.



**Figure 2.4** One quadrant of the relative residual fields (top figures) and the absolute residual fields (bottom figures) in the  $xy$  plane for the  $X^2-Y^2$  shim coils designed using minimum inductance (a, c) and minimum power methods (b, d). Within the ROI and in the  $xy$  plane, the average relative residual fields are  $<2\%$  and the average absolute residual fields are  $<10^{-7}$  T when evaluated using both design methods. The magnetic fields produced by the coils designed using minimum power and minimum inductance methods were scaled to have the same efficiency ( $17 \text{ mT} / \text{m}^2/\text{A}$ ).



**Figure 2.5** One quadrant of the relative residual fields (top figures) and the absolute residual fields (bottom figures) in the  $yz$  plane for the  $X^2-Y^2$  shim coils designed using minimum inductance (a, c) and minimum power methods (b, d). Within the ROI and in the  $yz$  plane, the average relative residual fields are  $<4\%$  and the average absolute residual fields are  $<10^{-6}$  T when evaluated using both design methods. The magnetic fields produced by the coils designed using minimum power and minimum inductance methods were scaled to have the same efficiency ( $17 \text{ mT}/\text{m}^2/\text{A}$ ).

Table 2.1 summarizes the  $ML$  and  $MR$  values for the ten different shim axes. Percent differences of the merits of inductance and of the merits of resistance were calculated for coils designed with the minimum power and the minimum inductance methods. The absolute values of  $MR$  and  $ML$  cannot be compared between different shim axes; however, they can be used to compare designs for any given shim axis. In all cases, regardless of discrete or continuous evaluation, coils designed using the minimum inductance method have higher  $ML$  values, while coils designed using the minimum power method have higher  $MR$  values, as expected. However, it is equally clear that the differences between the design algorithms are small. When the stream functions were sampled with the same number of levels, the improvement in  $ML$  provided by the minimum inductance method is less than 10% of the value obtained using the minimum power method, in every design case. The improvements in  $MR$  provided by the minimum power method are less than 15% of the values obtained using the minimum inductance method. When the stream function sampling levels were adjusted to achieve constant coil efficiency, the improvements are 10 to 20% in inductive merit and 20 to 30% in resistive merit for the minimum inductance method and the minimum power method, respectively.

The merit of inductance calculated with the discrete method agrees with the merit of inductance calculated with the continuous method within 3.5% in all cases. This is expected because both efficiency and inductance are independent of current density. The difference between the merits of power calculated with the discrete and the continuous methods ranges between 10% and 30%. This larger discrepancy is observed because the resistance calculated by the discrete method is higher than the one calculated by the continuous method.

The results summarized in Table 2.1 are specific to the particular case of 10 cm-radius shim coils that correct for field inside an imaging region of 10 cm. The radii of the coils were chosen to be twice the radius of the imaging region. More work is required to extend these results to shim coil axes designed over a wider range of uniformity parameters.



In order to relate the results of this study to pulse sequence parameters for a simple example MRI pulse sequence, the effect of readout-gradient performance on a fast gradient echo sequence was simulated. The amplifier parameters were as follows: maximum voltage of 1200 V, maximum current of 400 A. The acquisition parameters were: receiver bandwidth of 125 kHz, 256 k-space data points along the readout direction, field-of-view equal to 10 cm. Gradient coils from both methods were scaled to have equal efficiency of 1.38 mT/m/A. The gradient coil designed using the minimum inductance method allowed a minimum  $TE$  of 1.13 ms and dissipated RMS power of 512 W, whereas the gradient coil designed using the minimum power method allowed a minimum  $TE$  of 1.15 ms and dissipated RMS power of 410 W. In this case then, the minimum inductance method results in a decrease of the minimum echo time of less than 2%, while the minimum power method results a decrease in power dissipation of 22%. For this application, it is probably most advantageous to utilize the minimum power design.

In this study, it has been shown that for shims coils of higher orders, minimum power algorithms yield coils with approximately 30% reduced power dissipation as compared to minimum inductance algorithms; while minimum inductance algorithms yield coils with approximately 20% reduced switching times. The question becomes: which is more significant for MRI applications? In the opinion of the authors, for small animal imaging studies at high field, the reduction in switching times provided by minimum inductance coil designs is not significant compared to the reduction in power dissipation allowed by minimum power designs. Modern imaging pulse sequences employing steady-state methods typically require gradients operating at high strength with very high duty-cycles, where power dissipation is the primary limitation. Furthermore, high-power shimming essentially requires direct current (DC) operation of the shim coils, and as shimming requirements increase, the thermal dissipation within the shim set is also expected to limit operation. Regardless, the results of this study allow judgments regarding gradient and shim coil design algorithm to be made on an informed, application-specific basis.

Axis	Analysis	Inductive Merit			Resistive Merit		
		Min. Power	Min. Ind.	Percent	Min. Power	Min. Ind.	Percent
		Method	Method	Difference	Method	Method	difference
<b>Z</b>	Discrete	0.0957	0.101	5.40	0.00490	0.00460	6.32
	Continuous	0.0937	0.100	6.97	0.00620	0.00570	8.4
<b>Z<sup>2</sup></b>	Discrete	0.797	0.839	5.13	0.0373	0.0340	9.26
	Continuous	0.816	0.869	6.29	0.0462	0.0413	11.2
<b>Z<sup>3</sup></b>	Discrete	10.5	11.2	6.45	0.418	0.395	5.65
	Continuous	10.3	11.1	7.48	0.545	0.505	7.61
<b>Z<sup>4</sup></b>	Discrete	91.5	93.4	5.50	3.3282	3.0998	7.10
	Continuous	88.2	90.4	6.25	4.41	4.01	9.50
<b>X and Y</b>	Discrete	0.0870	0.0921	5.69	0.00400	0.00350	13.3
	Continuous	0.0879	0.0933	5.96	0.00520	0.00450	14.4
<b>XY and X<sup>2</sup>-Y<sup>2</sup></b>	Discrete	1.53	1.63	6.33	0.0589	0.0535	9.6
	Continuous	1.53	1.62	5.71	0.0799	0.0718	10.7
<b>YZ and XZ</b>	Discrete	2.14	2.34	8.93	0.0625	0.0581	7.29
	Continuous	2.17	2.33	7.11	0.0844	0.0752	11.53

**Table 2.1** Performance values for ten shim axes designed using minimum inductance and minimum power algorithms. In every design case, the improvement in *ML* provided by the minimum inductance method is less than 10% of the value obtained using the minimum power method and the improvements in *MR* provided by the minimum power method are less than 15% of the values obtained using the minimum inductance method. The merit of inductance calculated with the discrete method agrees with the merit of inductance calculated with the continuous method within 3.5% in all cases. The difference between the merits of power calculated with the discrete and the continuous methods ranges between 10% and 30%.

## 2.5 References or Bibliography

1. Li BS, Regal J, Gonen O. SNR versus resolution in 3D <sup>1</sup>H MRS of the human brain at high magnetic fields. *Magn Reson Med* 2001;46(6):1049-1053.
2. Barker PB, Hearshen DO, Boska MD. Single-voxel proton MRS of the human brain at 1.5T and 3.0T. *Magn Reson Med* 2001;45(5):765-769.
3. Turner R. Gradient coil design-a review of methods. *Magn Reson Med* 1993;11:903-920.
4. Turner R. A target field approach to optimal coil design. *J Phys [D]* 1986;19:L147-L151.
5. Turner R. Minimum inductance coils. *J Phys [E]* 1988;21:948-995.
6. Carlson JW, Derby KA, Hawryszko KC, Weideman M. Design and evaluation of shielded gradient coils. *Magn Reson Med* 1992;26(2):191-206.
7. Bowtell R, Robyr P. Multilayer Gradient Coil Design. *J Magn Reson* 1998;131(2):286-294.
8. Forbes LK, Crozier S. A Novel target-field method for finite-length magnetic resonance shim coils: I. zonal shims. *J Phys [D]* 2001;34:3447-3455
9. Forbes LK, Crozier S. A Novel target-field method for finite-length magnetic resonance shim coils: II. tesseral shims. *J Phys [D]* 2002;35:839-849
10. Forbes LK, Crozier S. A Novel target-field method for magnetic resonance shim coils: III. shielded zonal and tesseral coilsShims. *J Phys [D]* 2003;36,:68-80.
11. Poole M, Bowtell R. Novel gradient coil designed using a boundary element method. *Concept Magn Reson [B]* 2007;31B:162-175

12. Turner R. Comparison of minimum inductance and minimum power gradient coil design strategies. 1992. Berkeley, CA. p 4031.
13. Jackson JD. Classical Electrodynamics. New York: John Wiley & Sons; 1998.
14. Reitz JR, Milford FJ, Christy RW. Foundation of electromagnetic Theory. New York: Addison Wesley; 1989.
15. Hildebrand FB. Advanced Calculus for Applications: Prentice-Hall; 1976.
16. Abramowitz M, Stegun IA. Hand Book of Mathematical Functions. New York: Dover; 1965.
17. Chronik BA, Rutt BK. Constrained length minimum inductance gradient coil design. Magn Reson Med 1998;39(2):270-278.
18. Peeren GN. Stream function approach for determining optimal surface current. J Com Phys 2003;191(1):305-321

## 2.6 Appendix A

To complete the derivation of the current density for the minimum power method, the  $z$ -component of the magnetic field should be expanded in cylindrical harmonics using the Green's function theory (13):

$$B_z(\rho, \phi, z) = -\mu_0 a \sum_{m=-\infty}^{\infty} \int_{-\infty}^{\infty} dk e^{im\phi} e^{i2\pi kz} j_\phi^m(k) |k| I_m(|2\pi k \rho|) K'_m(|2\pi k a|) \quad (\text{A1})$$

where  $a$  is the radius of the coil.  $I_m$  and  $K_m$  are the modified Bessel functions. The power dissipation in the coil can also be expanded in cylindrical harmonics (3):

$$P = \frac{\rho a}{2\pi t} \sum_{m=-\infty}^{\infty} \int_{-\infty}^{\infty} dk |j_\phi^m(k)|^2 \left( 1 + \frac{m^2}{(2\pi k a)^2} \right) \quad (\text{A2})$$

where  $\rho$  is the resistivity and  $t$  is thickness of the conductor. The functional,  $U\{j_\phi^m(k)\}$ , consists of power,  $P\{j_\phi^m(k)\}$ , and the field constraints deviation from the calculated field:

$$U\{j_\phi^m(k)\} = P\{j_\phi^m(k)\} + \sum_{n=1}^N \lambda_n [B_z(\rho_n, \phi_n, z_n) - B_{zn}] \quad (\text{A3})$$

$B_{zn}$  are the  $z$ -components of the desired magnetic field,  $N$  is the number of the field target points and  $\lambda_n$  are Lagrange multipliers. The minimum value of  $P$ , subject to the field constraints, is given when:

$$\frac{dU\{j_\phi^m(k)\}}{dj_\phi^m(k)} = 0. \quad (\text{A4})$$

Taking the derivative of  $U$  with respect to the reciprocal current density,  $j_\phi^m(k)$ , setting it equal to zero, and solving for  $j_\phi^m(k)$  yields:

$$j_\varphi^m(k) = \sum_{n=1}^N \lambda_n a_n \quad (\text{A5})$$

where:

$$a_n = \frac{\mu_0 t \pi}{\rho} \frac{1}{\left(1 + \frac{m^2}{(2\pi k a)^2}\right)} e^{im\phi} e^{i2\pi k z} |k| I_m(|2\pi k \rho_n|) K'_m(|2\pi k a|). \quad (\text{A6})$$

Once the set of  $\lambda_n$  is known in Eq. [A5], Eq. [A6] gives the reciprocal current density,  $j_\varphi^m(k)$ . To find  $\lambda_n$ , the field constraint equations:

$$B_z(\rho_n, \varphi_n, z_n) - B_{zn} = 0 \quad (\text{A7})$$

should be considered. Eq. [A5] can be substituted back into Eq. [A1] to write  $B_z$  in terms of  $\lambda_n$ . Substituting this expression for  $B_z$  into Eq. [A7] yields:

$$\left[ -\mu_0 a \sum_{n=1}^N \sum_{m=-\infty}^{\infty} \int dk e^{im\phi} e^{i2\pi k z} \lambda_n a_n |k| I_m(|2\pi k \rho|) K'_m(|2\pi k a|) \right] - B_{zn} = 0. \quad (\text{A8})$$

Eq. [A8] is a set of linearly independent equations that can be assembled into a matrix equation:

$$[M][\lambda_n] = [B_{zn}] \quad (\text{A9})$$

and solved for the set of  $\{\lambda_n\}$  using the singular value decomposition method. The elements of the matrix  $M$  are the integrals as a function of the constraint coordinates:

$$M(n, n') = \frac{-\pi\mu_0^2 ta}{\rho} \sum_{m=-\infty}^{\infty} \int_{-\infty}^{\infty} dk e^{im(\phi_n + \phi_{n'})} e^{i2\pi k(z_n + z_{n'})} \frac{|k|^2 I_m(|2\pi k \rho_n|) I_m(|2\pi k \rho_{n'}|) K_m'^2(|2\pi k a|)}{1 + \frac{m^2}{(2\pi k a)^2}}. \quad (\text{A10})$$

Evaluating the elements of  $M$  using Eq. [A9], solving Eq. [A8] for the set of  $\{\lambda_n\}$ , and substituting  $\lambda_n$ 's into Eq.[A5] gives the current density,  $j_\phi^m(k)$ . The  $J_\phi(z, \phi)$  can be calculated by taking the inverse transform of  $j_\phi^m(k)$ . Since the current density is known, Eqs. [A1,A2] give us the magnetic field and the power, respectively.

# Chapter 3

## 3 Finite-length shim coil design using a Fourier series minimum inductance and minimum power algorithm

### 3.1 Introduction

Magnetic Resonance Imaging (MRI) and Magnetic Resonance Spectroscopy (MRS) are under continual development at high field strengths such as 7T and above because of the promise of increased signal to noise ratio (SNR), allowing the acquisition of high quality, more easily quantifiable spectra in MRS and higher resolution images in shorter times for MRI (1). However, the SNR advantages can be eroded by field inhomogeneities which increase with field strength (2). Dynamically controlled field correction systems with higher power and performance than those required by moderate field MRI scanners are being developed to address these problems. An essential component of any field correction system is the shim coil. The performance of the shim system is a function of coil inductance, resistance, and field efficiency, as well as the physical length and diameter of the wire pattern (3). In this study, the effects of coil aspect ratio (defined as the ratio of coil length to diameter) on figures of merit for inductance and resistance were systematically studied. More specifically, the advantages

---

A version of this chapter has been published: Hudson P, Hudson SD, Handler WB, Chronik BA. Finite-length shim coil design using a Fourier series minimum inductance and minimum power algorithm. Concepts Magn Reson Part B Magn Reson Eng 2010;37B(4):245-253.



(if any) of using minimum inductance versus minimum power design algorithms are evaluated as a function of coil aspect ratio. In this study, gradient coils are also evaluated, as they can be considered to be the first-order members of the shim coil family.

In some applications rapid switching of gradients and shims are either necessary or under investigation. Functional MRI (fMRI) typically requires single-shot images of the brain. Rapid gradient switching is necessary in order to cover the required amount of k-space within the transverse decay time of the magnetization. Rapid temporal adjustment of the shim values would be necessary if non-linear field effects due to eddy currents are significant or if field changes due to rapid subject motion are to be corrected for. Since switching time is proportional to coil's inductance, minimum inductance designs would be expected to result in the most rapid switching of shim fields. On the other hand, imaging applications such as magnetic resonance microscopy require very large magnetic field gradients in order to produce high-frequency spatial encoding in sufficiently short echo times. High field shim coils are necessary in order to try to correct for localized field inhomogeneities within the sample. These applications are often limited by power dissipation within the coils, and minimum power designs would be attractive in order to limit this problem.

The target field method (4,5) is an analytic method which has been used to produce gradient coils with either minimum inductance or power. A current distribution is obtained over a surface of a cylinder which achieves the desired magnetic field profile. The limitation of the method is that the length of the current density is not controlled, sometimes resulting in coils that are too long for the desired application. Modifications of this method have been described which allow for explicit constraint of the extent of the final current density as well as control over the position of the uniform gradient with respect to the current density (6). The limitation of this approach is that the large number of current constraints required result in relatively long computation times and sometimes unstable solutions for the desired current density. To constrain the length of the gradient coils more directly, Carlson *et al.* (7) used a much simpler approach to modify the target field technique. In their method the current density is expanded as a sum of odd

sinusoidal functions (sines) for the Z gradient and even sinusoidal functions (cosines) for the transverse gradients, over a finite region in the z-direction. In this paper, an extension of Carlson's method for the robust design of shim coils is introduced. A more general 2D Fourier series expansion of current density over the surface of a cylinder is used.

Because the terms of the expansion are all limited in the z direction, the method allows for explicit control over the final current density extent (and thus the coil length).

Magnetic field target points are specified over some region either within or outside the cylinder on which the current density expansion has been made. The method can be used to minimize inductance, resistance, or a weighted combination of the two.

### 3.2 Theory

For any magnetic coil design, the goal is to obtain a current density that produces a desired magnetic field subject to optimizing some set of parameters. For the design of cylindrical shims in MRI, only the axial component of the magnetic field,  $B_z(r, \phi, z)$ , is of interest. In the event that the coils are to be switched extremely quickly, it is possible that peripheral nerve stimulation (8) could become a limiting factor, necessitating consideration of the other components of the magnetic field; however, this will not be considered further in this work. For a current constrained to flow on a surface of an axially aligned cylinder, only the azimuthal component of the current density,  $J_\phi(r, \phi, z)$  contributes to this field component. The azimuthal component of the current density confined to the surface of a cylindrical coil of radius  $a$  and length  $2l$ , can be expanded as a Fourier series:

$$\begin{aligned} J_\phi(r, \phi, z) &= \delta(r - a) \sum_{n=-N}^N \sum_{m=-M}^M \lambda_{mn} e^{\frac{in\pi z}{l}} e^{im\phi} & |z| \leq l \\ J_\phi(r, \phi, z) &= 0 & |z| > l \end{aligned} \quad (3.1)$$

where  $2N+1$  is the number of terms allowed for expansion of the z-variation of current density,  $2M+1$  is the number of terms allowed for expansion of the  $\phi$ -variation of current density, and  $\lambda_{mn}$  are the unknown coefficients. The total number of terms in the

expansion is therefore  $(2M+1) \times (2N+1)$ . The goal of the algorithm is to obtain the set of 'm × n' coefficients in an optimal manner.

The axial component of the magnetic field,  $B_z(r, \phi, z)$  inside a coil (i.e.  $r < a$ ) can be represented in terms of cylindrical harmonics (9,10) :

$$B_z(r, \phi, z) = \frac{-\mu_0 a}{2\pi} \sum_{m=-M}^M \int_{-\infty}^{\infty} dk e^{im\phi} e^{ikz} j_\phi^m(k) |k| K'_m(|ka|) I_m(|kr|). \quad (3.2)$$

$I_m$  and  $K_m$  are the modified Bessel functions (11,12) and  $K'_m$  is the derivative of  $K_m$  which can be written:  $K'_m = -\frac{1}{2}(K_{m+1} + K_{m-1})$ .  $j_\phi^m(k)$  is the Fourier transform of the current density given in Eq.[3.1] and can be written as:

$$j_\phi^m(k) = I \sum_{m=-M}^M \sum_{n=-N}^N \lambda_{mn} e^{im\phi} \sin c(kl - n\pi). \quad (3.3)$$

Like the magnetic field, inductance can be represented in terms of the current density in reciprocal domain (2,8):

$$L = \frac{-\mu_0 a^2}{I^2} \sum_{m=-M}^M \int_{-\infty}^{\infty} dk |j_\phi^m(k)|^2 K'_m(|ka|) I'_m(|ka|) \quad (3.4)$$

where  $I$  is the current used to sample the current density. The power dissipated by the current density can be described as:

$$P = \frac{\rho a}{t} \sum_{m=-\infty}^{\infty} \int_{-\infty}^{\infty} dk |j_\phi^m(k)|^2 \left( 1 + \frac{m^2}{(ka)^2} \right). \quad (3.5)$$

where  $t$  and  $\rho$  are the thickness and the resistivity, respectively, of the wire assumed to be used in approximating the current density (3).

The goal is to calculate the unknown  $\lambda_{mn}$ 's to achieve a desired magnetic field in the region of interest (ROI), while minimizing inductance or power or a combination of both. A functional,  $U\{j_\phi^m(k)\}$  is introduced which consists of two terms:

$$U\{j_\phi^m(k)\} = \beta Z\{j_\phi^m(k)\} + \sum_{q=1}^Q \alpha \left( B_z(\rho_q, \phi_q, z_q) - B_{zq} \right)^2. \quad (3.6)$$

In the first term,  $Z$  could be power, inductance, or a combination of both. The second term is the sum of the squares of the field deviation from the desired field targets,  $B_{zq}$  (7).  $\alpha$  and  $\beta$  are weighting factors whose values determine the relative importance of the field uniformity within the region of interest.

Differentiating the functional with respect to  $\lambda_{mn}$  inside  $j_\phi^m(k)$  and setting it equal to zero, yields the set of optimal  $\lambda_{mn}$ :

$$\frac{dU}{d\lambda_{mn'}} = \beta \frac{dZ}{d\lambda_{mn'}} + \alpha \sum_{q=1}^Q 2 \left( B_z(r_q, \phi_q, z_q) - B_{zq} \right) \frac{dB_z}{d\lambda_{mn'}} = 0. \quad (3.7)$$

The equation above can be written as a set of linear equations that can be assembled into a matrix equation and solved for the matrix  $\underline{\lambda}$ :

$$(D + A)\underline{\lambda} = B \quad (3.8)$$

where  $B$  is an  $m \times n'$  matrix:

$$B(m, n') = \frac{\mu_0 a l}{\pi} \sum_{q=1}^Q \alpha B_{zq} \int_{-\infty}^{\infty} dk e^{im\phi_q} e^{ikz_q} |k| \sin c(kl - \pi n') K'_m(|ka|) I_m(|kr_q|) \quad (3.9)$$

$D$  is an  $m \times n \times n'$ , a 3-dimensional matrix:

$$D(m, n, n') = \frac{\mu_0^2 a^2 l^2}{2\pi^2} \alpha \left( \begin{array}{l} \sum_{q=-\infty}^{\infty} \int_{-\infty}^{\infty} dk e^{im\phi_q} e^{ikz_q} |k| \sin c(kl - \pi n) K'_m(|ka|) I_m(|kr_q|) \times \\ \sum_{q=-\infty}^{\infty} \int_{-\infty}^{\infty} dk e^{im\phi_q} e^{ikz_q} |k| \sin c(kl - \pi n') K'_m(|ka|) I_m(|kr_q|) \end{array} \right), \quad (3.10)$$

and  $A$  is an  $m \times n \times n'$  matrix whose specific form depends on whether inductance or resistance is within the functional. For minimum inductance design,  $A$  would be:

$$A(m, n, n') = \beta \frac{\mu_0 a^2 l^2}{I^2} \int_{-\infty}^{\infty} dk \sin c(kl - \pi n) \sin c(kl - \pi n') K'_m(|ka|) I'_m(|ka|). \quad (3.11)$$

For minimum power design,  $A$  would be:

$$A(m, n, n') = \beta \frac{\rho a l^2}{t} \int_{-\infty}^{\infty} dk \sin c(kl - \pi n) \sin c(kl - \pi n') \left( 1 + \left( \frac{m}{ka} \right)^2 \right). \quad (3.12)$$

To generate matrix Eq. [3.8], a set of field targets are specified with indices  $q = 1, 2, \dots, Q$ . The number of terms  $(2N + 1)$  to be allowed in the  $z$ -dimension of the Fourier series expansion must be chosen. Finally, the order of the shim coil to be designed ( $m'$ ) must be chosen. One is then able to calculate the elements of  $B$ ,  $D$  and  $A$  using the expressions provided above. Eq. [3.8] can then be solved for the matrix  $\underline{\lambda}$  using the singular value decomposition method. Having  $\underline{\lambda}$ , the final current density can then be evaluated using Eq. [3.1].

### 3.3 Methods

The algorithm described above was implemented in Matlab (version 7.5, The Mathworks, Inc., Natick, MD, USA) and applied to the design of sets of shim coils with diameter 40 cm and four lengths: 50 cm, 60 cm, 80 cm, and 100 cm. The following ten separate axes were designed using both minimum inductance and minimum power methods: X, Y, Z, XY, X<sup>2</sup>-Y<sup>2</sup>, YZ, XZ, Z<sup>2</sup>, Z<sup>3</sup> and Z<sup>4</sup>. For all coil lengths, identical magnetic field targets were used for both the minimum inductance and the minimum

power methods. Twenty field targets were located in a cylindrical volume spaced equally between  $z = \pm 0.15$  m, radius  $r = \pm 0.5a$  and  $\phi = \pm\pi$ . Increasing the number of field targets over the same region increases both the accuracy of the field and the size of the region of uniformity, at the expense of coil efficiency.

For the first order shims (gradients),  $2N+1 = 7$  terms in the Fourier series expansion of current density were used. For the higher order shims: XY,  $X^2-Y^2$ , YZ, XZ,  $Z^2$ ,  $Z^3$  and  $Z^4$ , 9 terms were used. It was found that for the coil dimensions investigated in this study, a higher number of terms did not significantly improve the field uniformity, inductance, or resistance. Zonal shim coils were designed by limiting the expansion to have only  $m = 0$  and tesseral shim coils were designed by limiting the expansion to have only the azimuthal order necessary for that shim; for the first order tesseral shims we included only  $m = \pm 1$  in the current density expansion, for the second order tesseral shims we included only  $m = \pm 2$ , etc.

The continuous current density was sampled using a finite set of current carrying loops in order to calculate realistic wire positions for actual coil designs. A stream function was introduced, which was defined by the cumulative integral of the current density with respect to  $z$ :

$$S(r, \phi, z) = \int_{-l}^z J_\phi(r, \phi, z') dz'. \quad (3.13)$$

Contours were taken of the stream function using Matlab's contouring. Discrete wire segments were positioned along the contours of the stream function to represent the final discretized wire pattern for each coil (13,14). The discretized wire pattern was organized into an array of elements characterized by their positions and lengths, each carrying current  $I$ . The magnetic field generated by each coil was then calculated using the Biot-Savart equation (9,10).

In order to calculate the efficiency,  $\eta$ , of each shim coil a function was fit to the calculated field using a linear least squares algorithm (15). The field was calculated over the cylindrical volume of length of 30 cm and radius of  $0.5 a$ . For each shim coil, the

mathematical function used in the fitting was the same function used to define the field constraints. For example, the function  $z^2$  was fit to the calculated  $Z^2$  shim coil field profile. The coefficient of each fit divided by the current used in the field calculation defined the field efficiency for each coil.

Inductance was calculated by applying the Neumann Formula (9,10) to the wire element array. Resistance was calculated by summing the resistances of the wire elements in the element array. The radial thickness of the wire used for coil fabrication was assumed to be constant. The width of the wire was assumed to be equal to the minimum wire spacing for that coil design. The cross-sectional area of each wire element would then be the thickness multiplied by the minimum spacing. It is assumed that the current density is uniform across the wire cross section.

In order to assure that the field uniformity produced for the minimum inductance and minimum power formulations were comparable, the weighting factors  $\alpha$  and  $\beta$  in Eq. [3.6] needed to be adjusted separately for each design. This was done iteratively during the design process for each design until the percent difference in mean squared errors over the ROI obtained using the two algorithms was less than five percent.

Relative field residuals were calculated for each coil as a method for characterizing overall field uniformity. They are defined as the percent difference between the calculated field and the assumed ideal shape of the field for that shim. These fields were calculated inside a cylindrical volume of radius of  $0.9a$  and a length of  $2a$  (approximately 6 times the volume of the ROI).

The results of the minimum inductance and minimum power design methods were compared by calculating inductive merit,  $ML$ , and resistive merit,  $MR$ . Inductive merit ( $ML$ ) was defined to be  $\eta/L^{1/2}$  and the resistive merit ( $MR$ ) was defined to be  $\eta/R^{1/2}$  for rectangular wire (16). Both inductive and resistive merit are defined such that they are independent of the number of loops used to approximate the current density. Because the coil radius was held constant for this entire study it was not necessary to include it within the figures of merit.

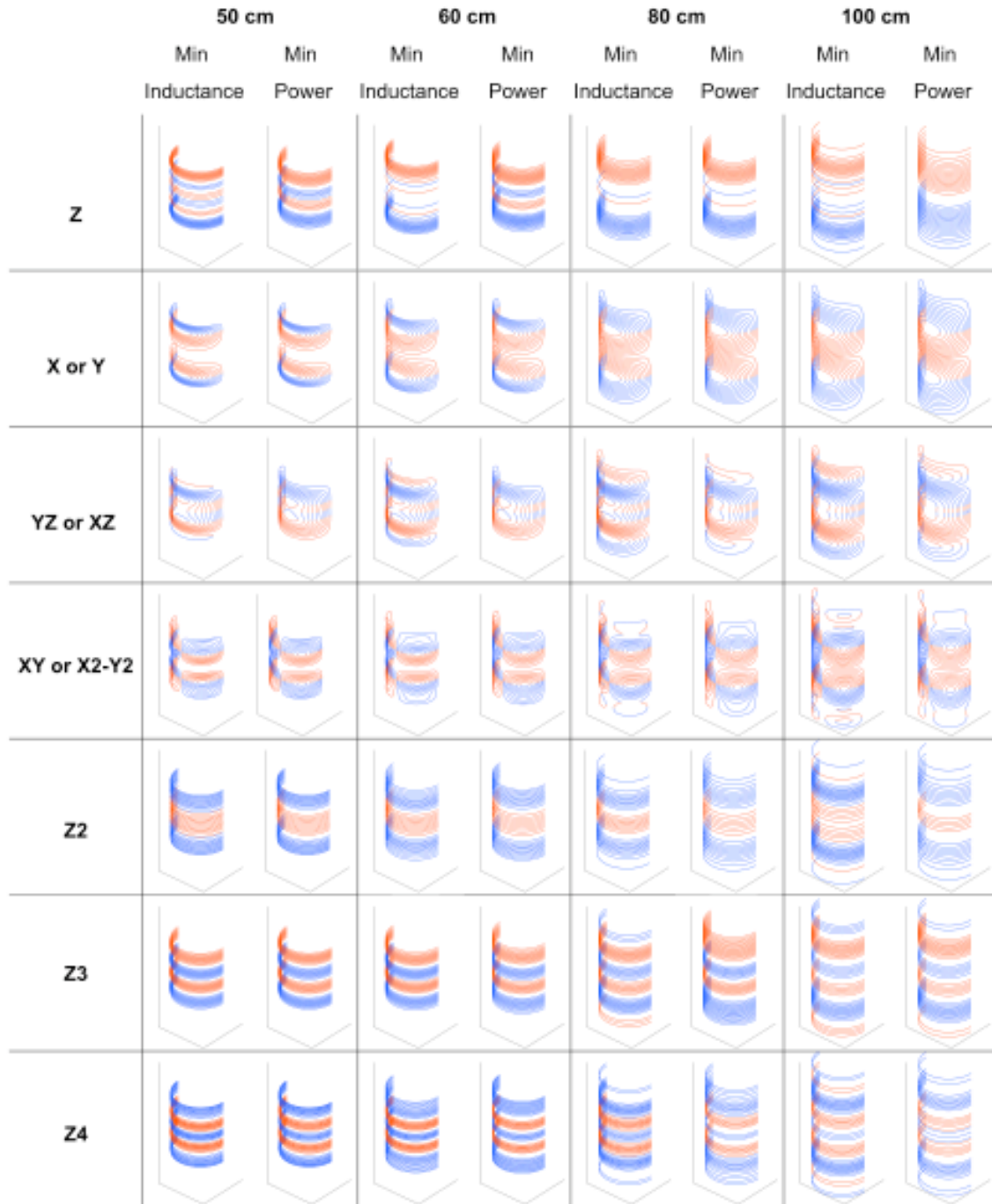


**Figure 3.1** Half-wire-patterns for ten coils: X, Y, Z, XY,  $X^2-Y^2$ , YZ, XZ,  $Z^2$ ,  $Z^3$ , and  $Z^4$  at four different lengths given by minimum inductance and minimum resistance methods. All coils are symmetric about the cuts chosen. The minimum resistance designs tend to feature less oscillation with less number of loops than minimum inductance designs at the same coil length.



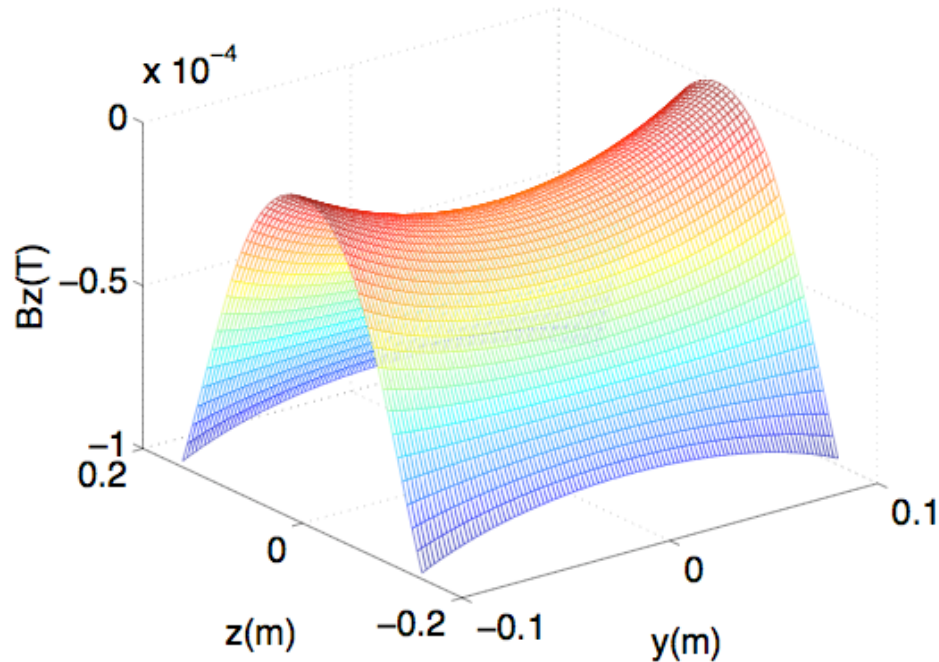


**Figure 3.2** The  $z$ -component of the magnetic field profile in the  $z$ - $y$  plane ( $x = 0$ ) for a  $Z^2$  shim coil with a radius of  $a = 0.2$  m. The region shown is larger than the originally specified region of interest, and it can be seen that the quadratic behavior of the magnetic field continues well outside the region of interest.

Both  $ML$  and  $MR$  were calculated for each coil, regardless of whether the coil was obtained using the minimum inductance or minimum resistance formulation. The percent difference in  $ML$  obtained by using the two formulations was calculated as the difference between  $ML$  for the minimum inductance design and  $ML$  for the minimum resistance design, divided by  $ML$  for the minimum inductance design. This yielded 40 comparisons (4 coil lengths and 10 shim axes per length). Similarly, the percent difference in  $MR$  obtained by using the two formulations was calculated as the difference between  $MR$  for the minimum resistance design and  $MR$  for the minimum inductance design, divided by  $MR$  for the minimum resistance design. This also yielded 40 comparisons.

### 3.4 Results and Discussion

Half-wire-patterns for all shim axes are summarized in Figure 3.1, for both minimum inductance and minimum resistance designs. The characteristic features of the two methods are apparent: minimum inductance designs tend to feature more higher-frequency oscillations within the current density as compared to minimum power designs. The observed oscillations in these designs are consistent with those obtained using other design methods in gradient coils (6)

As an example field profile, Figure 3.2 shows the calculated magnetic field profile for the 80 cm  $Z^2$  coil calculated in the  $yz$  plane. The quadratic behavior of the magnetic field continues well outside of the region of interest. The magnetic field profile for an 80 cm XY shim coil calculated in the  $xy$  plane within the region of interest (ROI) is shown in Figure 3.3. The deviation of magnetic field outside the region of interest was found to increase faster for the XY coil than for the  $Z^2$  coil in this case.

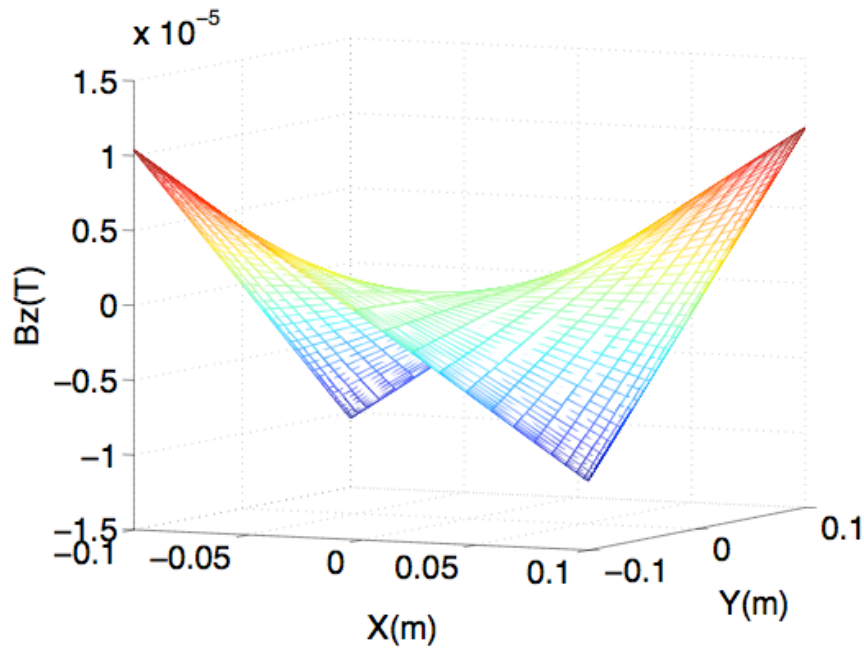


**Figure 3.3** The  $z$ -component of the magnetic field profile in the  $x$ - $y$  plane ( $z = 0$ ) for an XY shim coil with a radius of  $a = 0.2$  m.

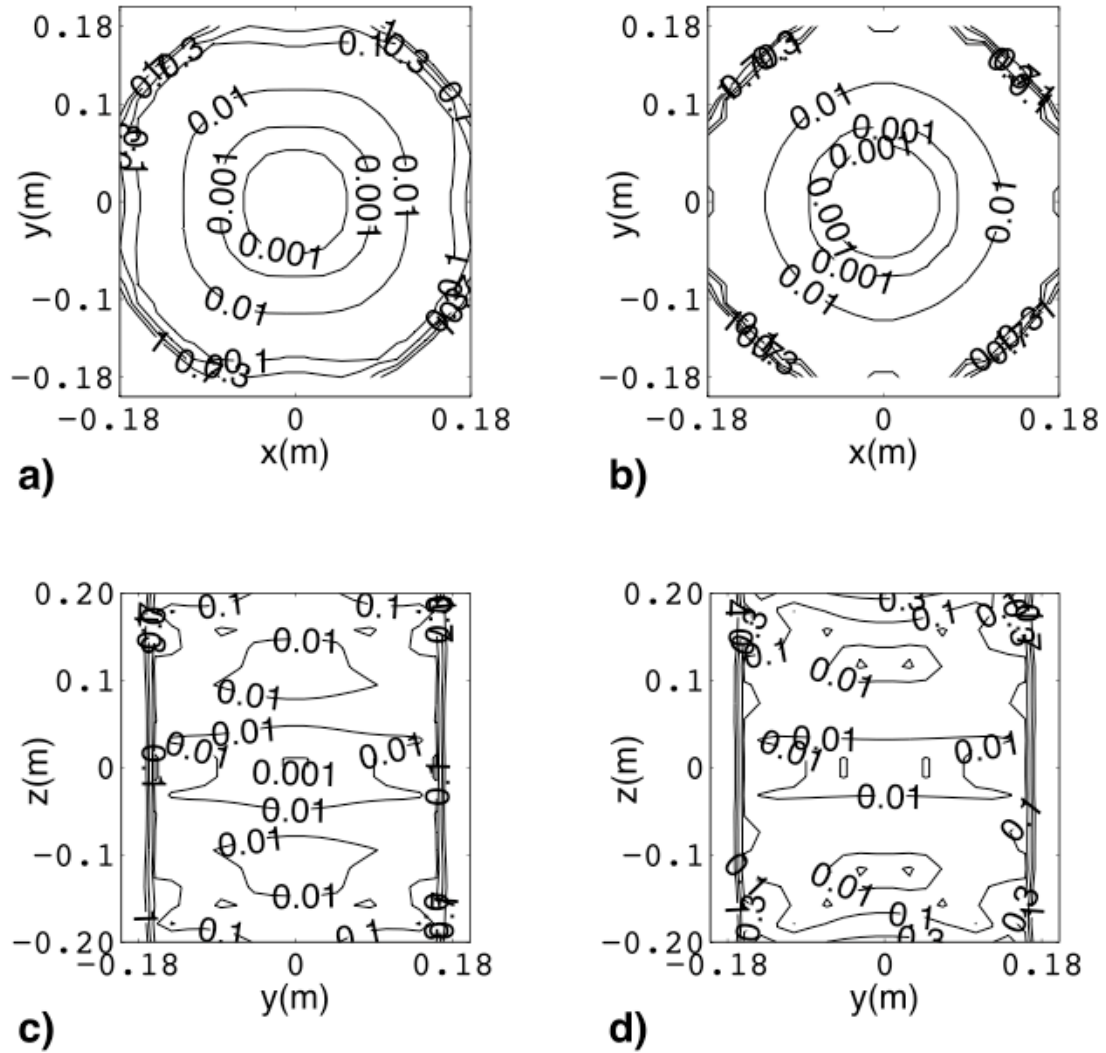


**Figure 3.4** The relative residual fields in the  $xy$  (a, b) and  $yz$  (c, d) planes for the 80 cm length XY shim coil designed using minimum inductance (left column; a, c) and minimum power methods (right column; b, d). The average relative residual fields within the ROI in the  $xy$  and  $yz$  planes are less than 5% for both formulations, indicating that both produced comparable field uniformity.

The field profiles obtained for all coils produced using the two different functionals were found to be almost identical over the prescribed ROI. The relative residual fields for the 80 cm XY coil are shown in Figure 3.4 for the  $xy$  and  $yz$  planes. For both methods, the mean residual fields evaluated over the ROI were found to be less than 5% for all tesseral coils and less than 3% for all zonal coils.

For all 28 distinct pairs of shim axes designed (note that for the three tesseral pairs of designs, the coils are simply rotations of each other and are therefore listed together in rows), Tables 3.1 and 3.2 list  $ML$  and  $MR$  respectively. As expected, in every case the minimum inductance design achieved better  $ML$  values than the minimum power design, and the minimum power design achieved better  $MR$  values than the minimum inductance design. However the differences between the two design methods were found to be very small. For all shim axes and all lengths considered, the differences in merit (either inductive or resistive merit) between the minimum inductance and minimum power designs were less than 6%. This maximum difference in merit would translate into an approximately 10% difference in either resistance or inductance for a completed coil (other parameters held constant).

This small difference must be weighed against the increased complexity and wire densities observed for the minimum inductance designs. The difference between the two methods does seem to increase for the highest order and shortest coil lengths, indicating that the choice of design method may become important as coil geometries become increasingly extreme. But for the large majority of designs evaluated in this study, there is very little difference in performance between the two methods.

	Inductive Merit ( $ML$ )							
	50 cm		60 cm		80 cm		100 cm	
	MinP	MinL	MinP	MinL	MinP	MinL	MinP	MinL
$Z$	0.016	0.016	0.016	0.017	0.017	0.017	0.016	0.016
$Z^2$	0.057	0.058	0.060	0.060	0.061	0.062	0.058	0.060
$Z^3$	0.27	0.27	0.27	0.28	0.28	0.30	0.27	0.27
$Z^4$	1.09	1.09	1.09	1.09	1.09	1.11	1.08	1.08
$X/Y$	1.08	1.08	1.09	1.09	1.10	1.11	1.09	1.09
$XZ/YZ$	0.052	0.064	0.058	0.066	0.063	0.069	0.059	0.067
$XY/X^2-Y^2$	0.086	0.090	0.096	0.099	0.088	0.091	0.088	0.091

**Table 3.1** Inductive merit,  $ML$ , values for all 28 distinct shim axis pairs designed using minimum inductance and minimum power algorithms. The differences in  $ML$  between the minimum inductance and minimum power designs were less than 6% in all cases. Across most shim axes, the 80 cm length designs had the highest inductive merit values.

	Resistive Merit ( $MR$ )							
	50 cm		60 cm		80 cm		100 cm	
	MinP	MinL	MinP	MinL	MinP	MinL	MinP	MinL
$Z$	0.0010	0.0009	0.0011	0.0010	0.0012	0.0011	0.0013	0.0012
$Z^2$	0.0035	0.0034	0.0038	0.0037	0.0040	0.0038	0.0038	0.0036
$Z^3$	0.014	0.014	0.015	0.015	0.016	0.015	0.014	0.014
$Z^4$	0.059	0.057	0.060	0.060	0.068	0.064	0.059	0.058
$X/Y$	4.3e-4	4.1e-4	4.5e-4	4.7e-4	6.2e-4	6.0e-4	5.8e-4	5.3e-4
$XZ/YZ$	0.0026	0.0025	0.0027	0.0026	0.0029	0.0028	0.0027	0.0026
$XY/X^2-Y^2$	0.0034	0.0033	0.0036	0.0034	0.0048	0.0046	0.0037	0.0036

**Table 3.2** Resistive merit,  $MR$ , values for all 28 distinct shim axis pairs designed using minimum inductance and minimum power algorithms. The differences in  $MR$  between the minimum inductance and minimum power designs were less than 6% in all cases. Across all shim axes, the 80 cm length designs had the highest resistive merit values.

When considering the effect of coil length on performance, it was also found across almost all shim axes that the 80 cm length designs (i.e. an aspect ratio of 2) had the highest merit values (both for resistance and inductance) while the 50 cm length (i.e. aspect ratio of 1.25) designs had the lowest merit values. The differences between the 50 cm and 80 cm length coil merits were always less than 25%. The 50 cm length was specifically included in this study because this would be the maximum length of shim coil that could effectively be used for human head imaging, as the ROI begins approximately 10 cm from the edge of the coil. These results indicate that the maximum penalty in power deposition, assuming constant field efficiency, expected by constraining the length of a shim coil to be compatible with human head imaging would be approximately 56% as compared to an unconstrained length coil. This is a significant increase in power and suggests that such a shim system may require additional efforts in terms of cooling and thermal monitoring; however, it also suggests that such a design would not have requirements beyond our existing methods for thermal management in gradient coil insert systems. If the longer coils were to be considered for use with the human head, asymmetric designs would clearly be necessary.

It is the view of the authors that the minimum power design is preferable to the minimum inductance approach due to the almost negligible difference in merits for coils resulting from the two design algorithms, coupled with the decreased complexity of the minimum power wire patterns. Furthermore, one would expect the power dissipated within any coil set to scale with the square of the scanner field strength (for the same object under investigation). These results suggest the increased use of minimum power design algorithms for the majority of shim and gradient coil applications, even in cases where switching and dynamic control is a primary requirement. These results motivate and guide the pursuit of high strength, minimum power coil systems for the most demanding imaging and spectroscopy applications at field strengths of 7T and above.

### 3.5 References or Bibliography

1. Li BS, Regal J, Gonen O. SNR versus resolution in 3D  $^1\text{H}$  MRS of the human brain at high magnetic fields. *Magn Reson Med* 2001;46(6):1049-1053.
2. Barker PB, Hearshen DO, Boska MD. Single-voxel proton MRS of the human brain at 1.5T and 3.0T. *Magn Reson Med* 2001;45(5):765-769.
3. Turner R. Gradient coil design-a review of methods. *Magn Reson Med* 1993;11:903-920.
4. Turner R. A target field approach to optimal coil design. *J Phys [D]* 1986;19:L147-L151.
5. Turner R. Minimum inductance coils. *J Phys [E]* 1988;21:948-995.
6. Chronik BA, Rutt BK. Constrained length minimum inductance gradient coil design. *Magn Reson Med* 1998;39(2):270-278.
7. Carlson JW, Derby KA, Hawryszko KC, Weideman M. Design and evaluation of shielded gradient coils. *Magn Reson Med* 1992;26(2):191-206.
8. Chronik BA, Ramachandran M. Simple anatomical measurements do not correlate significantly to individual peripheral nerve stimulation thresholds as measured in MRI gradient coils. *J Magn Reson Imaging* 2003;17(6):716-721.
9. Jackson JD. *Classical Electrodynamics*. New York: John Wiley & Sons; 1998.
10. Reitz JR, Milford FJ, Christy RW. *Foundation of electromagnetic Theory*. New York: Addison Wesley; 1989.
11. Hildebrand FB. *Advanced Calculus for Applications*: Prentice-Hall; 1976.
12. Abramowitz M, Stegun IA. *Hand Book of Mathematical Functions*. New York: Dover; 1965.

13. Peeren GN. Stream function approach for determining optimal surface current. *J Com Phys* 2003;191(1):305-321
14. Hudson P, Hudson SD, Handler WB, Scholl TJ, Chronik BA. Quantitative Comparison of Minimum Inductance and Minimum Power Algorithms for the Design of Shim Coils for Small Animal Imaging. *Concepts Magn Reson Part B Magn Reson Eng* 2010;37B(2):65-74.
15. Press WH TS, Vetterling WT, Flannery BP. *Numerical Recipes*. New York: Cambridge University Press; 2007.
16. Bowtell R, Robyr P. Multilayer Gradient Coil Design. *J Magn Reson* 1998;131(2):286-294.



## **Chapter 4**

# **4 A novel custom shim coil designed for spectroscopy to correct the field inhomogeneities in the medial temporal lobe of the human brain**

### **4.1 Introduction**

Magnetic resonance imaging and spectroscopy is moving towards higher magnetic field strength to benefit from the higher signal to noise ratio, that allows for higher resolution MR images and more quantifiable spectra of low concentration metabolites (1) to be collected. However at higher magnetic field,  $B_0$  inhomogeneities increase, causing artifacts in MR images and line broadening in MR spectra (2). These field inhomogeneities are particularly severe at tissue, bone, and air interfaces due to their magnetic susceptibility differences (3). A useful way to look at these field inhomogeneities is to factor them into two components: relatively large inhomogeneities with minimal variation between subjects, and smaller, subject specific inhomogeneities. We propose that very efficient, short, custom shim coils could be designed to compensate for the largest, most significant inhomogeneities that are approximately consistent between subjects, while system shims could be used to fine-tune the field on a sample specific basis. Optimal performance would be achieved by designing a separate custom coil for each specific imaging region. For example, separate coils could be designed for the frontal, temporal, parietal or occipital lobes of the human brain, and these insert shim

coils would be switched into and out-of the scanner on a study-specific basis. In this work, we demonstrate the efficacy of our shimming method by designing a custom shim coil for correcting the field inhomogeneities over the medial temporal lobe of the human brain.

Magnetic field generating coils such as gradient and shim coils are numerous and varied. These gradient and shim coils should be designed such that they only modify the  $z$ -component of the main magnetic field,  $B_0$ , since the main magnetic field generated by superconductive or resistive magnets is oriented in the  $z$ -direction. The design goal is to produce a highly efficient coil with uniform field over the region of interest while minimizing other important physical properties of the coil such as inductance, power, and torque. Historically, different techniques have been developed for designing gradient and shim coils with minimum power, minimum inductance or both. Turner and Bowley (4,5) developed a target field method for designing gradient coils with minimized inductance or power. The magnetic field, inductance and power due to an unknown current density were expanded as Fourier-Bessel functions. A current distribution was calculated over a surface of a cylinder or in a plane to achieve the desired magnetic field, while minimizing inductance or power. Carlson *et al.* modified Turner's method by expanding the current density with a truncated sinusoidal function to allow for finite length gradient coils. (6). Bowtell and Robyr designed multilayer, cylindrical gradient coils by allowing the current density to vary in the radial direction in addition to the axial and azimuthal directions (7). In their design algorithm, power and inductance of the coil were minimized simultaneously. Further developments by Forbes and Crozier in a series of papers (8-10), allowed for the design of shielded zonal and tesseral shim coils on cylindrical and planar surfaces.

Pissanetzky (11) introduced a boundary element method (BEM) that allows for the design of coils wound on an arbitrary surface. Using this method a current density is discretized into a mesh of triangles. The magnetic field, inductance and torque were derived in terms of discretized current density, allowing for a functional capable of simultaneously minimizing the square of the difference between the target field and the actual field, the inductance, the power loss, and the torque exerted on the coils. Further,

Lemdiasov and Ludwig (12) extended the boundary element method by removing the reliance on coil symmetry. Recently Poole and Bowtell (13) modified the boundary element method by adding a power term to the functional allowing the minimization of the power dissipation in the coil.

Since the boundary element method can be used to design current densities with symmetric or asymmetric geometry wound on an arbitrary surface to generate a specific magnetic field, we will use this method to design our region specific shim coil for the medial temporal lobe of human brain. This region of the brain is located in the vicinity of the sinus cavity where the magnetic susceptibility differences between air, tissue and bone create significant field inhomogeneities. Reduction of the field inhomogeneity in this region of the brain would allow for higher resolution MR spectroscopy of the hippocampi, possibly facilitating diagnosis of Alzheimer's disease (14) and other neuro-degenerative diseases via quantitative measurement of specific metabolite concentrations.

## 4.2 Methods

To specify the field targets in the BEM algorithm, the field inhomogeneity maps of three normal human heads were derived with a robust automated shimming technique using arbitrary mapping acquisition parameters (RASTAMAP) (17) using a head only 7T Varian system. Studies were conducted with approval of The University of Western Ontario Human Subject's form # 15018. This technique uses a gradient echo sequence to measure the field inhomogeneities with high precision. This fast, accurate and flexible pulse sequence can compensate for phase errors and generate absolute field maps regardless of field of view (FOV), resolution, acquisition geometry, or bandwidth, making it ideally suited for automated shimming applications. A multiecho, 3D gradient echo sequence consisting of eight echoes with linearly increasing echoes spacing was used for field mapping. An entire 3D volume with dimensions 19.2 cm by 19.2 cm by 14.4 cm encompassing a human head was acquired with one polarity and then repeated with the opposite polarity. All gradient spoiling was limited to the readout direction to minimize a possible magnetic field along phase encode directions. The acquisition parameters are a  $96 \times 96 \times 72$  acquisition matrix, 104 kHz readout bandwidth, 15 ms TR,

1.3 ms TE, echo spacing of 1.2 ms, incremental echo spacing increase of 0.2 ms and eight echoes for a total acquisition time of 2 min. A slice-selective *sinc* pulse with a  $6^\circ$  flip angle is used to restrict the FOV in the third dimension. To minimize the geometric distortion caused by static field gradients, the read out bandwidths of 100 kHz or higher were used. Once the field maps were acquired, the effect of the system shims had to be removed in order to acquire the unshimmed field maps. This was achieved by subtracting the shim fields from the field maps, taking into account the known current used for each shim during the field-mapping experiment. Linear (gradient) shim fields were not subtracted.

Within each 3D field map, a rectangular volume of dimensions of 8 cm by 5 cm by 4 cm (see figure 4. 1) encompassing the medial temporal lobe was chosen as the region of interest (ROI). Principle component analysis (PCA) was used as method of averaging the field maps within the ROI. PCA projects a data set into a new coordinate system where the first coordinate has the largest variance of the data set and the second coordinate has the largest variance uncorrelated to the first component etc. In this way the principal component of the data contains the “most important aspect” of all the data. Using this method, the most important features of all of the field maps were selected.

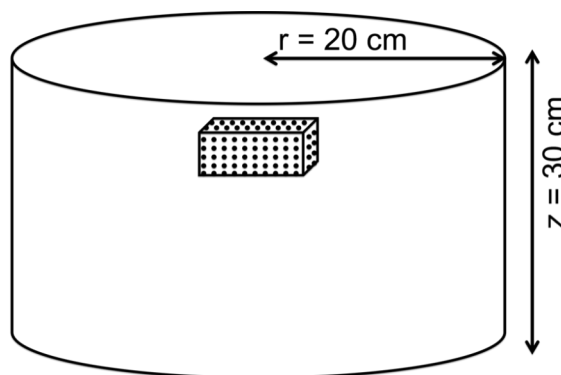


**Figure 4.1** A schematic view of a custom coil with a diameter of 40 cm and the length of 30 cm is shown. The coil’s region of interest has dimensions of 8 cm  $\times$  5 cm  $\times$  4 cm and is off centered.

Principle Component Analysis starts by considering a matrix  $\mathbf{B}$  comprised of vectors,  $\mathbf{B}_i$ , where  $i = 1, \dots, N$ .

$$\mathbf{B} = (\mathbf{B}_1, \dots, \mathbf{B}_i, \dots, \mathbf{B}_N) \quad (4.1)$$

The vectors,  $\mathbf{B}_i$ , are three dimensional field inhomogeneity maps of  $i^{th}$  subjects re-ordered into vectors, within a ROI. Therefore  $\mathbf{B}$  is an  $M \times N$  matrix where  $M$  is the number of magnetic field data points within the ROI and  $N$  is the number of subjects. In our experiment  $N = 3$ . The mean subtracted  $\mathbf{B}_{ms}$  could be calculated by subtracting the mean of each vector,  $\bar{\mathbf{B}}_i$ , from  $\mathbf{B}_i$ :

$$\mathbf{B}_{ms} = (\mathbf{B}_1 - \bar{\mathbf{B}}_1, \dots, \mathbf{B}_i - \bar{\mathbf{B}}_i, \dots, \mathbf{B}_N - \bar{\mathbf{B}}_N). \quad (4.2)$$

Next the covariance matrix was calculated in order to measure the correlation between each two vectors:

$$\mathbf{C} = \frac{1}{M} \mathbf{B}_{ms} \mathbf{B}_{ms}^T. \quad (4.3)$$

Using the covariance matrix, eigenvectors,  $\mathbf{V}$ , and eigenvalues,  $\lambda$ , could be calculated:

$$\mathbf{C}\mathbf{V} = \lambda\mathbf{V}. \quad (4.4)$$

If the eigenvector corresponding to the highest eigenvalue is multiplied by the mean subtracted matrix, the first principle component of the field maps is achieved. Similarly if the eigenvector corresponding to the second highest eigenvalue is multiplied by the mean subtracted matrix, the second principle component of the field maps, uncorrelated with the first principle component, is achieved, etc.

The first principal component, PCA field map, can then be used as the target magnetic field to design a custom shim coil for the correction of the field inhomogeneities within the specified ROI. A cylindrical surface mesh was created with

8300 elements, a diameter of 40 cm, and a length of 30 cm using Comsol Multiphysics (Burlington, MA) (see figure 4.2). The surface mesh was imported into Matlab for the use in BEM. C++ was also used for the calculation of some matrices described in Appendix B and the current density of the custom coil capable of correcting the field inhomogeneities in the region of interest was found.

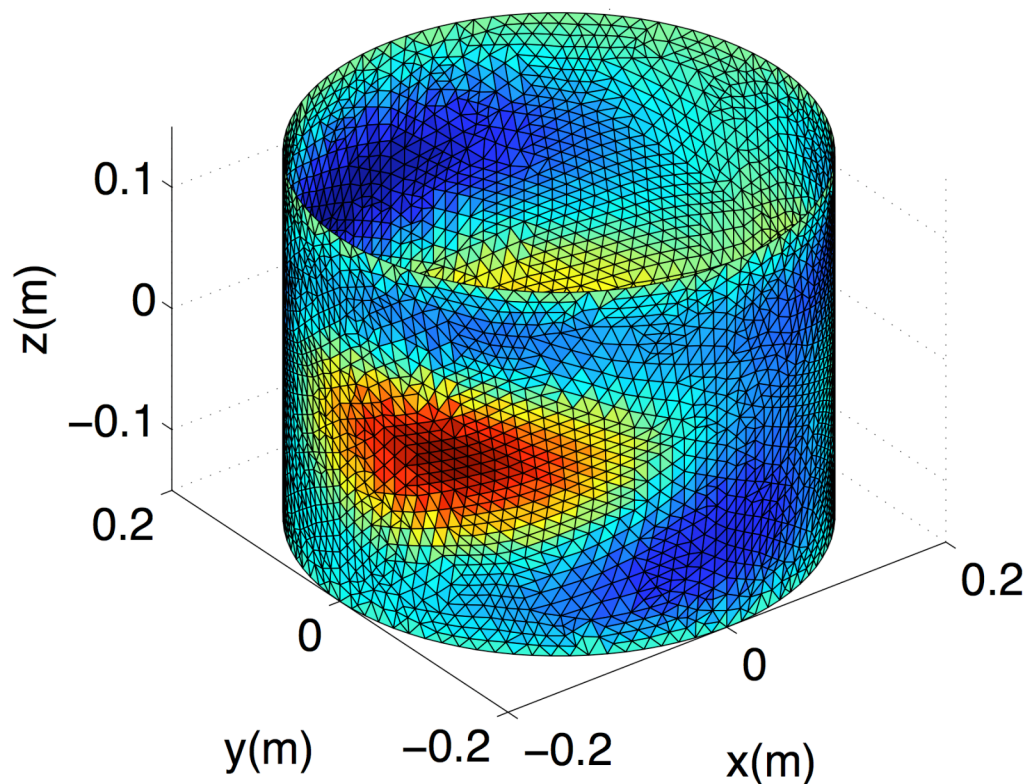


**Figure 4.2** A cylindrical surface mesh with 8300 elements, with a diameter of 40 cm, and a length of 30 cm was created using Comsol Multiphysics (Burlington, MA).

The boundary element method (BEM) relies on discretization of the surface current density into a set of basis functions over the elements of a mesh. These basis functions are weighted by some unknown coefficients. The magnetic field, power, and torque of the coil are derived in terms of the unknown coefficients via current density, and are used to create a functional. The functional is minimized to find the unknown coefficients of current density that yields the desired magnetic field, while optimizing the

power and torque properties. The complete derivation of the boundary element method is presented in Appendix B. This method is implemented in Matlab, version 7.5 (The Mathworks, Inc., Natick, MA, USA) and C++ for the design of a custom coil (see figure 4.2) to correct the field inhomogeneities in the medial temporal lobe.

For coil construction, the continuous current density should be approximated with a set of current carrying loops. To determine the position of the loops under the condition  $\nabla \cdot \mathbf{J} = \mathbf{0}$ , we define a stream function  $\mathbf{S}(\mathbf{r})$ :

$$\mathbf{S}(\mathbf{r}) = \int_{-\infty}^{\mathbf{r}} \mathbf{J}(\mathbf{r}') d\mathbf{r}'$$

The stream function was discretized into contours using the contouring function of Matlab version 7.5 (The Mathworks, Inc., Natick, MA, USA). The contours of the stream function are the intersections of the stream function with evenly spaced planes (levels). Wires were positioned along the contours of the stream function and each contour represented one or more closed loops on the coils cylindrical surface (18).

Once the wire pattern was obtained (see figure 4.5), it was discretized into an array of wire segments characterized by their positions and lengths. A Bio-Savart elemental equation was used to calculate the shim field within the region of interest (15,16). The coil inductance was evaluated by applying the Neumann formula (12,15,16) to the wire element array and the resistance was calculated by summing the resistances of the wire elements in the element array for rectangular wire. In this case the radial thickness of the conducting layer used for coil fabrication was assumed to be constant and the width of the conducting path was assumed to be equal to the minimum spacing. The cross-sectional area of each wire element would then be the thickness multiplied by the minimum spacing.

A computer simulation was performed, by adding the simulated custom shim as a channel to the system shims. Linear least squares fitting (19) was used to fit the simulated custom coil and system shims fields to the unshimmed field inhomogeneity

map within the region of interest. The fitting provided an estimate of the currents required for the real custom coil and the system shims for multiple subjects.

Once the currents were calculated, the field profile achievable with the simulated custom shim plus the system shims was determined for each subject and compared with the field profile attainable using the system shims only. This comparison was made by first converting the field profiles to frequency profiles using the gyromagnetic ratio, and then by calculating the standard deviation of histograms of the frequency profiles. For each subject, the histograms of three frequency profiles were calculated: the unshimmed frequency profile (unshimmed frequency inhomogeneity map), the frequency profile of the system shims subtracted from the unshimmed frequency profile and the frequency profile of the simulated custom shim plus the system shims subtracted from the unshimmed frequency profile. For each histogram the standard deviation was calculated and the results are shown in table 4.1. To investigate the sensitivity of the simulated customized shim coil to small differences in subject positioning within the coil, in computer we misaligned one of the subject's head with respect to the custom coil in the  $x$ -,  $y$ -, and  $z$ - directions and the standard deviations of the histograms of many misalignments were extracted and plotted versus the misalignments.

### **4.3 Results and Discussion**

Figure 4.3 parts a, d and g show sagittal anatomical images and parts b, e and h show sagittal images of unshimmed field inhomogeneity maps of all three-subject heads respectively. To specify the region encompassing the medial temporal lobe on the field inhomogeneity maps, the field map of each subject head was overlaid with the anatomical image and the results are shown in figure 4.3 parts c, f, and i. For each subject, the white rectangle, shown in part c, f, and i of figure 4.3, encompasses the hippocampi. The PCA field map was calculated from the field maps within the regions enclosed by these rectangles.



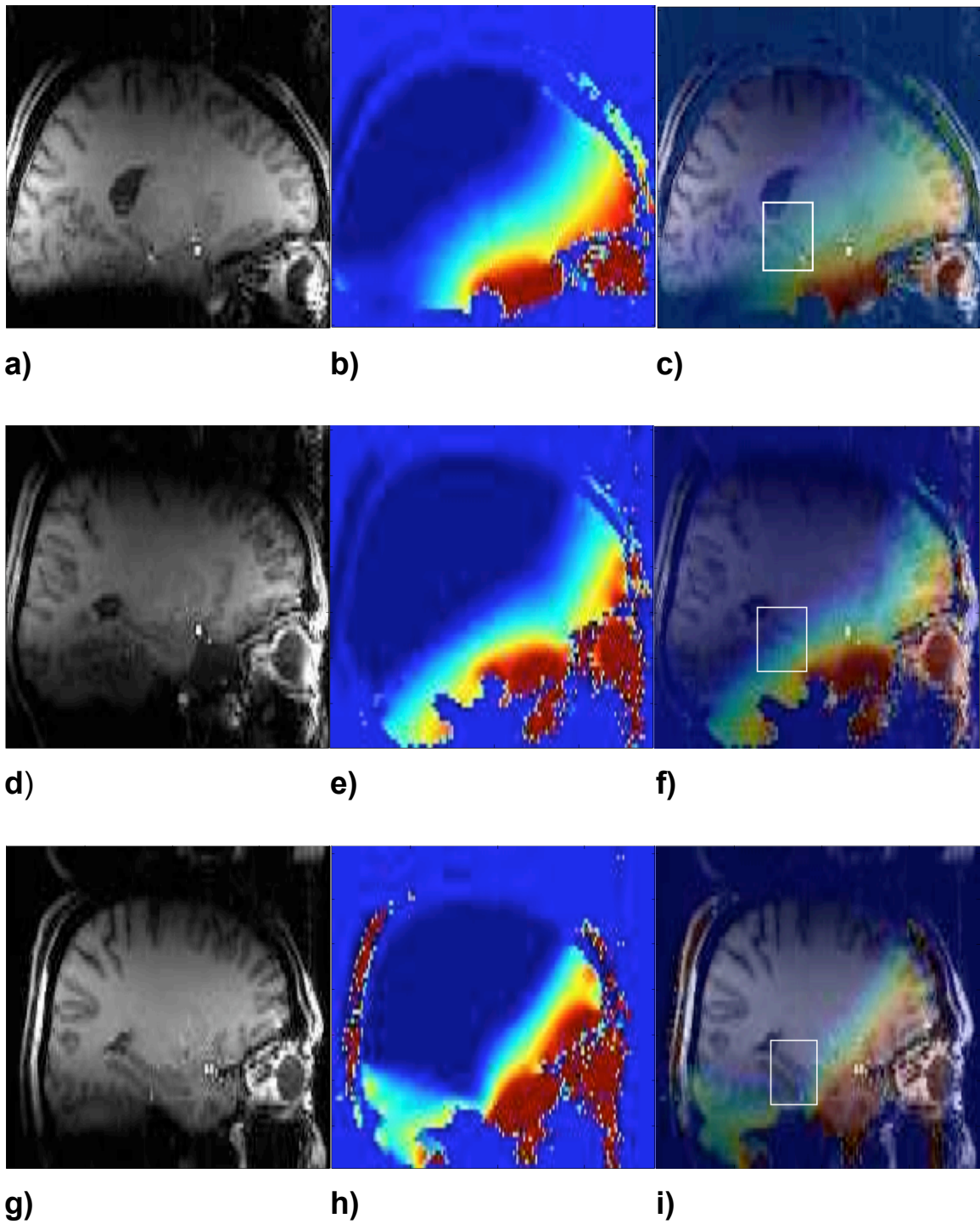


**Figure 4.3** parts a), d) and g) show sagittal anatomical images and parts b), e) and h) show sagittal images of the unshimmed field inhomogeneity maps of all three subject heads respectively. The field map of each subject head was overlaid with the anatomical image and the results are shown in parts c), f), and i). For each subject the white rectangle, shown in parts c), f), and i) encompasses the hippocampi.

The unwrapped wire pattern of the custom coil is shown in figure 4.4. The coil was modeled with 1 mm diameter wire and 60 windings. The inductance of the coil was calculated to be 960  $\mu\text{H}$  and the resistance of the coil was calculated to be 1.65  $\Omega$ .

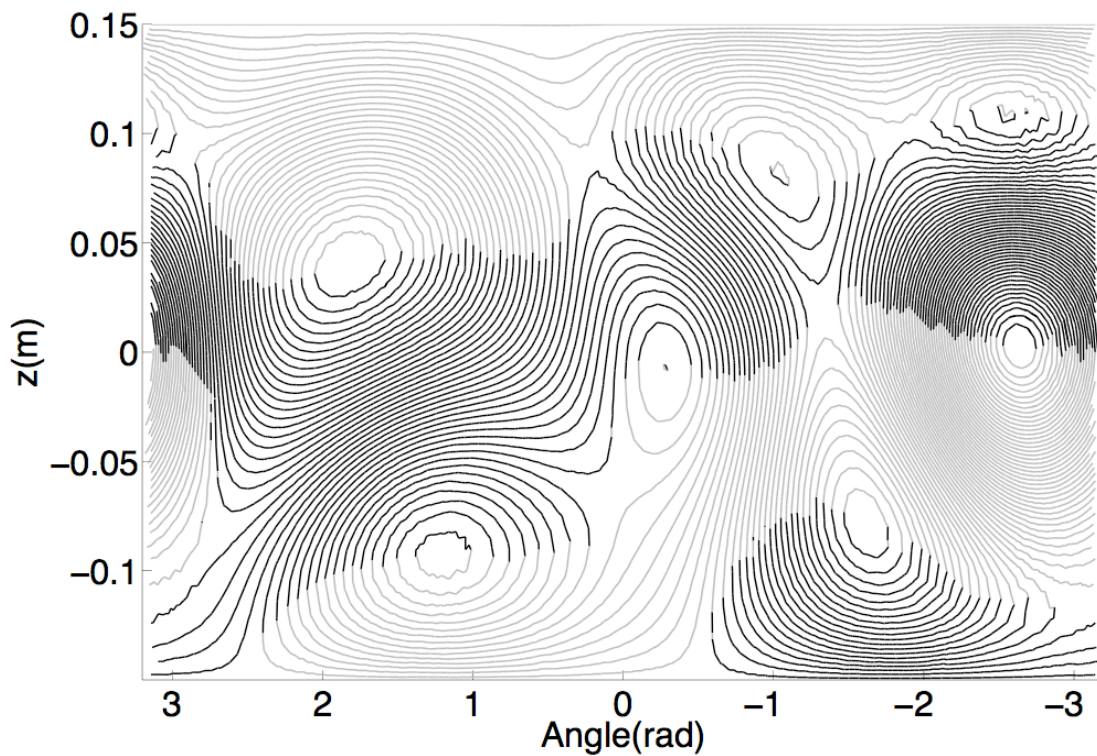


**Figure 4.4** The wire pattern of the coil is shown with 1 mm diameter wire and 60 windings. The inductance of the coil was calculated to be 960  $\mu\text{H}$  and the resistance of the coil was 1.65  $\Omega$ .

Figure 4.5 shows the  $z$ -component of the magnetic field generated by the custom coil along  $x$ ,  $y$  and  $z$ -axes, within the region of interest.

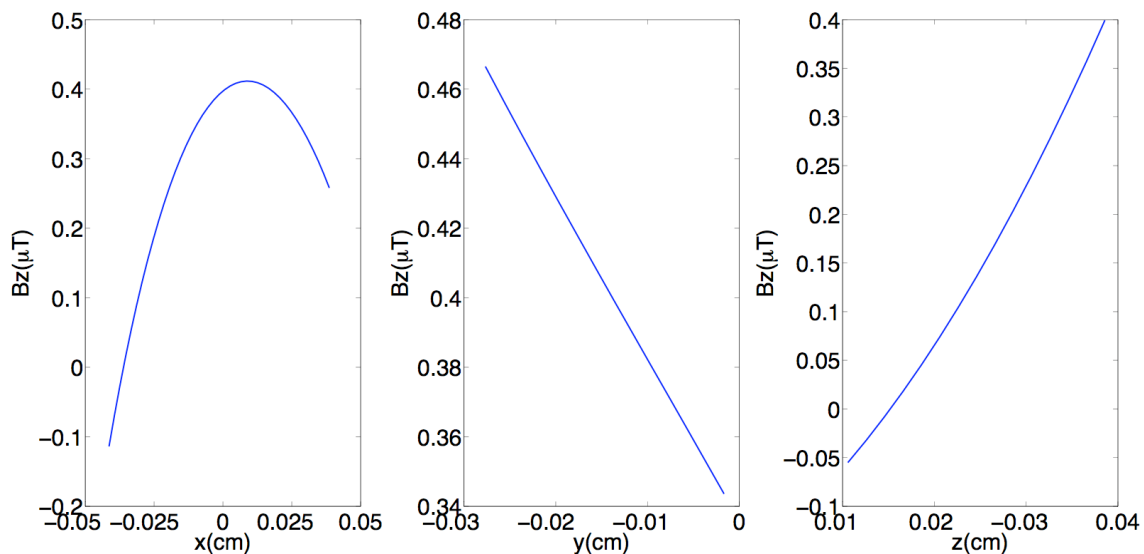
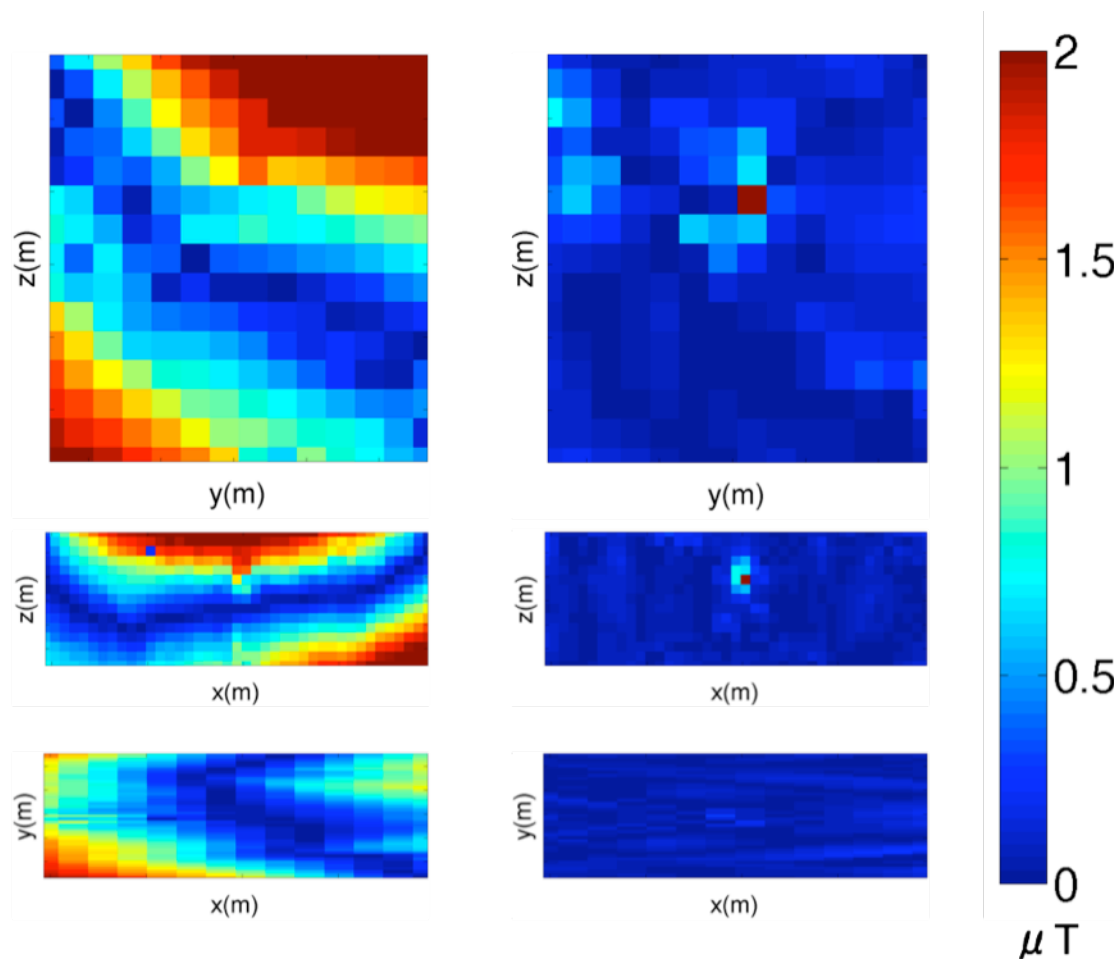


**Figure 4.5** The  $z$ -component of the magnetic field is shown along  $x$ ,  $y$  and  $z$ -axes, within the region of interest.

Figure 4.6 shows the field inhomogeneity profiles across three slices through the center of the region of interest after a) no shimming and b) shimming using the simulated custom coil plus system shims. For each slice, the customized shim is expected to reduce the field inhomogeneity by a factor of 1.3 when added to the system shims as compared to that obtained using the shim system only.

Figure 4.7 parts a, b, and c show the histograms of the frequency inhomogeneities for all three subjects. Each figure shows the histogram of the unshimmed frequency inhomogeneities, the histogram of the residual frequency inhomogeneities after shimmed with the system shims and the histogram of the residual frequency inhomogeneities after shimmed with the simulated custom plus system shims. It should be mentioned that in computer software each subject's head was moved in the  $z$ -direction in order to locate the medial temporal lobe in the region of interest of the simulated custom coil. The subject's head was only moved in the  $z$ -direction since in practice that could be the only possible translation when a subject head is located in an MRI scanner. In all three cases when the simulated custom shim is added to the system shims, the simulated histogram becomes narrower which mean that the inhomogeneity is decreased.



a)

b)

**Figure 4.6** Planar slices of the field inhomogeneity through the centre of the region of interest when a) no shims, b) simulated custom shim and the existing system shims were used. The simulated custom shim reduces the field inhomogeneity by a factor of 1.3 when added to the system shims as compared to that obtained using the shim system only.

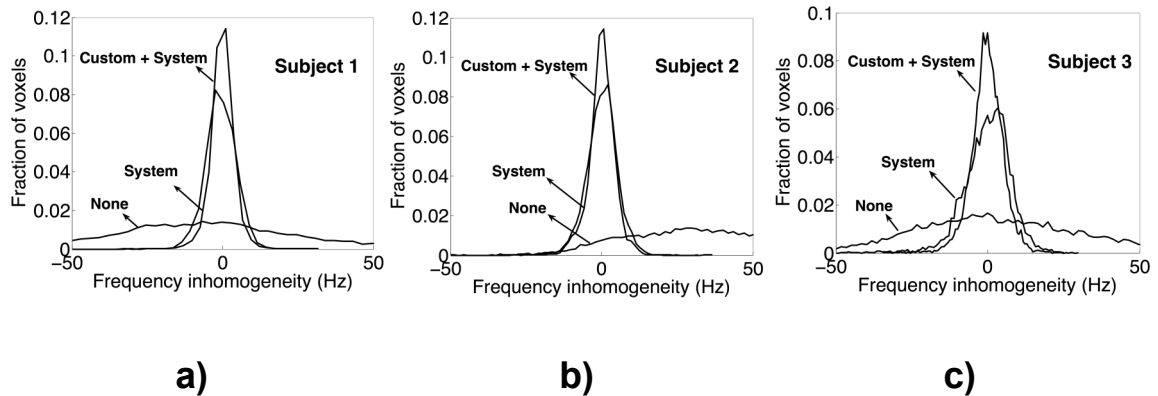


**Figure 4.7** Parts **a)**, **b)**, and **c)** show the simulated histograms of the frequency inhomogeneities for three subjects. Each figure shows the histogram of the unshimmed frequency inhomogeneities, the residual frequency inhomogeneities after shimmed with the system shims and the residual frequency inhomogeneities after shimmed with the simulated custom plus system shims. In all three subjects the line-width of the histogram of frequency inhomogeneities decreases after the addition of the custom coil to the system.

To calculate the reduction of the field inhomogeneity quantitatively, the standard deviation of each histogram was calculated and the results are shown in table 4.1. As shown in the table, the standard deviation of frequency inhomogeneity histograms was decreased by 70% when the system shims was applied alone. When the simulated custom shim was added to the system shims, the standard deviation was decreased by another 30%. In our field mapping measurements, two subjects were males and one subject was a female. As shown in figure 4.3, all three heads are different in shape and size. However, the improvement in the field inhomogeneities is consistent among all three subjects after adding the custom shim to the system shims. We believe that if the custom coil is applied to more subjects, it will improve the field inhomogeneities consistently.

Standard Deviation, $\sigma$ (Hz)			
	Subject #1	Subject #2	Subject #3
No shim	31.1	33.9	27.3
System shims	5.72	5.95	7.92
Custom+ system shims	4.71	4.90	5.42

**Table 4.1** Calculated standard deviations of the frequency inhomogeneities when no shim, system shims, and the simulated custom plus system shims were used for all three subjects. The addition of the custom shim improves the field inhomogeneities by up to 30%.

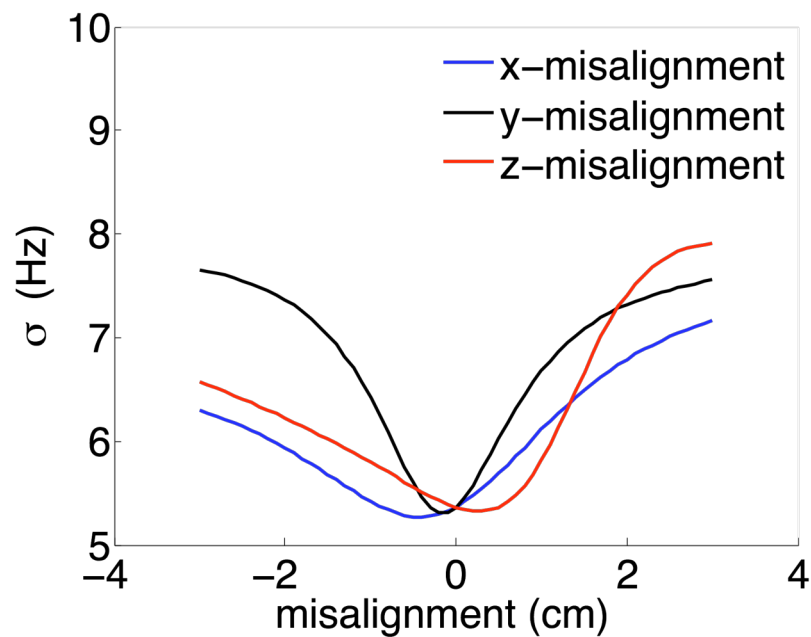


**Figure 4.8** The standard deviation of residual frequency inhomogeneities after shimmed with the simulated custom plus system shims was calculated for many misalignments of one subject's head within the custom coil. This figure shows that the misalignment of up to  $\pm 1$  cm could be tolerated in  $x$ -,  $y$ - and  $z$ - directions.

## 4.4 Conclusions

The results predict that a simulated custom coil insert would allow improvements in shimming of up to 30% for this specific head MRI system. This improvement was achieved when a custom shim was designed for a 7T head only MR system where the system shims are specifically designed for head. We believe that such a custom coil would improve head shimming significantly when used in whole body MRI scanners. We are currently studying the improvement of field inhomogeneity by adding a custom coil to a whole body 3T MR system. As mentioned, the current required for the custom coil is small, which means it would need no cooling and it would not experience large Lorentz forces.

Our goal is to develop a series of coil inserts, each customized to a different region of the brain or other anatomical area. These coils would be inserted into the scanner bore as necessary for different studies.

## 4.5 References or Bibliography

1. Takahashi M, Uematsu H, Hatabu H. MR imaging at high magnetic fields. *European Journal of Radiology* 2003;46(1):45-52.
2. Haacke EM, Tkach JA, Parrish TB. Reduction of  $T_2^*$  dephasing in gradient field-echo imaging. *Radiology* 1989;170(2):457-462.
3. Truonga TK, Clymerb BD, Chakeresa DW, Schmalbroc P. Three-dimensional numerical simulations of susceptibility-induced magnetic field inhomogeneities in the human head. *Magn Reson Imaging* 2002;20(10):759-770.
4. Turner R. A target field approach to optimal coil design. *J Phys [D]* 1986;19:L147-L151.
5. Turner R. Minimum inductance coils. *J Phys [E]* 1988;21:948-995.
6. Carlson JW, Derby KA, Hawryszko KC, Weideman M. Design and evaluation of shielded gradient coils. *Magn Reson Med* 1992;26(2):191-206.
7. Bowtell R, Robyr P. Multilayer Gradient Coil Design. *J Magn Reson* 1998;131(2):286-294.
8. Forbes LK, Crozier S. A Novel target-field method for finite-length magnetic resonance shim coils: I. zonal shims. *J Phys [D]* 2001;34:3447-3455
9. Forbes LK, Crozier S. A Novel target-field method for finite-length magnetic resonance shim coils: II. tesseral shims. *J Phys [D]* 2002;35:839-849
10. Forbes LK, Crozier S. A Novel target-field method for magnetic resonance shim coils: III. shielded zonal and tesseral coilsShims. *J Phys [D]* 2003;36,:68-80.
11. Pissanetzky S. Minimum Energy MRI Gradient Coils of General Geometry. *Measurement Science and Technology* 1992;3(7):667-673.



12. Lemdiasov RA, Ludwig R. A Stream Function Method For Gradient Coil Design. *Concepts in Magnetic Resonance Part B* 2005;26B(1):67-80.
13. Poole M, Bowtell R. Novel gradient coil designed using a boundary element method. *Concept Magn Reson [B]* 2007;31B:162-175
14. Soher BJ, Doraiswamy PM, Charles HC. A review of 1H MR spectroscopy findings in Alzheimer's disease. *Neuroimaging Clin N Am* 2005;15(4):847-852.
15. Reitz JR, Milford FJ, Christy RW. *Foundation of electromagnetic Theory*. New York: Addison Wesley; 1989.
16. Jackson JD. *Classical Electrodynamics*. New York: John Wiley & Sons; 1998.
17. Klassen LM, Menon RS. Robust Automated Shimming Technique Using Arbitrary Mapping Acquisition Parameters. *Magn Reson Med* 2004;51:881-887.
18. Hudson P, Hudson SD, Handler WB, Scholl TJ, Chronik BA. Quantitative Comparison of Minimum Inductance and Minimum Power Algorithms for the Design of Shim Coils for Small Animal Imaging. *Concepts Magn Reson Part B Magn Reson Eng* 2010;37B(2):65-74.
19. Press WH TS, Vetterling WT, Flannery BP. *Numerical Recipes*. New York: Cambridge University Press; 2007.

## 4.6 Appendix B

The goal is to find an optimal current distribution flowing on a cylindrical or any arbitrary shape surfaces to achieve a desired magnetic field in region of interest. The coil surface could be discretized into a mesh of triangles of the surface (12). The points at the corners of these triangles are called “nodes”. A current element includes all neighboring triangles of the chosen non-boundary node (see Figure 4.9a). For each node,  $n$ , a basis function,  $\mathbf{f}_n(\mathbf{r})$ , is defined to describe a circulating current around the nodes through the adjoining triangles.

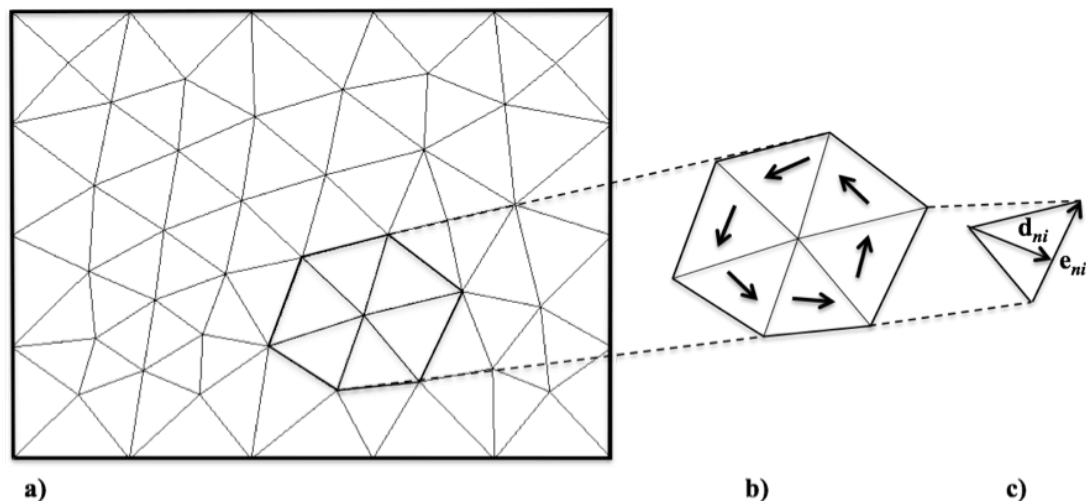


**Figure 4.9** The discretized current carrying surface is shown in a), the current element and the basis function  $\mathbf{f}_n$  for the  $n^{\text{th}}$  node are shown in b), and the length,  $\mathbf{d}_{ni}$ , and the width,  $\mathbf{e}_{ni}$ , vectors of one of the triangles associated with the selected node are shown in c).

A current density on a surface is described as the summation of all basis functions for  $N$  nodes and weighted by  $I_n$ :

$$\mathbf{J}(\mathbf{r}) \approx \sum_{n=1}^N I_n \mathbf{f}_n(\mathbf{r}) \quad (\text{B1})$$

Each basis function,  $\mathbf{f}_n(\mathbf{r})$ , could be described as:

$$\mathbf{f}_n(\mathbf{r}) = \frac{\mathbf{e}_{ni}}{|\mathbf{e}_{ni}|} \frac{1}{|\mathbf{d}_{ni}|} = \mathbf{v}_{ni} \quad i = 1, \dots, N_n \quad \text{if } \mathbf{r} \text{ belongs to } \Delta_n \quad (\text{B2})$$

where in each neighboring triangle vector  $\mathbf{e}$  is the opposite edge and vector  $\mathbf{d}$  is the minimum distance vector and perpendicular to  $\mathbf{e}$  (see Figure 4.9b).  $N_n$  is the number of triangles in a particular current element and  $\Delta_{ni}$  denotes an  $i^{\text{th}}$  triangle belonging to node  $n$ . This formalism for the basis function provides a system, in which the current density is divergence-free on the surface,  $\nabla \cdot \mathbf{J}(\mathbf{r}) = 0$ . Using Eq. [B1] the magnetic vector potential  $\mathbf{A}(\mathbf{r})$  can be written as (15,16):

$$\mathbf{A}(\mathbf{r}) = \frac{\mu_0}{4\pi} \int \frac{\mathbf{J}(\mathbf{r}')}{|\mathbf{r} - \mathbf{r}'|} dS' \approx \frac{\mu_0}{4\pi} \sum_{n=1}^N I_n \int \frac{\mathbf{f}_n(\mathbf{r}')}{|\mathbf{r} - \mathbf{r}'|} dS'. \quad (\text{B3})$$

The magnetic field is then:

$$\mathbf{B}(\mathbf{r}) = \nabla \times \mathbf{A}(\mathbf{r}) \approx \frac{\mu_0}{4\pi} \sum_{n=1}^N I_n \int \nabla \times \frac{\mathbf{f}_n(\mathbf{r}')}{|\mathbf{r} - \mathbf{r}'|} dS' = \frac{\mu_0}{4\pi} \sum_{n=1}^N I_n \int \nabla \frac{1}{|\mathbf{r} - \mathbf{r}'|} \times \mathbf{f}_n(\mathbf{r}') dS'. \quad (\text{B4})$$

To simplify the notation in the equation above, we introduce  $\mathbf{c}_n$ :

$$\mathbf{B}_z(\mathbf{r}) = \sum_{n=1}^N I_n \mathbf{c}_n(\mathbf{r}) \quad (\text{B5})$$

where:

$$\mathbf{c}_n(\mathbf{r}) = \frac{\mu_0}{4\pi} \int \left[ \frac{-f_{ny}(\mathbf{r}')(x - x') + f_{nx}(\mathbf{r}')(y - y')}{|\mathbf{r} - \mathbf{r}'|^3} \right] dS'. \quad (\text{B6})$$

In Eq. [B7], the integration over the surface,  $\int dS'$ , is now equivalent to integration over the surface of elements containing the node  $n$ . Because the basis functions are made

up of  $N_n$  parts, the  $c_n(\mathbf{r})$  matrix is calculated by summing over the set of functions linked to each triangle associated with each node:

$$c_n(\mathbf{r}) = \frac{\mu_0}{4\pi} \sum_{i=1}^{N_n} \int \left[ \frac{-v_{niy}(\mathbf{r}')(\mathbf{x} - \mathbf{x}') + v_{nix}(\mathbf{r}')(\mathbf{y} - \mathbf{y}')}{|\mathbf{r} - \mathbf{r}'|^3} \right] dS' \quad (\text{B7})$$

The power dissipation,  $P$ , in the coil can be written as (16):

$$P(\mathbf{r}) = \frac{\rho}{t} \int \int \mathbf{J}(\mathbf{r}') \cdot \mathbf{J}(\mathbf{r}) dS' dS \quad (\text{B8})$$

Where  $t$  is the thickness and  $\rho$  is the resistivity of the coil. Using the discretized current density, Eq. [B1], the discretized version of power could be written as:

$$P(\mathbf{r}) \approx \frac{\rho}{t} \sum_{m=1}^N \sum_{n=1}^N I_n I_m \int \int \mathbf{f}_n(\mathbf{r}) \cdot \mathbf{f}_m(\mathbf{r}') dS' dS = \sum_{m=1}^N \sum_{n=1}^N I_n I_m P_{mn} \quad (\text{B9})$$

where  $I_a$  is the current flowing on the surface of the coil which could be normalized to one. Similarly the inductance could be discretized using Eq. [B1], which will form a quadratic system of equations:

$$L(\mathbf{r}) \approx \frac{\mu_0}{4\pi} \sum_{n=1}^N \sum_{m=1}^N I_n I_m \int \int \frac{\mathbf{f}_n(\mathbf{r}) \cdot \mathbf{f}_m(\mathbf{r}')}{|\mathbf{r} - \mathbf{r}'|} dS' dS = \frac{\mu_0}{4\pi} \sum_{m=1}^N \sum_{n=1}^N I_n I_m L_{mn} \quad (\text{B10})$$

where  $L_{mn}$  is the self-inductance matrix that could be expanded in terms of  $v_{ni}$  using Eq. [B2]:

$$L_{mn} \approx \frac{\mu_0}{4\pi} \int \int \frac{\mathbf{f}_n(\mathbf{r}) \cdot \mathbf{f}_m(\mathbf{r}')}{|\mathbf{r} - \mathbf{r}'|} dS' dS = \frac{\mu_0}{4\pi} \sum_i \sum_j v_{mi} v_{nj} \int \int \frac{dS' dS}{|\mathbf{r}_{mi} - \mathbf{r}'_{nj}|}. \quad (\text{B11})$$

The current density,  $\mathbf{J}(\mathbf{r}')$ , experiences the torque vector,  $\mathbf{M}$ , in the external main magnetic field,  $\mathbf{B}_0$  (16):

$$\mathbf{M} = \int \mathbf{r} \times [\mathbf{J}(\mathbf{r}') \times \mathbf{B}_0] dS \quad (\text{B12})$$

Therefore three components of the torque are described and discretized as:

$$M_x = B_0 \int \int J_x z dS \approx B_0 \sum_{n=1}^N I_n \int f_{nx} z dS = B_0 \sum_{n=1}^N I_n \sum_{i=1}^{N_n} \int v_{nx} z dS, \quad (\text{B13})$$

$$M_y = B_0 \int \int J_y z dS \approx B_0 \sum_{n=1}^N I_n \int f_{ny} z dS = B_0 \sum_{n=1}^N I_n \sum_{i=1}^{N_n} \int v_{ny} z dS, \quad (\text{B14})$$

$$\begin{aligned} M_z &= -B_0 \int \int (J_x x + J_y y) dS \approx -B_0 \sum_{n=1}^N I_n \int (f_{nx} x + f_{ny} y) dS \\ &= -B_0 \sum_{n=1}^N I_n \sum_{i=1}^{N_n} \int (v_{nx} x + v_{ny} y) dS. \end{aligned} \quad (\text{B15})$$

To optimize the physical parameters of the coil such as self inductance,  $\mathbf{L}$ , resistance,  $\mathbf{R}$ , and torque,  $\mathbf{M}$ , and to create a magnetic field,  $\mathbf{B}_z$  that matches the desired target field  $\mathbf{B}_z^t$ , we introduce a functional that consists of the deviation of the magnetic field from the desired target field, self inductance,  $\mathbf{L}$ , power,  $\mathbf{P}$ , and torque,  $\mathbf{M}$ :

$$\begin{aligned}
U &= \frac{1}{2} \sum_{k=1}^K W(\mathbf{r}_k) \left( \mathbf{B}_z(\mathbf{r}_k) - \mathbf{B}'_z(\mathbf{r}_k) + \mathbf{B}_{\text{off},z} \right)^2 + \frac{\alpha}{2} L \\
&+ \frac{\beta}{2} P - \sum_{p=1}^P \left( \lambda_{px} M_{px} + \lambda_{py} M_{py} + \lambda_{pz} M_{pz} \right) \\
&= \frac{1}{2} \sum_{k=1}^K W(\mathbf{r}_k) \left( \mathbf{B}_z(\mathbf{r}_k) - \mathbf{B}'_z(\mathbf{r}_k) + \mathbf{B}_{\text{off},z} \right)^2 \\
&+ \frac{\alpha}{2} \sum_{m=1}^N \sum_{n=1}^N I_n I_m L_{mn} + \frac{\beta}{2} \sum_{m=1}^N \sum_{n=1}^N I_n I_m P_{mn} \\
&- B_0 \sum_{p=1}^P \lambda_{px} \sum_{n=1}^N \delta_{n \in p} I_n \int f_{nx} z dS \\
&- B_0 \sum_{p=1}^P \lambda_{py} \sum_{n=1}^N \delta_{n \in p} I_n \int f_{ny} z dS \\
&+ B_0 \sum_{p=1}^P \lambda_{pz} \sum_{n=1}^N \delta_{n \in p} I_n \int (f_{nx} x + f_{ny} y) dS
\end{aligned} \tag{B16}$$

where  $W(\mathbf{r}_k)$  is a weighting function that can be set to adjust the accuracy with which the magnetic field is generated by the coil,  $\mathbf{B}_{\text{off},z}$  is a field offset that is obtained as a solution in the minimization,  $\alpha$  and  $\beta$  are weighting factors whose values determine the importance of self-inductance minimization and power minimization respectively.  $\lambda_{px}$ ,  $\lambda_{py}$  and  $\lambda_{pz}$  are Lagrange multipliers for the  $p^{\text{th}}$  surface.  $\delta_{n \in p}$  is a term that is equal to 1 if the node  $n$  belongs to the  $p^{\text{th}}$  surface, and 0 if it does not. This term allows for torque minimization on any number of surfaces. By differentiating the functional with respect to each unknown variable such as  $I_n$  values,  $\mathbf{B}_{\text{off},z}$  and the Lagrange multipliers,  $\lambda$  and setting it to zero,  $I_n$  values,  $\mathbf{B}_{\text{off},z}$  and the Lagrange multipliers,  $\lambda$  could be found:

$$\begin{aligned}
0 = \frac{\partial U}{\partial I_m} &= \sum_{m=1}^{N'} \underbrace{\left( \sum_{k=1}^K W(\mathbf{r}_k) c_m(\mathbf{r}_k) c_n(\mathbf{r}_k) + \alpha L_{mn} + \beta P_{mn} \right)}_A I_n \\
&+ \underbrace{B_{\text{off},z}}_B \sum_{k=1}^K W(\mathbf{r}_k) c_m(\mathbf{r}_k) + \sum_{p=1}^P \underbrace{\hat{\lambda}_{px} \delta_{n \in p} \int_{-T_{pA}} -f_{mx} z dS}_{-T_{pA}} \\
&+ \sum_{p=1}^P \underbrace{\hat{\lambda}_{py} \delta_{n \in p} \int_{T_{pB}} -f_{my} z dS}_{T_{pB}} + \sum_{p=1}^P \underbrace{\hat{\lambda}_{pz} \delta_{n \in p} \int_{T_{pC}} (f_{mx} x + f_{my} y) dS}_{T_{pC}} \\
&- \underbrace{\sum_{k=1}^K W(\mathbf{r}_k) c_m(\mathbf{r}_k) B'_z(\mathbf{r}_k)}_E, \quad m = 1, \dots, N
\end{aligned} \tag{B17}$$

$$0 = \frac{\partial U}{\partial B_{\text{off},z}} = \sum_{m=1}^{N'} \underbrace{\left( \sum_{k=1}^K W(\mathbf{r}_k) c_n(\mathbf{r}_k) \right)}_C I_n + \underbrace{B_{\text{off},z}}_D \sum_{k=1}^K W(\mathbf{r}_k) - \underbrace{\sum_{k=1}^K W(\mathbf{r}_k) B'_z(\mathbf{r}_k)}_F \tag{B18}$$

$$0 = \frac{\partial U}{\partial \hat{\lambda}_{p'x}} = \sum_{n=1}^{N'} \underbrace{\left( \delta_{n \in p'} \int_{T_A} -f_{nx} z dS \right)}_{T_A} I_n \quad p' = 1, \dots, P \tag{B19}$$

$$0 = \frac{\partial U}{\partial \hat{\lambda}_{p'y}} = \sum_{n=1}^{N'} \underbrace{\left( \delta_{n \in p'} \int_{T_B} -f_{ny} z dS \right)}_{T_B} I_n \quad p' = 1, \dots, P \tag{B20}$$

$$0 = \frac{\partial U}{\partial \hat{\lambda}_{p'z}} = \sum_{n=1}^{N'} \underbrace{\left( \delta_{n \in p'} \int_{T_C} (f_{nx} x + f_{ny} y) dS \right)}_{T_C} I_n \quad p' = 1, \dots, P \tag{B21}$$

In Eq [B20],  $\hat{\lambda}$  is a Lagrange multiplier combined with the static magnetic field,  $\mathbf{B}_0$  and in Eqs [B22-B23],  $\mathbf{P}$  is the number of surfaces composing the coil. Eqs. [B20] to [B24] could be assembled into a global matrix equation:

$$\mathbf{Z}\mathbf{I} = \mathbf{b} \quad (\text{B22})$$

If the number of surfaces  $\mathbf{P} = 1$ , the matrix equation could be shown as:

$$\underbrace{\begin{pmatrix} \left( \begin{array}{ccc} \ddots & \dots & \cdot \\ \vdots & \mathbf{A} & \vdots \\ \cdot & \dots & \ddots \end{array} \right) \left( \begin{array}{c} \vdots \\ \mathbf{B} \\ \vdots \end{array} \right) \left( \begin{array}{c} \vdots \\ -\mathbf{T}_{pA} \\ \vdots \end{array} \right) \left( \begin{array}{c} \vdots \\ -\mathbf{T}_{pB} \\ \vdots \end{array} \right) \left( \begin{array}{c} \vdots \\ -\mathbf{T}_{pC} \\ \vdots \end{array} \right) \\ \left( \dots \mathbf{C} \dots \right) \mathbf{0} \quad \mathbf{0} \quad \mathbf{0} \quad \mathbf{0} \\ \left( \dots \mathbf{T}_{pA} \dots \right) \mathbf{0} \quad \mathbf{0} \quad \mathbf{0} \quad \mathbf{0} \\ \left( \dots \mathbf{T}_{pB} \dots \right) \mathbf{0} \quad \mathbf{0} \quad \mathbf{0} \quad \mathbf{0} \\ \left( \dots \mathbf{T}_{pC} \dots \right) \mathbf{0} \quad \mathbf{0} \quad \mathbf{0} \quad \mathbf{0} \end{pmatrix} \begin{pmatrix} \left( \begin{array}{c} \vdots \\ \mathbf{I}_n \\ \vdots \end{array} \right) \\ \mathbf{B}_{off,z} \\ \lambda_{px} \\ \lambda_{py} \\ \lambda_{pz} \end{pmatrix} \right)}_{\mathbf{Z}} = \underbrace{\begin{pmatrix} \left( \begin{array}{c} \vdots \\ \mathbf{E} \\ \vdots \end{array} \right) \\ \mathbf{F} \\ \mathbf{0} \\ \mathbf{0} \\ \mathbf{0} \end{pmatrix}}_{\mathbf{b}} \quad (\text{B23})$$

Eq. [B25] is inverted to find  $\mathbf{I}$ , which contains  $\mathbf{I}_n$  values. Once  $\mathbf{I}_n$  values are known, the current density  $\mathbf{J}(\mathbf{r})$  could be found using Eq. [B1]. Having the current density, magnetic field, power, self-inductance and torque could simply be found using Eqs [B4,B9,B12] and [B15].



# Chapter 5

## 5 Conclusions

### 5.1 Thesis Summary

The problem of having magnetic field inhomogeneities caused by different magnetic susceptibilities within the human body was discussed in this thesis. In particular, with the recent movement towards higher magnetic field resonance imaging to benefit from higher signal to noise ratio (SNR), the field inhomogeneities become more intense and problematic as their magnitude scales with the strength of the magnetic field. As discussed in this thesis, many methods have been proposed to reduce the field inhomogeneities by either using ferroschims or shim coils which results in better quality MR images and more quantifiable MR spectra. This thesis has focused on designing high performance gradient and shim coils using a variety of methods to maximally decrease the magnetic field inhomogeneity present in the object being scanned. An extension of powerful gradient design tools based on constrained current minimum inductance was expanded to minimize power instead. Upon conclusion of this research an extension of the computationally simple Fourier series method was expanded to include arbitrary shim design. Finally, the recent innovation on the boundary element method for designing coils to produce arbitrary fields was applied to shimming the hippocampus specifically, as a test case.

A set of gradient and shim coils customized for small animal imaging was designed using minimum inductance and minimum power target field methods. A quantitative comparison of shim performance in terms of merit of inductance,  $ML$ , and merit of resistance,  $MR$ , for shim coils designed using both design algorithms showed

that the difference in  $ML$  and the difference in  $MR$  was less than 15%. Minimum inductance designs tend to feature oscillations within the current density; while minimum power designs tend to feature less rapidly-varying current densities and a lower power dissipation. Overall, the differences in coil performance obtained by the two methods were small. Using, the target field method, the length of the gradient and shim coils could not be controlled. Therefore, we decided to extend the Carlson Fourier series technique developed for designing gradient coils with finite length. By introducing a truncated 2D-Fourier series expansion of current density in the design algorithm, we designed a set of shim coils.

This technique is mathematically simple, easy to implement, computationally fast and allows for simple design of a shim set for use with short-bore magnets. A prototype set of shim coils was designed using Fourier series minimum inductance and minimum power algorithms. A quantitative comparison of shim coil performance in terms of merit of inductance,  $ML$ , and merit of resistance,  $MR$ , was made for coils, of length 50 cm, 60 cm, 80 cm, and 100 cm, designed using minimum power and minimum inductance algorithms. In each design case, the difference in  $ML$  and the difference in  $MR$  given by the two design methods was less than 6%. Across shim axes, the 80 cm length designs had the highest merit values (for both power and inductance). We concluded that the decreased complexity of the minimum power designs in terms of the wire pattern outweighs the slight decrease in the merits and the minimum power designs outperform the minimum inductance designs. This design method makes it possible to easily design a shim set of any desired order for any radius and length of surface, which makes the engineering of such a coil straightforward.

The boundary element method (BEM) capable of designing shim coils with widely varying geometry and off centered region of interest (ROI) is a powerful method that we used to design region specific custom shim coils. With the new idea of dividing the field inhomogeneities into two factors; relatively large inhomogeneities with minimal variation between subjects, and smaller, subject specific inhomogeneities, custom shim coils could be designed to correct for the large inhomogeneities that are consistent between subjects. Then the existing system shims could be used to correct the field on a

sample specific basis. We designed a custom coil to correct for the large field inhomogeneities existed in the medial temporal of the brain. The results showed an improvement of up to 30% in the field homogeneities when the custom coil was added to the head only 7T scanner. The subject misalignment of up to  $\pm 1$  cm with respect to the custom coil could be tolerated. In this study, a head only MRI scanner was used, where shim coils are specifically designed and built for the head. We believe that the custom coil could improve the field inhomogeneities by up to 50% when inserted in a whole body MRI scanner. The power of this method is that any geometry and any physically possible field can be produced, making it an extremely powerful and versatile tool. The only problem with methods such as these is that the coils are essentially coarse as they are produced on a mesh and often need further manipulation to make them useful from an engineering perspective.

## 5.2 Future Work

The Fourier series method has been used by another student to build a shim set which will be used for dynamic shimming. The benefit of the method was in the simplicity of the design.

A test case custom shim coil that has been designed for the medial temporal of the brain will be constructed and tested in the head only 7T MRI scanner. The custom coil will be located concentrically outside the RF coil and inside the magnet bore. The diameter of the coil will be limited by the diameter of the magnet bore and the RF coil. Therefore the dimensions of the coil could be different than the one designed in chapter 4.

It has been shown by simulation that the custom coil is considerably effective at reducing the susceptibility induced magnetic field inhomogeneities in the medial temporal lobe where the hippocampi are located. This region of the brain suffers from large field inhomogeneities caused by magnetic susceptibility differences at tissue/air interfaces. The presence of the large field inhomogeneities ultimately increases the complexity of metabolite quantification in  $^1\text{H}$  spectroscopy of the hippocampus. Our goal is to increase

the accuracy of metabolites measurement in the spectrum of the hippocampus by applying the custom coil to correct for the significant field inhomogeneities existed in this region of the brain. Accurate quantification of metabolite spectra could possibly facilitate diagnosis of Alzheimer's disease and other neuro-degenerative diseases. Ultimately we are planning to design and build separate coils for the frontal, temporal, parietal or occipital lobes of the human brain, and these shim coils would be switched into and out-of the scanner on a study-specific basis.

### **5.3 Final Conclusions**

With the design of efficient traditional gradient and shim coils is now being trivial, region specific custom coils described in this thesis are promising tools for shimming at high fields, where shimming is of utmost importance. It has been shown by simulation that these coils significantly reduce the magnetic field inhomogeneities caused by differences in magnetic susceptibility in the head. This new approach to shimming has the potential to improve the quality of MR images and spectra that benefits from increased signal to noise ratio (SNR) at high magnetic field strength.

# Letters of Permission

Rightslink Printable License

3/10/11 4:07 PM

## JOHN WILEY AND SONS LICENSE TERMS AND CONDITIONS

Mar 10, 2011

This is a License Agreement between Parisa Hudson ("You") and John Wiley and Sons ("John Wiley and Sons") provided by Copyright Clearance Center ("CCC"). The license consists of your order details, the terms and conditions provided by John Wiley and Sons, and the payment terms and conditions.

**All payments must be made in full to CCC. For payment instructions, please see information listed at the bottom of this form.**

License Number	2625520882787
License date	Mar 10, 2011
Licensed content publisher	John Wiley and Sons
Licensed content publication	Concepts in Magnetic Resonance: Part A, Bridging Education and Research
Licensed content title	Quantitative comparison of minimum inductance and minimum power algorithms for the design of shim coils for small animal imaging
Licensed content author	Parisa Hudson, Stephen D. Hudson, William B. Handler, Timothy J. Scholl, Blaine A. Chronik
Licensed content date	Apr 1, 2010
Start page	65
End page	74
Type of use	Dissertation/Thesis
Requestor type	Author of this Wiley article
Format	Print and electronic
Portion	Full article
Will you be translating?	No
Order reference number	
Total	0.00 USD

[Terms and Conditions](#)

### TERMS AND CONDITIONS

This copyrighted material is owned by or exclusively licensed to John Wiley & Sons, Inc. or one of its group companies (each a "Wiley Company") or a society for whom a Wiley Company has exclusive publishing rights in relation to a particular journal (collectively "WILEY"). By clicking "accept" in connection with completing this licensing transaction, you agree that the following terms and conditions apply to this transaction (along with the billing and payment terms and conditions established by the Copyright Clearance Center Inc., ("CCC's Billing and Payment terms

time at <http://myaccount.copyright.com>)

#### Terms and Conditions

1. The materials you have requested permission to reproduce (the "Materials") are protected by copyright.
2. You are hereby granted a personal, non-exclusive, non-sublicensable, non-transferable, worldwide, limited license to reproduce the Materials for the purpose specified in the licensing process. This license is for a one-time use only with a maximum distribution equal to the number that you identified in the licensing process. Any form of republication granted by this licence must be completed within two years of the date of the grant of this licence (although copies prepared before may be distributed thereafter). The Materials shall not be used in any other manner or for any other purpose. Permission is granted subject to an appropriate acknowledgement given to the author, title of the material/book/journal and the publisher and on the understanding that nowhere in the text is a previously published source acknowledged for all or part of this Material. Any third party material is expressly excluded from this permission.
3. With respect to the Materials, all rights are reserved. Except as expressly granted by the terms of the license, no part of the Materials may be copied, modified, adapted (except for minor reformatting required by the new Publication), translated, reproduced, transferred or distributed, in any form or by any means, and no derivative works may be made based on the Materials without the prior permission of the respective copyright owner. You may not alter, remove or suppress in any manner any copyright, trademark or other notices displayed by the Materials. You may not license, rent, sell, loan, lease, pledge, offer as security, transfer or assign the Materials, or any of the rights granted to you hereunder to any other person.
4. The Materials and all of the intellectual property rights therein shall at all times remain the exclusive property of John Wiley & Sons Inc or one of its related companies (WILEY) or their respective licensors, and your interest therein is only that of having possession of and the right to reproduce the Materials pursuant to Section 2 herein during the continuance of this Agreement. You agree that you own no right, title or interest in or to the Materials or any of the intellectual property rights therein. You shall have no rights hereunder other than the license as provided for above in Section 2. No right, license or interest to any trademark, trade name, service mark or other branding ("Marks") of WILEY or its licensors is granted hereunder, and you agree that you shall not assert any such right, license or interest with respect thereto.
5. NEITHER WILEY NOR ITS LICENSORS MAKES ANY WARRANTY OR REPRESENTATION OF ANY KIND TO YOU OR ANY THIRD PARTY, EXPRESS, IMPLIED OR STATUTORY, WITH RESPECT TO THE MATERIALS OR THE ACCURACY OF ANY INFORMATION CONTAINED IN THE MATERIALS, INCLUDING, WITHOUT LIMITATION, ANY IMPLIED WARRANTY OF MERCHANTABILITY, ACCURACY, SATISFACTORY QUALITY, FITNESS FOR A PARTICULAR PURPOSE, USABILITY, INTEGRATION OR NON-INFRINGEMENT AND ALL SUCH WARRANTIES ARE HEREBY EXCLUDED BY WILEY AND ITS LICENSORS AND WAIVED BY YOU.
6. WILEY shall have the right to terminate this Agreement immediately upon breach of this Agreement by you.
7. You shall indemnify, defend and hold harmless WILEY, its Licensors and their respective directors, officers, agents and employees, from and against any actual or threatened claims, demands, causes of action or proceedings arising from any breach of this Agreement by you.
8. IN NO EVENT SHALL WILEY OR ITS LICENSORS BE LIABLE TO YOU OR ANY OTHER PARTY OR ANY OTHER PERSON OR ENTITY FOR ANY SPECIAL, CONSEQUENTIAL, INCIDENTAL, INDIRECT, EXEMPLARY OR PUNITIVE DAMAGES, HOWEVER CAUSED, ARISING OUT OF OR IN CONNECTION WITH THE DOWNLOADING, PROVISIONING, VIEWING OR USE OF THE MATERIALS REGARDLESS OF THE FORM OF ACTION, WHETHER FOR BREACH OF CONTRACT, BREACH OF WARRANTY,

TORT, NEGLIGENCE, INFRINGEMENT OR OTHERWISE (INCLUDING, WITHOUT LIMITATION, DAMAGES BASED ON LOSS OF PROFITS, DATA, FILES, USE, BUSINESS OPPORTUNITY OR CLAIMS OF THIRD PARTIES), AND WHETHER OR NOT THE PARTY HAS BEEN ADVISED OF THE POSSIBILITY OF SUCH DAMAGES. THIS LIMITATION SHALL APPLY NOTWITHSTANDING ANY FAILURE OF ESSENTIAL PURPOSE OF ANY LIMITED REMEDY PROVIDED HEREIN.

9. Should any provision of this Agreement be held by a court of competent jurisdiction to be illegal, invalid, or unenforceable, that provision shall be deemed amended to achieve as nearly as possible the same economic effect as the original provision, and the legality, validity and enforceability of the remaining provisions of this Agreement shall not be affected or impaired thereby.

10. The failure of either party to enforce any term or condition of this Agreement shall not constitute a waiver of either party's right to enforce each and every term and condition of this Agreement. No breach under this agreement shall be deemed waived or excused by either party unless such waiver or consent is in writing signed by the party granting such waiver or consent. The waiver by or consent of a party to a breach of any provision of this Agreement shall not operate or be construed as a waiver of or consent to any other or subsequent breach by such other party.

11. This Agreement may not be assigned (including by operation of law or otherwise) by you without WILEY's prior written consent.

12. Any fee required for this permission shall be non-refundable after thirty (30) days from receipt.

13. These terms and conditions together with CCC's Billing and Payment terms and conditions (which are incorporated herein) form the entire agreement between you and WILEY concerning this licensing transaction and (in the absence of fraud) supersedes all prior agreements and representations of the parties, oral or written. This Agreement may not be amended except in writing signed by both parties. This Agreement shall be binding upon and inure to the benefit of the parties' successors, legal representatives, and authorized assigns.

14. In the event of any conflict between your obligations established by these terms and conditions and those established by CCC's Billing and Payment terms and conditions, these terms and conditions shall prevail.

15. WILEY expressly reserves all rights not specifically granted in the combination of (i) the license details provided by you and accepted in the course of this licensing transaction, (ii) these terms and conditions and (iii) CCC's Billing and Payment terms and conditions.

16. This Agreement will be void if the Type of Use, Format, Circulation, or Requestor Type was misrepresented during the licensing process.

17. This Agreement shall be governed by and construed in accordance with the laws of the State of New York, USA, without regards to such state's conflict of law rules. Any legal action, suit or proceeding arising out of or relating to these Terms and Conditions or the breach thereof shall be instituted in a court of competent jurisdiction in New York County in the State of New York in the United States of America and each party hereby consents and submits to the personal jurisdiction of such court, waives any objection to venue in such court and consents to service of process by registered or certified mail, return receipt requested, at the last known address of such party. . BY CLICKING ON THE "I ACCEPT" BUTTON, YOU ACKNOWLEDGE THAT YOU HAVE READ AND FULLY UNDERSTAND EACH OF THE SECTIONS OF AND PROVISIONS SET FORTH IN THIS AGREEMENT AND THAT YOU ARE IN AGREEMENT WITH AND ARE WILLING TO ACCEPT ALL OF YOUR OBLIGATIONS AS SET FORTH IN THIS AGREEMENT.

v1.4

**Gratis licenses (referencing \$0 in the Total field) are free. Please retain this printable license for your reference. No payment is required.**

**If you would like to pay for this license now, please remit this license along with your payment made payable to "COPYRIGHT CLEARANCE CENTER" otherwise you will be invoiced within 48 hours of the license date. Payment should be in the form of a check or money order referencing your account number and this invoice number RLNK10947231.**

**Once you receive your invoice for this order, you may pay your invoice by credit card. Please follow instructions provided at that time.**

**Make Payment To:  
Copyright Clearance Center  
Dept 001  
P.O. Box 843006  
Boston, MA 02284-3006**

**For suggestions or comments regarding this order, contact Rightslink Customer Support: [customercare@copyright.com](mailto:customercare@copyright.com) or +1-877-622-5543 (toll free in the US) or +1-978-646-2777.**

---

---



**JOHN WILEY AND SONS LICENSE  
TERMS AND CONDITIONS**

Mar 10, 2011

This is a License Agreement between Parisa Hudson ("You") and John Wiley and Sons ("John Wiley and Sons") provided by Copyright Clearance Center ("CCC"). The license consists of your order details, the terms and conditions provided by John Wiley and Sons, and the payment terms and conditions.

**All payments must be made in full to CCC. For payment instructions, please see information listed at the bottom of this form.**

License Number	2625521409201
License date	Mar 10, 2011
Licensed content publisher	John Wiley and Sons
Licensed content publication	Concepts in Magnetic Resonance: Part A, Bridging Education and Research
Licensed content title	Finite-length shim coil design using a fourier series minimum inductance and minimum power algorithm
Licensed content author	Parisa Hudson, Stephen D. Hudson, William B. Handler, Blaine A. Chronik
Licensed content date	Oct 1, 2010
Start page	245
End page	253
Type of use	Dissertation/Thesis
Requestor type	Author of this Wiley article
Format	Print and electronic
Portion	Full article
Will you be translating?	No
Order reference number	
Total	0.00 USD

Terms and Conditions

**TERMS AND CONDITIONS**

This copyrighted material is owned by or exclusively licensed to John Wiley & Sons, Inc. or one of its group companies (each a "Wiley Company") or a society for whom a Wiley Company has exclusive publishing rights in relation to a particular journal (collectively "WILEY"). By clicking "accept" in connection with completing this licensing transaction, you agree that the following terms and conditions apply to this transaction (along with the billing and payment terms and conditions established by the Copyright Clearance Center Inc., ("CCC's Billing and Payment terms and conditions"), at the time that you opened your Rightslink account (these are available at any

time at <http://myaccount.copyright.com>)

#### Terms and Conditions

1. The materials you have requested permission to reproduce (the "Materials") are protected by copyright.
2. You are hereby granted a personal, non-exclusive, non-sublicensable, non-transferable, worldwide, limited license to reproduce the Materials for the purpose specified in the licensing process. This license is for a one-time use only with a maximum distribution equal to the number that you identified in the licensing process. Any form of republication granted by this licence must be completed within two years of the date of the grant of this licence (although copies prepared before may be distributed thereafter). The Materials shall not be used in any other manner or for any other purpose. Permission is granted subject to an appropriate acknowledgement given to the author, title of the material/book/journal and the publisher and on the understanding that nowhere in the text is a previously published source acknowledged for all or part of this Material. Any third party material is expressly excluded from this permission.
3. With respect to the Materials, all rights are reserved. Except as expressly granted by the terms of the license, no part of the Materials may be copied, modified, adapted (except for minor reformatting required by the new Publication), translated, reproduced, transferred or distributed, in any form or by any means, and no derivative works may be made based on the Materials without the prior permission of the respective copyright owner. You may not alter, remove or suppress in any manner any copyright, trademark or other notices displayed by the Materials. You may not license, rent, sell, loan, lease, pledge, offer as security, transfer or assign the Materials, or any of the rights granted to you hereunder to any other person.
4. The Materials and all of the intellectual property rights therein shall at all times remain the exclusive property of John Wiley & Sons Inc or one of its related companies (WILEY) or their respective licensors, and your interest therein is only that of having possession of and the right to reproduce the Materials pursuant to Section 2 herein during the continuance of this Agreement. You agree that you own no right, title or interest in or to the Materials or any of the intellectual property rights therein. You shall have no rights hereunder other than the license as provided for above in Section 2. No right, license or interest to any trademark, trade name, service mark or other branding ("Marks") of WILEY or its licensors is granted hereunder, and you agree that you shall not assert any such right, license or interest with respect thereto.
5. NEITHER WILEY NOR ITS LICENSORS MAKES ANY WARRANTY OR REPRESENTATION OF ANY KIND TO YOU OR ANY THIRD PARTY, EXPRESS, IMPLIED OR STATUTORY, WITH RESPECT TO THE MATERIALS OR THE ACCURACY OF ANY INFORMATION CONTAINED IN THE MATERIALS, INCLUDING, WITHOUT LIMITATION, ANY IMPLIED WARRANTY OF MERCHANTABILITY, ACCURACY, SATISFACTORY QUALITY, FITNESS FOR A PARTICULAR PURPOSE, USABILITY, INTEGRATION OR NON-INFRINGEMENT AND ALL SUCH WARRANTIES ARE HEREBY EXCLUDED BY WILEY AND ITS LICENSORS AND WAIVED BY YOU.
6. WILEY shall have the right to terminate this Agreement immediately upon breach of this Agreement by you.
7. You shall indemnify, defend and hold harmless WILEY, its Licensors and their respective directors, officers, agents and employees, from and against any actual or threatened claims, demands, causes of action or proceedings arising from any breach of this Agreement by you.
8. IN NO EVENT SHALL WILEY OR ITS LICENSORS BE LIABLE TO YOU OR ANY OTHER PARTY OR ANY OTHER PERSON OR ENTITY FOR ANY SPECIAL, CONSEQUENTIAL, INCIDENTAL, INDIRECT, EXEMPLARY OR PUNITIVE DAMAGES, HOWEVER CAUSED, ARISING OUT OF OR IN CONNECTION WITH THE DOWNLOADING, PROVISIONING, VIEWING OR USE OF THE MATERIALS REGARDLESS OF THE FORM OF ACTION, WHETHER FOR BREACH OF CONTRACT, BREACH OF WARRANTY,

TORT, NEGLIGENCE, INFRINGEMENT OR OTHERWISE (INCLUDING, WITHOUT LIMITATION, DAMAGES BASED ON LOSS OF PROFITS, DATA, FILES, USE, BUSINESS OPPORTUNITY OR CLAIMS OF THIRD PARTIES), AND WHETHER OR NOT THE PARTY HAS BEEN ADVISED OF THE POSSIBILITY OF SUCH DAMAGES. THIS LIMITATION SHALL APPLY NOTWITHSTANDING ANY FAILURE OF ESSENTIAL PURPOSE OF ANY LIMITED REMEDY PROVIDED HEREIN.

9. Should any provision of this Agreement be held by a court of competent jurisdiction to be illegal, invalid, or unenforceable, that provision shall be deemed amended to achieve as nearly as possible the same economic effect as the original provision, and the legality, validity and enforceability of the remaining provisions of this Agreement shall not be affected or impaired thereby.

10. The failure of either party to enforce any term or condition of this Agreement shall not constitute a waiver of either party's right to enforce each and every term and condition of this Agreement. No breach under this agreement shall be deemed waived or excused by either party unless such waiver or consent is in writing signed by the party granting such waiver or consent. The waiver by or consent of a party to a breach of any provision of this Agreement shall not operate or be construed as a waiver of or consent to any other or subsequent breach by such other party.

11. This Agreement may not be assigned (including by operation of law or otherwise) by you without WILEY's prior written consent.

12. Any fee required for this permission shall be non-refundable after thirty (30) days from receipt.

13. These terms and conditions together with CCC's Billing and Payment terms and conditions (which are incorporated herein) form the entire agreement between you and WILEY concerning this licensing transaction and (in the absence of fraud) supersedes all prior agreements and representations of the parties, oral or written. This Agreement may not be amended except in writing signed by both parties. This Agreement shall be binding upon and inure to the benefit of the parties' successors, legal representatives, and authorized assigns.

14. In the event of any conflict between your obligations established by these terms and conditions and those established by CCC's Billing and Payment terms and conditions, these terms and conditions shall prevail.

15. WILEY expressly reserves all rights not specifically granted in the combination of (i) the license details provided by you and accepted in the course of this licensing transaction, (ii) these terms and conditions and (iii) CCC's Billing and Payment terms and conditions.

16. This Agreement will be void if the Type of Use, Format, Circulation, or Requestor Type was misrepresented during the licensing process.

17. This Agreement shall be governed by and construed in accordance with the laws of the State of New York, USA, without regards to such state's conflict of law rules. Any legal action, suit or proceeding arising out of or relating to these Terms and Conditions or the breach thereof shall be instituted in a court of competent jurisdiction in New York County in the State of New York in the United States of America and each party hereby consents and submits to the personal jurisdiction of such court, waives any objection to venue in such court and consents to service of process by registered or certified mail, return receipt requested, at the last known address of such party. . BY CLICKING ON THE "I ACCEPT" BUTTON, YOU ACKNOWLEDGE THAT YOU HAVE READ AND FULLY UNDERSTAND EACH OF THE SECTIONS OF AND PROVISIONS SET FORTH IN THIS AGREEMENT AND THAT YOU ARE IN AGREEMENT WITH AND ARE WILLING TO ACCEPT ALL OF YOUR OBLIGATIONS AS SET FORTH IN THIS AGREEMENT.

v1.4

**Gratis licenses (referencing \$0 in the Total field) are free. Please retain this printable license for your reference. No payment is required.**

**If you would like to pay for this license now, please remit this license along with your payment made payable to "COPYRIGHT CLEARANCE CENTER" otherwise you will be invoiced within 48 hours of the license date. Payment should be in the form of a check or money order referencing your account number and this invoice number RLNK10947231.**

**Once you receive your invoice for this order, you may pay your invoice by credit card. Please follow instructions provided at that time.**

**Make Payment To:  
Copyright Clearance Center  
Dept 001  
P.O. Box 843006  
Boston, MA 02284-3006**

**For suggestions or comments regarding this order, contact Rightslink Customer Support: [customercare@copyright.com](mailto:customercare@copyright.com) or +1-877-622-5543 (toll free in the US) or +1-978-646-2777.**

---

---

**BMJ PUBLISHING GROUP LTD. LICENSE  
TERMS AND CONDITIONS**

Mar 11, 2011

This is a License Agreement between Parisa Hudson ("You") and BMJ Publishing Group Ltd. ("BMJ Publishing Group Ltd.") provided by Copyright Clearance Center ("CCC"). The license consists of your order details, the terms and conditions provided by BMJ Publishing Group Ltd., and the payment terms and conditions.

**All payments must be made in full to CCC. For payment instructions, please see information listed at the bottom of this form.**

License Number	2626121330161
License date	Mar 11, 2011
Licensed content publisher	BMJ Publishing Group Ltd.
Licensed content publication	Journal of Neurology, Neurosurgery and Psychiatry
Licensed content title	Quantitative MRI of the wrist and nerve conduction studies in patients with idiopathic carpal tunnel syndrome
Licensed content author	S Uchiyama, T Itsubo, T Yasutomi, H Nakagawa, M Kamimura, H Kato
Licensed content date	Aug 1, 2005
Volume number	76
Issue number	8
Type of Use	Thesis/Dissertation
Requestor type	Individual
Format	Print and electronic
Portion	Figure/table/extract
Number of figure/table/extracts	1
Will you be translating?	No
Circulation/distribution	10000
Title of your thesis / dissertation	Pushing the boundaries in gradient and shim design for MRI
Expected completion date	Mar 2011
Estimated size(pages)	120
BMJ VAT number	674738491
Billing Type	Invoice
Billing Address	1151 Richmond Street

Department of Physics and Astronomy  
 London, ON N6A3K7  
 Canada

Customer reference info

Permissions Cost	0.00 USD
VAT (0.0%)	0.00 USD
Total	0.00 USD

Terms and Conditions

### BMJ Group Terms and Conditions for Permissions

When you submit your order you are subject to the terms and conditions set out below. You will also have agreed to the Copyright Clearance Center's ("CCC") terms and conditions regarding billing and payment <https://s100.copyright.com/App/PaymentTermsAndConditions.jsp>. CCC are acting as the BMJ Publishing Group Limited's ("BMJ Group's") agent.

Subject to the terms set out herein, the BMJ Group hereby grants to you (the Licensee) a non-exclusive, non-transferable licence to re-use material as detailed in your request for this/those purpose(s) only and in accordance with the following conditions:

1) **Scope of Licence:** Use of the Licensed Material(s) is restricted to the ways specified by you during the order process and any additional use(s) outside of those specified in that request, require a further grant of permission.

2) **Acknowledgement:** In all cases, due acknowledgement to the original publication with permission from the BMJ Group should be stated adjacent to the reproduced Licensed Material. The format of such acknowledgement should read as follows:

"Reproduced from [publication title, author(s), volume number, page numbers, copyright notice year] with permission from BMJ Publishing Group Ltd."

3) **Third Party Material:** BMJ Group acknowledges to the best of its knowledge, it has the rights to licence your reuse of the Licensed Material, subject always to the caveat that images/diagrams, tables and other illustrative material included within, which have a separate copyright notice, are presumed as excluded from the licence. Therefore, you should ensure that the Licensed Material you are requesting is original to BMJ Group and does not carry the copyright of another entity (as credited in the published version). If the credit line on any part of the material you have requested in any way indicates that it was reprinted or adapted by BMJ Group with permission from another source, then you should seek permission from that source directly to re-use the Licensed Material, as this is outside of the licence granted herein.

4) **Altering/Modifying Material:** The text of any material for which a licence is granted may not be altered in any way without the prior express permission of the BMJ Group. Subject to Clause 3 above however, single figure adaptations do not require BMJ Group's approval; however, the adaptation should be credited as follows:

"Adapted by permission from BMJ Publishing Group Limited. [publication title, author, volume number, page numbers, copyright notice year]"

5) **Reservation of Rights:** The BMJ Group reserves all rights not specifically granted in the combination of (i) the licence details provided by you and accepted in the course of this licensing transaction, (ii) these terms and conditions and (iii) CCC's Billing and Payment Terms and Conditions.

**6) Timing of Use:** First use of the Licensed Material must take place within 12 months of the grant of permission.

**7) Creation of Contract and Termination:** Once you have submitted an order via Rightslink and this is received by CCC, and subject to you completing accurate details of your proposed use, this is when a binding contract is in effect and our acceptance occurs. As you are ordering rights from a periodical, to the fullest extent permitted by law, you will have no right to cancel the contract from this point other than for BMJ Group's material breach or fraudulent misrepresentation or as otherwise permitted under a statutory right. Payment must be made in accordance with CCC's Billing and Payment Terms and conditions. In the event that you breach any material condition of these terms and condition or any of CCC's Billing and Payment Terms and Conditions, the license is automatically terminated upon written notice from the BMJ Group or CCC or as otherwise provided for in CCC's Billing and Payment Terms and Conditions, where these apply.. Continued use of materials where a licence has been terminated, as well as any use of the Licensed Materials beyond the scope of an unrevoked licence, may constitute intellectual property rights infringement and BMJ Group reserves the right to take any and all action to protect its intellectual property rights in the Licensed Materials.

**8. Warranties:** BMJ Group makes no express or implied representations or warranties with respect to the Licensed Material and to the fullest extent permitted by law this is provided on an "as is" basis. For the avoidance of doubt BMJ Group does not warrant that the Licensed Material is accurate or fit for any particular purpose.

**9. Limitation of Liability:** To the fullest extent permitted by law, the BMJ Group disclaims all liability for any indirect, consequential or incidental damages (including without limitation, damages for loss of profits, information or interruption) arising out of the use or inability to use the Licensed Material or the inability to obtain additional rights to use the Licensed Material. To the fullest extent permitted by law, the maximum aggregate liability of the BMJ Group for any claims, costs, proceedings and demands for direct losses caused by BMJ Group's breaches of its obligations herein shall be limited to twice the amount paid by you to CCC for the licence granted herein.

**10. Indemnity:** You hereby indemnify and hold harmless the BMJ Group and their respective officers, directors, employees and agents, from and against any and all claims, costs, proceeding or demands arising out of your unauthorised use of the Licensed Material.

**11. No Transfer of License:** This licence is personal to you, and may not be assigned or transferred by you without prior written consent from the BMJ Group or its authorised agent(s). BMJ Group may assign or transfer any of its rights and obligations under this Agreement, upon written notice to you.

**12. No Amendment Except in Writing:** This licence may not be amended except in a writing signed by both parties (or, in the case of BMJ Group, by CCC on the BMJ Group's behalf).

**13. Objection to Contrary terms:** BMJ Group hereby objects to any terms contained in any purchase order, acknowledgment, check endorsement or other writing prepared by you, which terms are inconsistent with these terms and conditions or CCC's Billing and Payment Terms and Conditions. These terms and conditions, together with CCC's Billing and Payment Terms and Conditions (which to the extent they are consistent are incorporated herein), comprise the entire agreement between you and BMJ Group (and CCC) and the Licensee concerning this licensing transaction. In the event of any conflict between your obligations established by these terms and conditions and those established by CCC's Billing and Payment Terms and Conditions, these terms and conditions shall control.

**14. Revocation:** BMJ Group or CCC may, within 30 days of issuance of this licence, deny the

permissions described in this licence at their sole discretion, for any reason or no reason, with a full refund payable to you should you have not been able to exercise your rights in full. Notice of such denial will be made using the contact information provided by you. Failure to receive such notice from BMJ Group or CCC will not, to the fullest extent permitted by law alter or invalidate the denial. For the fullest extent permitted by law in no event will BMJ Group or CCC be responsible or liable for any costs, expenses or damage incurred by you as a result of a denial of your permission request, other than a refund of the amount(s) paid by you to BMJ Group and/or CCC for denied permissions.

**15. Restrictions to the license:**

**15.1 Promotion:** BMJ Group will not give permission to reproduce in full or in part any Licensed Material for use in the promotion of the following:

- a) non-medical products that are harmful or potentially harmful to health: alcohol, baby milks and/or, sun beds
- b) medical products that do not have a product license granted by the Medicines and Healthcare products Regulatory Agency (MHRA) or its international equivalents. Marketing of the product may start only after data sheets have been released to members of the medical profession and must conform to the marketing authorization contained in the product license.

**16. Translation:** This permission is granted for non-exclusive world English language rights only unless explicitly stated in your licence. If translation rights are granted, a professional translator should be employed and the content should be reproduced word for word preserving the integrity of the content.

**17. General:** Neither party shall be liable for failure, default or delay in performing its obligations under this Licence, caused by a Force Majeure event which shall include any act of God, war, or threatened war, act or threatened act of terrorism, riot, strike, lockout, individual action, fire, flood, drought, tempest or other event beyond the reasonable control of either party.

17.1 In the event that any provision of this Agreement is held to be invalid, the remainder of the provisions shall continue in full force and effect.

17.2 There shall be no right whatsoever for any third party to enforce the terms and conditions of this Agreement. The Parties hereby expressly wish to exclude the operation of the Contracts (Rights of Third Parties) Act 1999 and any other legislation which has this effect and is binding on this agreement.

17.3 To the fullest extent permitted by law, this Licence will be governed by the laws of England and shall be governed and construed in accordance with the laws of England. Any action arising out of or relating to this agreement shall be brought in courts situated in England save where it is necessary for BMJ Group for enforcement to bring proceedings to bring an action in an alternative jurisdiction.



**Gratis licenses (referencing \$0 in the Total field) are free. Please retain this printable license for your reference. No payment is required.**

**If you would like to pay for this license now, please remit this license along with your payment made payable to "COPYRIGHT CLEARANCE CENTER" otherwise you will be invoiced within 48 hours of the license date. Payment should be in the form of a check or money order referencing your account number and this invoice number RLNK10947971.**

**Once you receive your invoice for this order, you may pay your invoice by credit card. Please follow instructions provided at that time.**

**Make Payment To:  
Copyright Clearance Center  
Dept 001  
P.O. Box 843006  
Boston, MA 02284-3006**

**For suggestions or comments regarding this order, contact Rightslink Customer Support: [customercare@copyright.com](mailto:customercare@copyright.com) or +1-877-622-5543 (toll free in the US) or +1-978-646-2777.**

---

---

**ELSEVIER LICENSE  
TERMS AND CONDITIONS**

Mar 11, 2011

This is a License Agreement between Parisa Hudson ("You") and Elsevier ("Elsevier") provided by Copyright Clearance Center ("CCC"). The license consists of your order details, the terms and conditions provided by Elsevier, and the payment terms and conditions.

**All payments must be made in full to CCC. For payment instructions, please see information listed at the bottom of this form.**

Supplier	Elsevier Limited The Boulevard, Langford Lane Kidlington, Oxford, OX5 1GB, UK
Registered Company Number	1982084
Customer name	Parisa Hudson
Customer address	1151 Richmond Street London, ON N6A3K7
License number	2625730516310
License date	Mar 11, 2011
Licensed content publisher	Elsevier
Licensed content publication	Journal of Magnetic Resonance
Licensed content title	Sample-specific diamagnetic and paramagnetic passive shimming
Licensed content author	Kevin M. Koch, Peter B. Brown, Douglas L. Rothman, Robin A. de Graaf
Licensed content date	September 2006
Licensed content volume number	182
Licensed content issue number	1
Number of pages	9
Start Page	66
End Page	74
Type of Use	reuse in a thesis/dissertation
Intended publisher of new work	other
Portion	figures/tables/illustrations

Number of figures/tables/illustrations	1
Format	both print and electronic
Are you the author of this Elsevier article?	No
Will you be translating?	No
Order reference number	
Title of your thesis/dissertation	Pushing the boundaries in gradient and shim design for MRI
Expected completion date	Mar 2011
Estimated size (number of pages)	120
Elsevier VAT number	GB 494 6272 12
Permissions price	0.00 USD
VAT/Local Sales Tax	0.0 USD / 0.0 GBP
Total	0.00 USD
Terms and Conditions	

### INTRODUCTION

1. The publisher for this copyrighted material is Elsevier. By clicking "accept" in connection with completing this licensing transaction, you agree that the following terms and conditions apply to this transaction (along with the Billing and Payment terms and conditions established by Copyright Clearance Center, Inc. ("CCC"), at the time that you opened your Rightslink account and that are available at any time at <http://myaccount.copyright.com>).

### GENERAL TERMS

2. Elsevier hereby grants you permission to reproduce the aforementioned material subject to the terms and conditions indicated.

3. Acknowledgement: If any part of the material to be used (for example, figures) has appeared in our publication with credit or acknowledgement to another source, permission must also be sought from that source. If such permission is not obtained then that material may not be included in your publication/copies. Suitable acknowledgement to the source must be made, either as a footnote or in a reference list at the end of your publication, as follows:

"Reprinted from Publication title, Vol /edition number, Author(s), Title of article / title of chapter, Pages No., Copyright (Year), with permission from Elsevier [OR APPLICABLE SOCIETY COPYRIGHT OWNER]." Also Lancet special credit - "Reprinted from The Lancet, Vol. number, Author(s), Title of article, Pages No., Copyright (Year), with permission from Elsevier."

4. Reproduction of this material is confined to the purpose and/or media for which permission is hereby given.
5. Altering/Modifying Material: Not Permitted. However figures and illustrations may be altered/adapted minimally to serve your work. Any other abbreviations, additions, deletions and/or any other alterations shall be made only with prior written authorization of Elsevier Ltd. (Please contact Elsevier at [permissions@elsevier.com](mailto:permissions@elsevier.com))
6. If the permission fee for the requested use of our material is waived in this instance, please be advised that your future requests for Elsevier materials may attract a fee.
7. Reservation of Rights: Publisher reserves all rights not specifically granted in the combination of (i) the license details provided by you and accepted in the course of this licensing transaction, (ii) these terms and conditions and (iii) CCC's Billing and Payment terms and conditions.
8. License Contingent Upon Payment: While you may exercise the rights licensed immediately upon issuance of the license at the end of the licensing process for the transaction, provided that you have disclosed complete and accurate details of your proposed use, no license is finally effective unless and until full payment is received from you (either by publisher or by CCC) as provided in CCC's Billing and Payment terms and conditions. If full payment is not received on a timely basis, then any license preliminarily granted shall be deemed automatically revoked and shall be void as if never granted. Further, in the event that you breach any of these terms and conditions or any of CCC's Billing and Payment terms and conditions, the license is automatically revoked and shall be void as if never granted. Use of materials as described in a revoked license, as well as any use of the materials beyond the scope of an unrevoked license, may constitute copyright infringement and publisher reserves the right to take any and all action to protect its copyright in the materials.
9. Warranties: Publisher makes no representations or warranties with respect to the licensed material.
10. Indemnity: You hereby indemnify and agree to hold harmless publisher and CCC, and their respective officers, directors, employees and agents, from and against any and all claims arising out of your use of the licensed material other than as specifically authorized pursuant to this license.
11. No Transfer of License: This license is personal to you and may not be sublicensed, assigned, or transferred by you to any other person without publisher's written permission.
12. No Amendment Except in Writing: This license may not be amended except in a writing signed by both parties (or, in the case of publisher, by CCC on publisher's behalf).
13. Objection to Contrary Terms: Publisher hereby objects to any terms contained in any purchase order, acknowledgment, check endorsement or other writing prepared by you, which terms are inconsistent with these terms and conditions or CCC's Billing and Payment terms and conditions. These terms and conditions, together with CCC's Billing and

Payment terms and conditions (which are incorporated herein), comprise the entire agreement between you and publisher (and CCC) concerning this licensing transaction. In the event of any conflict between your obligations established by these terms and conditions and those established by CCC's Billing and Payment terms and conditions, these terms and conditions shall control.

14. **Revocation:** Elsevier or Copyright Clearance Center may deny the permissions described in this License at their sole discretion, for any reason or no reason, with a full refund payable to you. Notice of such denial will be made using the contact information provided by you. Failure to receive such notice will not alter or invalidate the denial. In no event will Elsevier or Copyright Clearance Center be responsible or liable for any costs, expenses or damage incurred by you as a result of a denial of your permission request, other than a refund of the amount(s) paid by you to Elsevier and/or Copyright Clearance Center for denied permissions.

### LIMITED LICENSE

The following terms and conditions apply only to specific license types:

15. **Translation:** This permission is granted for non-exclusive world **English** rights only unless your license was granted for translation rights. If you licensed translation rights you may only translate this content into the languages you requested. A professional translator must perform all translations and reproduce the content word for word preserving the integrity of the article. If this license is to re-use 1 or 2 figures then permission is granted for non-exclusive world rights in all languages.

16. **Website:** The following terms and conditions apply to electronic reserve and author websites:

**Electronic reserve:** If licensed material is to be posted to website, the web site is to be password-protected and made available only to bona fide students registered on a relevant course if:

This license was made in connection with a course,

This permission is granted for 1 year only. You may obtain a license for future website posting,

All content posted to the web site must maintain the copyright information line on the bottom of each image,

A hyper-text must be included to the Homepage of the journal from which you are licensing at <http://www.sciencedirect.com/science/journal/xxxxx> or the Elsevier homepage for books at <http://www.elsevier.com> , and

Central Storage: This license does not include permission for a scanned version of the material to be stored in a central repository such as that provided by Heron/XanEdu.

17. **Author website** for journals with the following additional clauses:

All content posted to the web site must maintain the copyright information line on the bottom of each image, and

the permission granted is limited to the personal version of your paper. You are not allowed to download and post the published electronic version of your article (whether PDF or

HTML, proof or final version), nor may you scan the printed edition to create an electronic version,

A hyper-text must be included to the Homepage of the journal from which you are licensing at <http://www.sciencedirect.com/science/journal/xxxxx> , As part of our normal production process, you will receive an e-mail notice when your article appears on Elsevier's online service ScienceDirect ([www.sciencedirect.com](http://www.sciencedirect.com)). That e-mail will include the article's Digital Object Identifier (DOI). This number provides the electronic link to the published article and should be included in the posting of your personal version. We ask that you wait until you receive this e-mail and have the DOI to do any posting.

Central Storage: This license does not include permission for a scanned version of the material to be stored in a central repository such as that provided by Heron/XanEdu.

**18. Author website** for books with the following additional clauses:

Authors are permitted to place a brief summary of their work online only.

A hyper-text must be included to the Elsevier homepage at <http://www.elsevier.com>

All content posted to the web site must maintain the copyright information line on the bottom of each image

You are not allowed to download and post the published electronic version of your chapter, nor may you scan the printed edition to create an electronic version.

Central Storage: This license does not include permission for a scanned version of the material to be stored in a central repository such as that provided by Heron/XanEdu.

**19. Website** (regular and for author): A hyper-text must be included to the Homepage of the journal from which you are licensing at

<http://www.sciencedirect.com/science/journal/xxxxx> . or for books to the Elsevier homepage at <http://www.elsevier.com>

**20. Thesis/Dissertation:** If your license is for use in a thesis/dissertation your thesis may be submitted to your institution in either print or electronic form. Should your thesis be published commercially, please reapply for permission. These requirements include permission for the Library and Archives of Canada to supply single copies, on demand, of the complete thesis and include permission for UMI to supply single copies, on demand, of the complete thesis. Should your thesis be published commercially, please reapply for permission.

**21. Other Conditions:**

v1.6

**Gratis licenses (referencing \$0 in the Total field) are free. Please retain this printable license for your reference. No payment is required.**

**If you would like to pay for this license now, please remit this license along with your payment made payable to "COPYRIGHT CLEARANCE CENTER" otherwise you will be invoiced within 48 hours of the license date. Payment should be in the form of a check**

or money order referencing your account number and this invoice number  
**RLNK10947473.**  
Once you receive your invoice for this order, you may pay your invoice by credit card.  
Please follow instructions provided at that time.

**Make Payment To:**  
**Copyright Clearance Center**  
**Dept 001**  
**P.O. Box 843006**  
**Boston, MA 02284-3006**

For suggestions or comments regarding this order, contact Rightslink Customer  
Support: [customer care@copyright.com](mailto:customer care@copyright.com) or +1-877-622-5543 (toll free in the US) or +1-  
978-646-2777.

---

---

**JOHN WILEY AND SONS LICENSE  
TERMS AND CONDITIONS**

Mar 11, 2011

This is a License Agreement between Parisa Hudson ("You") and John Wiley and Sons ("John Wiley and Sons") provided by Copyright Clearance Center ("CCC"). The license consists of your order details, the terms and conditions provided by John Wiley and Sons, and the payment terms and conditions.

**All payments must be made in full to CCC. For payment instructions, please see information listed at the bottom of this form.**

License Number	2625711445513
License date	Mar 11, 2011
Licensed content publisher	John Wiley and Sons
Licensed content publication	Magnetic Resonance in Medicine
Licensed content title	Multi-gradient echo with susceptibility inhomogeneity compensation (MGESIC): Demonstration of fMRI in the olfactory cortex at 3.0 T
Licensed content author	Qing X. Yang, Bernard J. Dardzinski, Shizhe Li, Paul J. Eslinger, Michael B. Smith
Licensed content date	Mar 1, 1997
Start page	331
End page	335
Type of use	Dissertation/Thesis
Requestor type	University/Academic
Format	Print and electronic
Portion	Figure/table
Number of figures/tables	1
Number of extracts	
Original Wiley figure/table number(s)	Figure 3
Will you be translating?	No
Order reference number	
Total	0.00 USD

[Terms and Conditions](#)

**TERMS AND CONDITIONS**

This copyrighted material is owned by or exclusively licensed to John Wiley & Sons, Inc. or one of its group companies (each a "Wiley Company") or a society for whom a Wiley Company has



exclusive publishing rights in relation to a particular journal (collectively "WILEY"). By clicking "accept" in connection with completing this licensing transaction, you agree that the following terms and conditions apply to this transaction (along with the billing and payment terms and conditions established by the Copyright Clearance Center Inc., ("CCC's Billing and Payment terms and conditions"), at the time that you opened your Rightslink account (these are available at any time at <http://myaccount.copyright.com>)

#### Terms and Conditions

1. The materials you have requested permission to reproduce (the "Materials") are protected by copyright.
2. You are hereby granted a personal, non-exclusive, non-sublicensable, non-transferable, worldwide, limited license to reproduce the Materials for the purpose specified in the licensing process. This license is for a one-time use only with a maximum distribution equal to the number that you identified in the licensing process. Any form of republication granted by this licence must be completed within two years of the date of the grant of this licence (although copies prepared before may be distributed thereafter). The Materials shall not be used in any other manner or for any other purpose. Permission is granted subject to an appropriate acknowledgement given to the author, title of the material/book/journal and the publisher and on the understanding that nowhere in the text is a previously published source acknowledged for all or part of this Material. Any third party material is expressly excluded from this permission.
3. With respect to the Materials, all rights are reserved. Except as expressly granted by the terms of the license, no part of the Materials may be copied, modified, adapted (except for minor reformatting required by the new Publication), translated, reproduced, transferred or distributed, in any form or by any means, and no derivative works may be made based on the Materials without the prior permission of the respective copyright owner. You may not alter, remove or suppress in any manner any copyright, trademark or other notices displayed by the Materials. You may not license, rent, sell, loan, lease, pledge, offer as security, transfer or assign the Materials, or any of the rights granted to you hereunder to any other person.
4. The Materials and all of the intellectual property rights therein shall at all times remain the exclusive property of John Wiley & Sons Inc or one of its related companies (WILEY) or their respective licensors, and your interest therein is only that of having possession of and the right to reproduce the Materials pursuant to Section 2 herein during the continuance of this Agreement. You agree that you own no right, title or interest in or to the Materials or any of the intellectual property rights therein. You shall have no rights hereunder other than the license as provided for above in Section 2. No right, license or interest to any trademark, trade name, service mark or other branding ("Marks") of WILEY or its licensors is granted hereunder, and you agree that you shall not assert any such right, license or interest with respect thereto.
5. NEITHER WILEY NOR ITS LICENSORS MAKES ANY WARRANTY OR REPRESENTATION OF ANY KIND TO YOU OR ANY THIRD PARTY, EXPRESS, IMPLIED OR STATUTORY, WITH RESPECT TO THE MATERIALS OR THE ACCURACY OF ANY INFORMATION CONTAINED IN THE MATERIALS, INCLUDING, WITHOUT LIMITATION, ANY IMPLIED WARRANTY OF MERCHANTABILITY, ACCURACY, SATISFACTORY QUALITY, FITNESS FOR A PARTICULAR PURPOSE, USABILITY, INTEGRATION OR NON-INFRINGEMENT AND ALL SUCH WARRANTIES ARE HEREBY EXCLUDED BY WILEY AND ITS LICENSORS AND WAIVED BY YOU.
6. WILEY shall have the right to terminate this Agreement immediately upon breach of this Agreement by you.
7. You shall indemnify, defend and hold harmless WILEY, its Licensors and their respective directors, officers, agents and employees, from and against any actual or threatened claims, demands, causes of action or proceedings arising from any breach of this Agreement by you.

8. IN NO EVENT SHALL WILEY OR ITS LICENSORS BE LIABLE TO YOU OR ANY OTHER PARTY OR ANY OTHER PERSON OR ENTITY FOR ANY SPECIAL, CONSEQUENTIAL, INCIDENTAL, INDIRECT, EXEMPLARY OR PUNITIVE DAMAGES, HOWEVER CAUSED, ARISING OUT OF OR IN CONNECTION WITH THE DOWNLOADING, PROVISIONING, VIEWING OR USE OF THE MATERIALS REGARDLESS OF THE FORM OF ACTION, WHETHER FOR BREACH OF CONTRACT, BREACH OF WARRANTY, TORT, NEGLIGENCE, INFRINGEMENT OR OTHERWISE (INCLUDING, WITHOUT LIMITATION, DAMAGES BASED ON LOSS OF PROFITS, DATA, FILES, USE, BUSINESS OPPORTUNITY OR CLAIMS OF THIRD PARTIES), AND WHETHER OR NOT THE PARTY HAS BEEN ADVISED OF THE POSSIBILITY OF SUCH DAMAGES. THIS LIMITATION SHALL APPLY NOTWITHSTANDING ANY FAILURE OF ESSENTIAL PURPOSE OF ANY LIMITED REMEDY PROVIDED HEREIN.

9. Should any provision of this Agreement be held by a court of competent jurisdiction to be illegal, invalid, or unenforceable, that provision shall be deemed amended to achieve as nearly as possible the same economic effect as the original provision, and the legality, validity and enforceability of the remaining provisions of this Agreement shall not be affected or impaired thereby.

10. The failure of either party to enforce any term or condition of this Agreement shall not constitute a waiver of either party's right to enforce each and every term and condition of this Agreement. No breach under this agreement shall be deemed waived or excused by either party unless such waiver or consent is in writing signed by the party granting such waiver or consent. The waiver by or consent of a party to a breach of any provision of this Agreement shall not operate or be construed as a waiver of or consent to any other or subsequent breach by such other party.

11. This Agreement may not be assigned (including by operation of law or otherwise) by you without WILEY's prior written consent.

12. Any fee required for this permission shall be non-refundable after thirty (30) days from receipt.

13. These terms and conditions together with CCC's Billing and Payment terms and conditions (which are incorporated herein) form the entire agreement between you and WILEY concerning this licensing transaction and (in the absence of fraud) supersedes all prior agreements and representations of the parties, oral or written. This Agreement may not be amended except in writing signed by both parties. This Agreement shall be binding upon and inure to the benefit of the parties' successors, legal representatives, and authorized assigns.

14. In the event of any conflict between your obligations established by these terms and conditions and those established by CCC's Billing and Payment terms and conditions, these terms and conditions shall prevail.

15. WILEY expressly reserves all rights not specifically granted in the combination of (i) the license details provided by you and accepted in the course of this licensing transaction, (ii) these terms and conditions and (iii) CCC's Billing and Payment terms and conditions.

16. This Agreement will be void if the Type of Use, Format, Circulation, or Requestor Type was misrepresented during the licensing process.

17. This Agreement shall be governed by and construed in accordance with the laws of the State of New York, USA, without regards to such state's conflict of law rules. Any legal action, suit or proceeding arising out of or relating to these Terms and Conditions or the breach thereof shall be instituted in a court of competent jurisdiction in New York County in the State of New York in the United States of America and each party hereby consents and submits to the personal jurisdiction of such court, waives any objection to venue in such court and consents to service of process by registered or certified mail, return receipt requested, at the last known address of such party. . BY CLICKING ON THE "I ACCEPT" BUTTON, YOU ACKNOWLEDGE THAT YOU HAVE READ

AND FULLY UNDERSTAND EACH OF THE SECTIONS OF AND PROVISIONS SET FORTH IN THIS AGREEMENT AND THAT YOU ARE IN AGREEMENT WITH AND ARE WILLING TO ACCEPT ALL OF YOUR OBLIGATIONS AS SET FORTH IN THIS AGREEMENT.

v1.4

**Gratis licenses (referencing \$0 in the Total field) are free. Please retain this printable license for your reference. No payment is required.**

**If you would like to pay for this license now, please remit this license along with your payment made payable to "COPYRIGHT CLEARANCE CENTER" otherwise you will be invoiced within 48 hours of the license date. Payment should be in the form of a check or money order referencing your account number and this invoice number RLNK10947439.**

**Once you receive your invoice for this order, you may pay your invoice by credit card. Please follow instructions provided at that time.**

**Make Payment To:  
Copyright Clearance Center  
Dept 001  
P.O. Box 843006  
Boston, MA 02284-3006**

**For suggestions or comments regarding this order, contact Rightslink Customer Support: [customercare@copyright.com](mailto:customercare@copyright.com) or +1-877-622-5543 (toll free in the US) or +1-978-646-2777.**

---

---

**ELSEVIER LICENSE  
TERMS AND CONDITIONS**

Mar 11, 2011

This is a License Agreement between Parisa Hudson ("You") and Elsevier ("Elsevier") provided by Copyright Clearance Center ("CCC"). The license consists of your order details, the terms and conditions provided by Elsevier, and the payment terms and conditions.

**All payments must be made in full to CCC. For payment instructions, please see information listed at the bottom of this form.**

Supplier	Elsevier Limited The Boulevard, Langford Lane Kidlington, Oxford, OX5 1GB, UK
Registered Company Number	1982084
Customer name	Parisa Hudson
Customer address	1151 Richmond Street London, ON N6A3K7
License number	2625730516310
License date	Mar 11, 2011
Licensed content publisher	Elsevier
Licensed content publication	Journal of Magnetic Resonance
Licensed content title	Sample-specific diamagnetic and paramagnetic passive shimming
Licensed content author	Kevin M. Koch, Peter B. Brown, Douglas L. Rothman, Robin A. de Graaf
Licensed content date	September 2006
Licensed content volume number	182
Licensed content issue number	1
Number of pages	9
Start Page	66
End Page	74
Type of Use	reuse in a thesis/dissertation
Intended publisher of new work	other
Portion	figures/tables/illustrations

Number of figures/tables/illustrations	1
Format	both print and electronic
Are you the author of this Elsevier article?	No
Will you be translating?	No
Order reference number	
Title of your thesis/dissertation	Pushing the boundaries in gradient and shim design for MRI
Expected completion date	Mar 2011
Estimated size (number of pages)	120
Elsevier VAT number	GB 494 6272 12
Permissions price	0.00 USD
VAT/Local Sales Tax	0.0 USD / 0.0 GBP
Total	0.00 USD
Terms and Conditions	

### INTRODUCTION

1. The publisher for this copyrighted material is Elsevier. By clicking "accept" in connection with completing this licensing transaction, you agree that the following terms and conditions apply to this transaction (along with the Billing and Payment terms and conditions established by Copyright Clearance Center, Inc. ("CCC"), at the time that you opened your Rightslink account and that are available at any time at <http://myaccount.copyright.com>).

### GENERAL TERMS

2. Elsevier hereby grants you permission to reproduce the aforementioned material subject to the terms and conditions indicated.

3. Acknowledgement: If any part of the material to be used (for example, figures) has appeared in our publication with credit or acknowledgement to another source, permission must also be sought from that source. If such permission is not obtained then that material may not be included in your publication/copies. Suitable acknowledgement to the source must be made, either as a footnote or in a reference list at the end of your publication, as follows:

"Reprinted from Publication title, Vol /edition number, Author(s), Title of article / title of chapter, Pages No., Copyright (Year), with permission from Elsevier [OR APPLICABLE SOCIETY COPYRIGHT OWNER]." Also Lancet special credit - "Reprinted from The Lancet, Vol. number, Author(s), Title of article, Pages No., Copyright (Year), with permission from Elsevier."

4. Reproduction of this material is confined to the purpose and/or media for which permission is hereby given.
5. Altering/Modifying Material: Not Permitted. However figures and illustrations may be altered/adapted minimally to serve your work. Any other abbreviations, additions, deletions and/or any other alterations shall be made only with prior written authorization of Elsevier Ltd. (Please contact Elsevier at [permissions@elsevier.com](mailto:permissions@elsevier.com))
6. If the permission fee for the requested use of our material is waived in this instance, please be advised that your future requests for Elsevier materials may attract a fee.
7. Reservation of Rights: Publisher reserves all rights not specifically granted in the combination of (i) the license details provided by you and accepted in the course of this licensing transaction, (ii) these terms and conditions and (iii) CCC's Billing and Payment terms and conditions.
8. License Contingent Upon Payment: While you may exercise the rights licensed immediately upon issuance of the license at the end of the licensing process for the transaction, provided that you have disclosed complete and accurate details of your proposed use, no license is finally effective unless and until full payment is received from you (either by publisher or by CCC) as provided in CCC's Billing and Payment terms and conditions. If full payment is not received on a timely basis, then any license preliminarily granted shall be deemed automatically revoked and shall be void as if never granted. Further, in the event that you breach any of these terms and conditions or any of CCC's Billing and Payment terms and conditions, the license is automatically revoked and shall be void as if never granted. Use of materials as described in a revoked license, as well as any use of the materials beyond the scope of an unrevoked license, may constitute copyright infringement and publisher reserves the right to take any and all action to protect its copyright in the materials.
9. Warranties: Publisher makes no representations or warranties with respect to the licensed material.
10. Indemnity: You hereby indemnify and agree to hold harmless publisher and CCC, and their respective officers, directors, employees and agents, from and against any and all claims arising out of your use of the licensed material other than as specifically authorized pursuant to this license.
11. No Transfer of License: This license is personal to you and may not be sublicensed, assigned, or transferred by you to any other person without publisher's written permission.
12. No Amendment Except in Writing: This license may not be amended except in a writing signed by both parties (or, in the case of publisher, by CCC on publisher's behalf).
13. Objection to Contrary Terms: Publisher hereby objects to any terms contained in any purchase order, acknowledgment, check endorsement or other writing prepared by you, which terms are inconsistent with these terms and conditions or CCC's Billing and Payment terms and conditions. These terms and conditions, together with CCC's Billing and

Payment terms and conditions (which are incorporated herein), comprise the entire agreement between you and publisher (and CCC) concerning this licensing transaction. In the event of any conflict between your obligations established by these terms and conditions and those established by CCC's Billing and Payment terms and conditions, these terms and conditions shall control.

14. **Revocation:** Elsevier or Copyright Clearance Center may deny the permissions described in this License at their sole discretion, for any reason or no reason, with a full refund payable to you. Notice of such denial will be made using the contact information provided by you. Failure to receive such notice will not alter or invalidate the denial. In no event will Elsevier or Copyright Clearance Center be responsible or liable for any costs, expenses or damage incurred by you as a result of a denial of your permission request, other than a refund of the amount(s) paid by you to Elsevier and/or Copyright Clearance Center for denied permissions.

### LIMITED LICENSE

The following terms and conditions apply only to specific license types:

15. **Translation:** This permission is granted for non-exclusive world **English** rights only unless your license was granted for translation rights. If you licensed translation rights you may only translate this content into the languages you requested. A professional translator must perform all translations and reproduce the content word for word preserving the integrity of the article. If this license is to re-use 1 or 2 figures then permission is granted for non-exclusive world rights in all languages.

16. **Website:** The following terms and conditions apply to electronic reserve and author websites:

**Electronic reserve:** If licensed material is to be posted to website, the web site is to be password-protected and made available only to bona fide students registered on a relevant course if:

This license was made in connection with a course,

This permission is granted for 1 year only. You may obtain a license for future website posting,

All content posted to the web site must maintain the copyright information line on the bottom of each image,

A hyper-text must be included to the Homepage of the journal from which you are licensing at <http://www.sciencedirect.com/science/journal/xxxxx> or the Elsevier homepage for books at <http://www.elsevier.com> , and

Central Storage: This license does not include permission for a scanned version of the material to be stored in a central repository such as that provided by Heron/XanEdu.

17. **Author website** for journals with the following additional clauses:

All content posted to the web site must maintain the copyright information line on the bottom of each image, and

the permission granted is limited to the personal version of your paper. You are not allowed to download and post the published electronic version of your article (whether PDF or

HTML, proof or final version), nor may you scan the printed edition to create an electronic version,

A hyper-text must be included to the Homepage of the journal from which you are licensing at <http://www.sciencedirect.com/science/journal/xxxxx> , As part of our normal production process, you will receive an e-mail notice when your article appears on Elsevier's online service ScienceDirect ([www.sciencedirect.com](http://www.sciencedirect.com)). That e-mail will include the article's Digital Object Identifier (DOI). This number provides the electronic link to the published article and should be included in the posting of your personal version. We ask that you wait until you receive this e-mail and have the DOI to do any posting.

Central Storage: This license does not include permission for a scanned version of the material to be stored in a central repository such as that provided by Heron/XanEdu.

**18. Author website** for books with the following additional clauses:

Authors are permitted to place a brief summary of their work online only.

A hyper-text must be included to the Elsevier homepage at <http://www.elsevier.com>

All content posted to the web site must maintain the copyright information line on the bottom of each image

You are not allowed to download and post the published electronic version of your chapter, nor may you scan the printed edition to create an electronic version.

Central Storage: This license does not include permission for a scanned version of the material to be stored in a central repository such as that provided by Heron/XanEdu.

**19. Website** (regular and for author): A hyper-text must be included to the Homepage of the journal from which you are licensing at

<http://www.sciencedirect.com/science/journal/xxxxx> . or for books to the Elsevier homepage at <http://www.elsevier.com>

**20. Thesis/Dissertation:** If your license is for use in a thesis/dissertation your thesis may be submitted to your institution in either print or electronic form. Should your thesis be published commercially, please reapply for permission. These requirements include permission for the Library and Archives of Canada to supply single copies, on demand, of the complete thesis and include permission for UMI to supply single copies, on demand, of the complete thesis. Should your thesis be published commercially, please reapply for permission.

**21. Other Conditions:**

v1.6

**Gratis licenses (referencing \$0 in the Total field) are free. Please retain this printable license for your reference. No payment is required.**

**If you would like to pay for this license now, please remit this license along with your payment made payable to "COPYRIGHT CLEARANCE CENTER" otherwise you will be invoiced within 48 hours of the license date. Payment should be in the form of a check**



or money order referencing your account number and this invoice number  
**RLNK10947473.**  
Once you receive your invoice for this order, you may pay your invoice by credit card.  
Please follow instructions provided at that time.

**Make Payment To:**  
**Copyright Clearance Center**  
**Dept 001**  
**P.O. Box 843006**  
**Boston, MA 02284-3006**

For suggestions or comments regarding this order, contact Rightslink Customer  
Support: [customercare@copyright.com](mailto:customercare@copyright.com) or +1-877-622-5543 (toll free in the US) or +1-  
978-646-2777.

---

---

**ELSEVIER LICENSE  
TERMS AND CONDITIONS**

Mar 11, 2011

This is a License Agreement between Parisa Hudson ("You") and Elsevier ("Elsevier") provided by Copyright Clearance Center ("CCC"). The license consists of your order details, the terms and conditions provided by Elsevier, and the payment terms and conditions.

**All payments must be made in full to CCC. For payment instructions, please see information listed at the bottom of this form.**

Supplier	Elsevier Limited The Boulevard, Langford Lane Kidlington, Oxford, OX5 1GB, UK
Registered Company Number	1982084
Customer name	Parisa Hudson
Customer address	1151 Richmond Street London, ON N6A3K7
License number	2625720599093
License date	Mar 11, 2011
Licensed content publisher	Elsevier
Licensed content publication	Journal of Magnetic Resonance
Licensed content title	Dynamic shim updating on the human brain
Licensed content author	Kevin M. Koch, Scott McIntyre, Terence W. Nixon, Douglas L. Rothman, Robin A. de Graaf
Licensed content date	June 2006
Licensed content volume number	180
Licensed content issue number	2
Number of pages	11
Start Page	286
End Page	296
Type of Use	reuse in a thesis/dissertation
Portion	figures/tables/illustrations
Number of figures/tables/illustrations	1

Format	both print and electronic
Are you the author of this Elsevier article?	No
Will you be translating?	No
Order reference number	
Title of your thesis/dissertation	Pushing the boundaries in gradient and shim design for MRI
Expected completion date	Mar 2011
Estimated size (number of pages)	120
Elsevier VAT number	GB 494 6272 12
Permissions price	0.00 USD
VAT/Local Sales Tax	0.0 USD / 0.0 GBP
Total	0.00 USD
Terms and Conditions	

### INTRODUCTION

1. The publisher for this copyrighted material is Elsevier. By clicking "accept" in connection with completing this licensing transaction, you agree that the following terms and conditions apply to this transaction (along with the Billing and Payment terms and conditions established by Copyright Clearance Center, Inc. ("CCC"), at the time that you opened your Rightslink account and that are available at any time at <http://myaccount.copyright.com>).

### GENERAL TERMS

2. Elsevier hereby grants you permission to reproduce the aforementioned material subject to the terms and conditions indicated.

3. Acknowledgement: If any part of the material to be used (for example, figures) has appeared in our publication with credit or acknowledgement to another source, permission must also be sought from that source. If such permission is not obtained then that material may not be included in your publication/copies. Suitable acknowledgement to the source must be made, either as a footnote or in a reference list at the end of your publication, as follows:

"Reprinted from Publication title, Vol /edition number, Author(s), Title of article / title of chapter, Pages No., Copyright (Year), with permission from Elsevier [OR APPLICABLE SOCIETY COPYRIGHT OWNER]." Also Lancet special credit - "Reprinted from The Lancet, Vol. number, Author(s), Title of article, Pages No., Copyright (Year), with permission from Elsevier."

4. Reproduction of this material is confined to the purpose and/or media for which permission is hereby given.

5. **Altering/Modifying Material: Not Permitted.** However figures and illustrations may be altered/adapted minimally to serve your work. Any other abbreviations, additions, deletions and/or any other alterations shall be made only with prior written authorization of Elsevier Ltd. (Please contact Elsevier at [permissions@elsevier.com](mailto:permissions@elsevier.com))

6. If the permission fee for the requested use of our material is waived in this instance, please be advised that your future requests for Elsevier materials may attract a fee.

7. **Reservation of Rights:** Publisher reserves all rights not specifically granted in the combination of (i) the license details provided by you and accepted in the course of this licensing transaction, (ii) these terms and conditions and (iii) CCC's Billing and Payment terms and conditions.

8. **License Contingent Upon Payment:** While you may exercise the rights licensed immediately upon issuance of the license at the end of the licensing process for the transaction, provided that you have disclosed complete and accurate details of your proposed use, no license is finally effective unless and until full payment is received from you (either by publisher or by CCC) as provided in CCC's Billing and Payment terms and conditions. If full payment is not received on a timely basis, then any license preliminarily granted shall be deemed automatically revoked and shall be void as if never granted. Further, in the event that you breach any of these terms and conditions or any of CCC's Billing and Payment terms and conditions, the license is automatically revoked and shall be void as if never granted. Use of materials as described in a revoked license, as well as any use of the materials beyond the scope of an unrevoked license, may constitute copyright infringement and publisher reserves the right to take any and all action to protect its copyright in the materials.

9. **Warranties:** Publisher makes no representations or warranties with respect to the licensed material.

10. **Indemnity:** You hereby indemnify and agree to hold harmless publisher and CCC, and their respective officers, directors, employees and agents, from and against any and all claims arising out of your use of the licensed material other than as specifically authorized pursuant to this license.

11. **No Transfer of License:** This license is personal to you and may not be sublicensed, assigned, or transferred by you to any other person without publisher's written permission.

12. **No Amendment Except in Writing:** This license may not be amended except in a writing signed by both parties (or, in the case of publisher, by CCC on publisher's behalf).

13. **Objection to Contrary Terms:** Publisher hereby objects to any terms contained in any purchase order, acknowledgment, check endorsement or other writing prepared by you, which terms are inconsistent with these terms and conditions or CCC's Billing and Payment terms and conditions. These terms and conditions, together with CCC's Billing and Payment terms and conditions (which are incorporated herein), comprise the entire agreement between you and publisher (and CCC) concerning this licensing transaction. In the event of any conflict between your obligations established by these terms and

conditions and those established by CCC's Billing and Payment terms and conditions, these terms and conditions shall control.

14. **Revocation:** Elsevier or Copyright Clearance Center may deny the permissions described in this License at their sole discretion, for any reason or no reason, with a full refund payable to you. Notice of such denial will be made using the contact information provided by you. Failure to receive such notice will not alter or invalidate the denial. In no event will Elsevier or Copyright Clearance Center be responsible or liable for any costs, expenses or damage incurred by you as a result of a denial of your permission request, other than a refund of the amount(s) paid by you to Elsevier and/or Copyright Clearance Center for denied permissions.

#### LIMITED LICENSE

The following terms and conditions apply only to specific license types:

15. **Translation:** This permission is granted for non-exclusive world **English** rights only unless your license was granted for translation rights. If you licensed translation rights you may only translate this content into the languages you requested. A professional translator must perform all translations and reproduce the content word for word preserving the integrity of the article. If this license is to re-use 1 or 2 figures then permission is granted for non-exclusive world rights in all languages.

16. **Website:** The following terms and conditions apply to electronic reserve and author websites:

**Electronic reserve:** If licensed material is to be posted to website, the web site is to be password-protected and made available only to bona fide students registered on a relevant course if:

This license was made in connection with a course,

This permission is granted for 1 year only. You may obtain a license for future website posting,

All content posted to the web site must maintain the copyright information line on the bottom of each image,

A hyper-text must be included to the Homepage of the journal from which you are licensing at <http://www.sciencedirect.com/science/journal/xxxx> or the Elsevier homepage for books at <http://www.elsevier.com> , and

Central Storage: This license does not include permission for a scanned version of the material to be stored in a central repository such as that provided by Heron/XanEdu.

17. **Author website** for journals with the following additional clauses:

All content posted to the web site must maintain the copyright information line on the bottom of each image, and

the permission granted is limited to the personal version of your paper. You are not allowed to download and post the published electronic version of your article (whether PDF or HTML, proof or final version), nor may you scan the printed edition to create an electronic version,

A hyper-text must be included to the Homepage of the journal from which you are

licensing at <http://www.sciencedirect.com/science/journal/xxxxx> , As part of our normal production process, you will receive an e-mail notice when your article appears on Elsevier's online service ScienceDirect ([www.sciencedirect.com](http://www.sciencedirect.com)). That e-mail will include the article's Digital Object Identifier (DOI). This number provides the electronic link to the published article and should be included in the posting of your personal version. We ask that you wait until you receive this e-mail and have the DOI to do any posting.  
Central Storage: This license does not include permission for a scanned version of the material to be stored in a central repository such as that provided by Heron/XanEdu.

**18. Author website** for books with the following additional clauses:

Authors are permitted to place a brief summary of their work online only.

A hyper-text must be included to the Elsevier homepage at <http://www.elsevier.com>

All content posted to the web site must maintain the copyright information line on the bottom of each image

You are not allowed to download and post the published electronic version of your chapter, nor may you scan the printed edition to create an electronic version.

Central Storage: This license does not include permission for a scanned version of the material to be stored in a central repository such as that provided by Heron/XanEdu.

**19. Website** (regular and for author): A hyper-text must be included to the Homepage of the journal from which you are licensing at <http://www.sciencedirect.com/science/journal/xxxxx> . or for books to the Elsevier homepage at <http://www.elsevier.com>

**20. Thesis/Dissertation:** If your license is for use in a thesis/dissertation your thesis may be submitted to your institution in either print or electronic form. Should your thesis be published commercially, please reapply for permission. These requirements include permission for the Library and Archives of Canada to supply single copies, on demand, of the complete thesis and include permission for UMI to supply single copies, on demand, of the complete thesis. Should your thesis be published commercially, please reapply for permission.

**21. Other Conditions:**

v1.6

**Gratis licenses (referencing \$0 in the Total field) are free. Please retain this printable license for your reference. No payment is required.**

**If you would like to pay for this license now, please remit this license along with your payment made payable to "COPYRIGHT CLEARANCE CENTER" otherwise you will be invoiced within 48 hours of the license date. Payment should be in the form of a check or money order referencing your account number and this invoice number RLNK10947451.**

**Once you receive your invoice for this order, you may pay your invoice by credit card.**

**Please follow instructions provided at that time.**

**Make Payment To:**  
**Copyright Clearance Center**  
**Dept 001**  
**P.O. Box 843006**  
**Boston, MA 02284-3006**

**For suggestions or comments regarding this order, contact Rightslink Customer Support: [customercare@copyright.com](mailto:customercare@copyright.com) or +1-877-622-5543 (toll free in the US) or +1-978-646-2777.**

---

---

# Curriculum Vitae

**Name:** Parisa Hudson

**Post-secondary Education and Degrees:** The University of Shiraz  
Shiraz, Fars, Iran  
1996-2000 B.A.

The University of Shahid Bahonar  
Kerman, Kerman, Iran  
2000-2003 M.A.

The University of Western Ontario  
London, Ontario, Canada  
2005-2010 Ph.D.

**Honours and Awards:** Western Graduate Thesis Research Award  
2010

**Related Work Experience**

Teaching Assistant  
The University of Shahid Bahonar  
2000-2003

Teaching Assistant  
The University of Western Ontario  
2005-2010

Teaching Support Centre Instructor  
The University of Western Ontario  
2007-2010

## Publications:

### Journal Articles:

Parisa Hudson, Stephen D. Hudson, William B. Handler, Timothy J. Scholl, and Blaine A. Chronik (2010) Quantitative comparison of minimum inductance and minimum power algorithms for the design of shim coils for small animal imaging. *Magnetic Resonance Engineering* 37B(2):65-74.

Parisa Hudson, Stephen D. Hudson, William B. Handler, and Blaine A. Chronik



(2010) Finite-length shim coil design using a fourier series minimum inductance and minimum power algorithm. *Magnetic Resonance Engineering* 37B(4):245-253.

Alireza Bahrampour, Mahyar Mahjoei, and Parisa Hudson (2007) Investigation of transient response of erbium-doped fiber lasers by semi-classical theory. *Journal of Optical Communications* 28(4):248-251.

### **Conference Presentations:**

Parisa Hudson, Chad T. Harris, William B. Handler, Timothy J. Scholl, and Blaine A. Chronik (2010) A single-axis composite shim coil insert for spectroscopy in the medial temporal lobe of the human brain. *International Society for Magnetic Resonance in Medicine, 18th Annual Meeting, Stockholm.*

Parisa Hudson, Blaine A. Chronik (2009) Design of a high power customized shim set insert for in vivo spectroscopy of deep brain structures in humans at 4T. *International Society for Magnetic Resonance in Medicine, 17th Annual Meeting, Hawaii.*

Parisa Hudson, Blaine A. Chronik (2008) Power versus Inductance: finite length shim coil design for high-field MRI. *International Society for Magnetic Resonance in Medicine, 16th Annual Meeting, Toronto.*

Parisa Hudson, Blaine A. Chronik (2007) Quantitative Comparison of Minimum Inductance and Minimum Power Algorithms for The Design of Small Animal Shim Coils. *International Society for Magnetic Resonance in Medicine, 15th Annual Meeting, Berlin.*

Parisa Hudson, Blaine A. Chronik (2007) Composite Shim Coil Design for System- Specific Field Corrections. *International Society for Magnetic Resonance in Medicine, 15th Annual Meeting, Berlin.*

Parisa Hudson, Blaine A. Chronik (2006) Magnetic Field Induced by PET Detector Scintillators in Dual Modality MRI/PET Inhomogeneity. *International Society for Magnetic Resonance in Medicine, 14th Annual Meeting, Seattle, WA.*

Parisa Hudson, Blaine A. Chronik (2005) Analysis of Magnetic Field Effects in MRI for Multi-Modality Imaging Systems. *Mathematics of Information Technology and Complex Systems Conference, Calgary, AB.*

Ali.Reza Bahrampour, Parisa Hudson, Mahyar Mahjoei (2003) Investigation of Relaxation-Oscillation Behavior of Erbium Doped Fiber by Semi-Classical Theory. *Proceeding of the Numerical Simulation of Semiconductor Optoelectronic Devices, IEEE/LEOS, Japan.*